U-PB DETRITAL ZIRCONS OF THE SYN-OROGENIC CARBONIFEROUS DEEP-WATER CLASTIC DEPOSITS IN THE OUACHITA MOUNTAINS, ARKANSAS, UNITED STATES

By

SHAUN T. PRINES

Bachelor of Science, 2018

University of Pittsburgh

Pittsburgh, Pennsylvania

Submitted to the Graduate Faculty of

the College of Science and Engineering

Texas Christian University

in partial fulfillment of the requirements for the degree

MASTER OF SCIENCE IN GEOLOGY

May 2020

Acknowledgements

I would like to thank the following for all the help they have given me during my two years at TCU.

First and foremost, my research advisor Dr. Xiangyang "Cheyenne" Xie for his patience and support with all the work I have ever done at TCU. His sense of humor made every single day in the "Xie Cave" enjoyable and fun. I truly believe I could not have had a better advisor or person helping me with my research during my time here at TCU. Also, I would like to thank my committee members Dr. Helge Alsleben and Dr. Walter L. Manger. I would like to greatly express my gratitude to Dr. Alsleben for his willingness to always answer my daily questions and for Dr. Manger for all his help in the field and providing insights for my research with his expertise on the geology of Arkansas. Additionally, I would like to thank family especially my mom Leslie and my grandma Bonnie who always gave their love and support to the fullest while I was working on my thesis. I would like to also thank my girlfriend Kayla for her constant love and support and always having to listen to me talk about detrital zircons. Lastly, I would like to thank all my friends I have made here at TCU with a special thank you to Brendan Talbert, Anthony Skaleski, Sam Walker, MG Moran, Marissa English, Blake Bezucha, Blake Warwick, Clayton Friemuth, and John Alvarez.

Also, I would like to express my sincerest gratitude the Atkins Fund from the Department of Geological Sciences and Science and Engineering Research Center (SERC) for the financial funding that made this research possible.

Table of Contents

List of Figures

List of Tables

INTRODUCTION

The collision between Laurentia and Gondwana, that produced late Paleozoic Ouachita Orogeny, resulted in the closure of the Rheic Ocean and uplifting of over 10,000 meters of Carboniferous deep-water, siliciclastic, sedimentary rocks that were deposited within the remnant Ouachita ocean basin along the southern margin of Laurentia (Figure 1) (Flawn et al., 1961; Viele and Thomas, 1989). Most of the Ouachita orogenic belt, which stretches from Mississippi to as far west as northern Mexico (Figure 1), is covered by Mesozoic and Cenozoic sediments. Being one of only two exposures, the Ouachita Mountains of southeastern Oklahoma and western Arkansas become an excellent laboratory to document the provenance of the syn-orogenic, Carboniferous deep-water interval. Despite numerous sedimentologic studies (Arbenz et al., 1989; Cline, 1960; Cline et al., 1968; Goldstein and Hendricks, 1962; Graham et al., 1975; Lowe, 1985, 1989; Moiola and Shanmugam, 1983; Morris, 1971, 1973, 1974, 1989; Morris et al., 1977; Sharrah, 2006; Sutherland, 1988), a thorough provenance study of these deep-water siliciclastic deposits has not yet been conducted. Different sources have been proposed including, the southern Ouachita orogenic belt, erosion of the ancestral Rockies to the north, or erosion of the eastern Appalachian orogenic belt (Danielson et al., 1988; Gleason et al., 1995; Morris, 1974; Thomas, 1985); as a result, the ultimate sources remain under debate.

Previous U-Pb detrital zircon analyses have proposed various potential sediment dispersal networks and delivery patterns to the Ouachita Mountains in the Carboniferous. For example, Gleason et al. (1995, 2002), McGuire (2017), and Shaulis (2010) proposed that Carboniferous sedimentation in the Ouachita Mountains was derived from recycled orogenic detritus from either the Appalachian foreland basins or the pre-Carboniferous seafloor assemblage of the Ouachita orogenic belt. Graham et al. (1975, 1976) suggested that sediment transport to the Ouachita Mountains in the Carboniferous was controlled via a large continental drainage system stemming from the Appalachian foreland using the modern Himalayan-Bengal deep-water fan as an analog. Whereas others have proposed a large scale, longitudinal, intra-basinal,

Amazon-scale drainage system that flowed parallel to the Appalachian foreland (Archer and Greb, 1995) and transcontinental, westward flowing, fluvial systems originating from the Appalachian hinterland (Gehrels et al., 2011). However, only a limited amount of detrital zircon data has been published on the Upper Paleozoic rocks of the Ouachita Mountains, leaving the provenance and sediment dispersal patterns of the Ouachita Mountains in question. Furthering the provenance record of the Carboniferous syn-orogenic, deep-water succession of the Ouachita Mountains grants additional insights for understanding the effects on sediment sourcing and dispersal patterns caused by the Late Paleozoic Ouachita orogeny in the Southern Midcontinent. In addition, a more complete provenance record of the upper Paleozoic rocks of the Ouachita Mountains provides further evidence for the influence of Late Paleozoic Taconic and Acadian orogenic events of eastern Appalachia dispersing sediment across Laurentia.

In this study, U-Pb detrital zircon geochronology has been applied to determine the provenance of the syn-orogenic, Carboniferous, deep-water succession of the Ouachita Mountains located in central Arkansas. Results show that the detrital zircon signatures of the syn-orogenic Carboniferous strata within the Ouachita Mountains are very similar suggesting that they were most likely derived from similar sediment sources. Additionally, minor variations in detrital signatures support the intermixing of sediment sources in the remnant ocean basin along the southern margin of Laurentia, which acted as a terminal sink during the Carboniferous. By comparing results to previously published detrital zircon data of Lower Paleozoic Laurentian sandstones, and combining paleogeographic, paleoclimate, paleotectonic, and sedimentologic data from Laurentia with previously proposed paleodrainage models (Archer and Greb, 1995; Kissock et al., 2018; Sutherland, 1988; Xie et al., 2018; Xie et al., 2016), I infer the origin and transport history of the deep-water deposits in the Ouachita Mountains, and can further reconstruct possible sediment dispersal pathways into the Southern Midcontinent during the Carboniferous.

GEOLOGIC BACKGROUND

Tectonic History

Prior to the formation of the Ouachita orogenic belt, the North American craton experienced a series of rifting events from the Precambrian to the Cambrian. This deformation led to the formation of the Iapetus Ocean along the southern margin of the continent (Viele and Thomas, 1989). Geophysical and well log data have helped to reconstruct the tectonic geometry of southern Laurentia during this time period. Geometric reconstructions suggest rifting along the southern margin has been characterized by a zigzag pattern (Thomas, 1976; Thomas, 2006; Viele and Thomas, 1989). Theses rifting events resulted in the formation of the remnant Ouachita ocean basin, also known as the Ouachita trough, along the southern embayment of the North American continent. The evolution of the remnant Ouachita ocean basin would continue throughout the Cambrian as a narrow, two-sided ocean basin, bounded on the north by the North American craton, and the Peri-Gondwana volcanic arc terranes to the south (Morris, 1974). Rift-related sedimentary basins such as the Illinois Basin, Reelfoot Rift, Rome Trough, and Southern Oklahoma Aulacogen, are all suggested to be a part of this same failed rift system (Lowe, 1985).

The pre-orogenic phase of the Ouachita orogeny comprises the beginning of the Ordovician to the end of the Early-Middle Mississippian. During this time, the Ouachita trough was a sediment starved, passive margin (Lowe, 1989). Basin-wide, sea level drops in the late Devonian caused a major shift in sedimentation resulting in the Ouachita trough transforming from a predominantly carbonate and shale environment to a predominantly carbonate and novaculite environment. These terrigenous clastic units represent regressional settings that favored increased carbonate deposition throughout the Ouachita trough (Haq and Schutter, 2008; Thomas, 1976). The dominant formation deposited during the late Devonian is the lower-middle Arkansas Novaculite, characterized as massive, light-colored, extremely fined grained, homogeneous, amorphous silica with interbedded siliceous chert nodules (Sholes et al., 1975). The increase

of volcanic detritus noted within the Arkansas Novaculite is mainly due to the advancement of subducting volcanic island arcs throughout the Devonian.

In the Early Mississippian, the southern margin of the North American craton was still a passive margin that had experienced limited tectonic activity since the rifting of Rodinia in the Precambrian. During this time, the Ouachita trough reached its maximum in terms of both depth and width (Viele and Thomas 1989), and a broad carbonate shelf blanketed a substantial area of the Southern Midcontinent (Xie et al., 2016). However, the advancement of the southern encroaching orogen began to alter sedimentation in the remnant Ouachita ocean basin during the Middle Mississippian (Sutherland, 1988). The progressive closure of the remnant Ouachita ocean basin combined with the relative sea level fall of the epeiric seas, resulted in a rapid influx of silty and sandy facies into the basin (Arbenz, 2008).

During the Late Mississippian and Early Pennsylvanian, Gondwana collided with the southern margin of Laurentia marking the onset of the Ouachita orogeny. The orogeny transformed the southern margin of the North American craton from a continental shelf, characterized by a passive margin, to a tectonically active cratonic margin (Viele and Thomas, 1989). This change resulted in contractional tectonics and the closure of the remnant Ouachita ocean basin along the southern margin, which led to the rapid deposition of clastic sediments succeeding the slow deposition of chert, novaculite, and siliceous shale in the basin (Sholes et al., 1975). These deep-water clastic deposits were thrusted northward onto shallow marine units during the Ouachita orogeny (Morris, 1974). The tectonic activity caused by the Ouachita orogeny along the southern margin of the North American craton ceased in the Early Permian, followed by periods of elevated weathering and erosion throughout the Late Paleozoic and Mesozoic responsible for the present-day state of the mountains (Cline, 1960).

Carboniferous deep-water interval of the Ouachita Mountains

The syn-orogenic Carboniferous succession of the Ouachita Mountains represents a classic deep-marine basin fan complex. The deposition of the Mississippian Stanley Group, which overlies the Devonian Arkansas Novaculite, marks the initial onset of syn-orogenic Carboniferous sedimentation in the Ouachita Mountains. The mixing of deep-water shales and sandstones with debris flows produced the bulk of the Stanley Shale (Cline, 1960; Morris, 1974) . The vast majority of detrital material comprising the Stanley Shale is derived from volcanic, granitic, and sedimentary terranes to the south of the submarine fan complex (Morris, 1989; Niem, 1976). Thick, relatively laterally extensive shale packages within the Stanley host the major thrust faults of the Ouachita Mountains (Coleman and Anonymous, 1990, 1993). The sandstones, siltstones, and shales of the Hot Springs Sandstone formation mark the lowermost sections of the Stanley submarine fan complex. At the top of the Stanley Group lies the discrete shale packages of the Chicksaw Creek member.

Succeeding the Stanley Group interval, the Jackfork Group represents a complex of generally westward-prograding submarine fans with deposition occurring along the axis of the closing ocean basin (Moiola and Shanmugam, 1983). The majority of the Jackfork was deposited by muddy and sandy turbidity currents and debris flows that emanated from systems northeast and southeast of the present-day Ouachita thrust belt (Arbenz et al., 1989; Danielson et al., 1988; Link et al., 1986; Pauli and Anonymous, 1999). Jackfork deposition indicates the basin floor was not affected by foreland basin thrusting inversion, due to its basin-wide similarity in thickness (Coleman et al., 2000). The Jackfork Group is distinct from the underlying Stanley Group—the majority of the Jackfork Group sandstones are composed of 95% quartz and substantially thicker on a bed-to-bed basis.

Overlying the Jackfork Group, the Lower-Middle Pennsylvanian Johns Valley Shale is composed of shales, thinly-bedded turbidities, and boulder-bed debrites, which host transported clasts of Cambrian-

Pennsylvanian basinal, shelf, and slope strata. These boulder deposits within the Johns Valley Shale represent the structural transformation of the remnant Ouachita ocean basin from a thrust driven system into a strike-slip driven system. This transition resulted in the basement uplift and erosion of the early syn- and pre-orogenic strata throughout the majority of the basin. (Coleman et al., 2000). Additionally, the Johns Valley Shale marks the first global sea-level drop following the major transgressions that occurred throughout the Early Pennsylvanian (Zou et al., 2017).

The last significant, syn-orogenic, depositional interval is the Atoka Formation, which overlies the Johns Valley Shale. The Atoka Formation is a relatively thick succession of lower and middle Pennsylvanian sandstone and shale. Atokan sedimentation represents a shallowing upward-sequence beginning with deep-water turbidities and concluding with fluvial-deltaic strata (Graham et al., 1976)

METHODS

Sampling and Unit Descriptions

Sampled rock units ranging in age from the Mississippian to the Lower-Middle Pennsylvanian were sampled from outcrops within, and adjacent to, the Ouachita thrust belt within the Ouachita Mountains. All the samples were taken from where lower, middle, and upper stratigraphic contacts are relatively clear. In total, six samples from the Stanley and Jackfork turbidities, and the Johns Valley shale were collected and processed for U-Pb detrital zircon analysis (Figures 2, 3, Table 1). The turbidities of the middle and upper section of the Mississippian Stanley Group consist of dark gray to olive-brown sandstones with, fine to coarse well-rounded texture, that are interbedded with thin, gray siliceous shales. Samples taken from the middle section of the Stanley Group display an increase in volcanic activity with interbedded quartzitic sandstones and tuff deposits (Stone et al., 1979). The majority of sandstone units within the Stanley Group range from 3 to 150 meters thick, and are mostly structureless without any distinct sedimentary features, although load casts, flute casts, tool marks, parallel laminations, and cross laminations are present in some

outcrops (Flawn et al., 1961; Morris, 1974). These types of bedding features are present in sand bodies from the upper section of the formation and were used to record paleocurrent measurements.

Samples of the Pennsylvanian Jackfork Group predominantly consists of brownish to yellow, thick bedded, turbidite and debris flow sandstones. Complete Bouma sequences are common throughout the Jackfork with the interbedding of sandstones, siltstones and shales. Sedimentary structures within the Jackfork Group include graded bedding, parallel laminations, interference ripples, cross-laminae, and convolute bedding. Deformation markings, such as load casts, are also common throughout the Jackfork Group. Sandstones within the formation range from 3 to 9 meters thick and are often cleaner, better sorted, and coarser grained than sandstones of the Stanley Group (Morris, 1974). Additionally, one shale unit was sampled from the lowermost sections of the Lower-Middle Pennsylvanian Johns Valley Formation. Overlying the Jackfork Group, the Johns Valley Formation ranges in thickness from 125 to 400 meters thick, and is characterized by black, heavily weathered, laminated shale (Flawn et al., 1961; Morris, 1974).

U-Pb Detrital Geochronology

Prior to geochronologic analysis, traditional zircon extraction methods were performed on each of the six samples. The samples were first cleaned, dried and crushed into gravel size pieces by a jaw crusher, and then reduced into a fine powder by a disk mill. All samples were processed and separated following standard mineral separation techniques in the following order: Wilfley table, Frantz-LB-1 magnetic separator, and heavy liquids. All grains were examined in alcohol under a binocular microscope to remove non-zircon minerals. The zircons were mounted in epoxy, polished, and imaged with reflected light using an optical microscope and SEM backscattered electron detector to identify possible fractures, inclusions, or overgrowths for the purpose of locating the laser spots for LA-MC-ICPMS (laser ablation multicollector inductively coupled plasma spectrometry).

U-Pb geochronology testing was conducted at the University of Arizona LaserChron Center. For statistical confidence, approximately 100 grains from each sample underwent LA-MC-ICPMS analysis. Zircon crystals were mostly randomly selected with exceptions for a grain smaller than the laser diameter, or if it lacked a homogenous section. The analyses involved a Photon Machines Analyte G2 excimer laser with a spot diameter of 20 microns for the ablation of the selected zircon grains. The ablation process involves three phases. First, each sample consists of one 15 second integration on peaks with the laser off. The laser then fires 15 one second integrations in order to perform the U-Pb analyses. Lastly, there is a 30 second delay to purge the previous sample and prepare for the next sample to be analyzed. The result of this process allows the ablated material's respective chemical concentrations of U, Th, and Pb to be measured after it is carried in helium to a plasma source of a Nu HR ICPMS. It is important to note that measurements at the LaserChron Center are made in static mode, using Faraday detectors with $3x10^{11}$ ohm resistors for ^{238}U, ^{232}Th, ^{208}Pb,^{206}Pb, and discrete dynode ion counters for ^{204}Pb and ^{202}Hg. Ion yields are ~0.8 mv per ppm.

Age uncertainties from common Pb errors were corrected as stated in Stacey and Kramers (1975) by using the Hg-corrected ^{204}Pb with assumption of initial Pb composition. Compositional values based on variations in Pb isotopic composition in modern igneous rocks can be applied for uncertainties of 1.5 for ^{204}Pb /^{204}Pb and 0.3 for $^{207}Pb/^{204}Pb$. On average inter-element fractionation of Pb/U is ~5%, and apparent fraction of Pb isotopes is ~0.2%. Correction for this fractionation can be obtained in-run analysis of fragments from a large zircon crystal with a known age of 563.5 ± 3.2 Ma (2-sigma error). Results of this calibration produces age uncertainties ranging from 1-2% (2-sigma) for both ^{206}Pb /^{207}Pb and $^{207}Pb/^{238}U$ ages. Grains older than 800 Ma correspond to the ^{206}Pb /^{207}Pb age, whereas younger grains correspond to the $^{207}Pb/^{238}U$ age.

The University of Arizona LaserChron Center uses U and Th concentrations calibrated at ~518 ppm of U and 68 ppm Th, ^{204}Pb /^{204}Pb = 18,000 with a concordant age of 563.5 ± 3.2 Ma (2σ), derived from the

Sri Lanka standard zircons. Other standards, such as the R33, derived from a dioritic dyke of the Braintree Complex of Vermont, and FC Duluth Gabbro from Minnesota, were also used during the analysis. ID-TIMS ages of the 419.3 ± 0.4 Ma and 1099 ± 2 Ma were used for the two different standards respectively (Black et al., 2004; Schmitz et al., 2003). U-Pb Concordia diagrams and normalized age probability diagrams were constructed to show age interpretations of the LA-MC-ICPMS analysis (Ludwig, 2008). All age probability and U-Pb Concordia diagrams were generated by using Isoplot 3.0 software and Excel programs courtesy of The University Arizona LaserChron Center. The Kernel Density Estimation diagrams (KDE) that provided statistical comparison were produced using the R statistic software provenance package (Vermeesch et al., 2016).

Additional statistical comparison methods such as a Multi-Dimensional Scaling (MDS) analysis were also applied for further visual representation of the results from this study. The MDS analysis is conducted by taking a given table of pairwise dissimilarities between samples and produces a map of points on which similar samples are clustered closely together, and dissimilar samples are plotted far apart from each other. The performance of a MDS analysis act as a powerful tool to extract geological insights and further characterize provenance interpretations through quantitative statistical analysis (Vermeesch et al., 2016).

NORTH AMERICAN DETRITAL ZIRCON SOURCES

Provenance interpretations are based on the well-defined and constrained Precambrian and Phanerozoic age provinces of North America (Figure 4). Potential sources for the syn-orogenic, Carboniferous, deep-water interval of the Ouachita Mountains consist of six different geochronologic provinces. Detailed description of each province can be found here in decreasing geochronological order.

Archean Province (>2500 Ma)

Archean-age grains are sourced from basement cored uplifts from both the Superior and Wyoming-Hearne Provinces of the Canadian Shield. The Canadian Shield is composed of the earliest Laurentian continental crust, and its formation occurred throughout the Paleoproterozoic with the collision of multiple Archean microcontinents. The Superior Province formed from the suturing of smaller Archean continental fragments at 2700-2800 Ma (Whitmeyer and Karlstrom, 2007). The Wyoming-Hearne Province formed at 2500-2700 Ma, and is composed of Precambrian igneous and metamorphic rocks (Wooden and Mueller, 1988). Most of the Archean grains represent the recycling of older sedimentary rocks, however, it remains possible that some grains may have been directly derived from the Superior Province, given that most of the Wyoming-Hearne Province was buried during the Paleozoic (Mckee and Oriel, 1967; Sloss, 1988).

Paleoproterozoic Province (~1600-2500 Ma)

Detrital zircon ages ranging from 2000 to 2500 Ma are interpreted as sourced from the Huronian and Snowy Pass Supergroups along the southernmost sections of the Canadian Shield (Whitmeyer and Karlstrom, 2007). Zircon ages ranging from 1800-1950 Ma are correlated to igneous and metasedimentary rocks that form the bulk of the Penokean Province located on the southern margin of the Canadian Shield (Whitmeyer and Karlstrom, 2007). The deformed and metamorphosed Archean basement rocks of the Trans-Hudson orogenic belt that represents the suture between the Wyoming-Hearne and Superior Provinces, may be potential source for grains with an age from 1800-1950 Ma (Van Schmus et al., 1993). However, the vast majority of the Trans-Hudson Province was buried during the Paleozoic, therefore a Penokean interpretation is favored for grains with an age of 1800-1950 Ma (Soreghan and Soreghan, 2013). In addition to Laurentian, craton-derived sediments, grains with an age range from 1950-2100 Ma might represent a Gondwanan crustal influence correlated to the Trans-Amazonian orogen (1800-2250 Ma) of South America (Hartmann, 2002).

Detrital zircon populations of 1600-1800 Ma are most likely associated with the metasedimentary and metavolcanic complexes of the Yavapai-Mazatzal terrane of central and southwestern Laurentia (Karlstrom et al., 2003; Van Schmus et al., 1993). The bulk of the Yavapai-Mazatzal terrane was exposed in Precambrian basement cored uplifts of the Ancestral Rocky Mountains during the Carboniferous and Early Permian (Soreghan and Soreghan, 2013). Additional sourcing is possible from the Nemaha Ridge and the Cambridge Uplift of the Southern Midcontinent Rift System. These structures acted as topographic highs incasing exposed Precambrian basement rocks that were capable of supplying sediment to the remnant Ouachita ocean basin in the Paleozoic (Bunker and Witzke, 1988; Gao et al., 2002; Woelk and Hinze, 1995).

Midcontinent Granite-Rhyolite Province (~1360-1500 Ma)

Detrital zircon grains with ages ranging from 1360-1500 Ma are associated with the igneous assemblages of the Midcontinent Granite-Rhyolite Province. Located to the southeast of the Yavapai-Mazatzal terranes, the Midcontinent Granite-Rhyolite Province extends across the North American midcontinent from northern Mexico to northeastern Canada (Nyman et al., 1994). The igneous activity of the Midcontinent Granite-Rhyolite Province was a result of an anorogenic, high-silica, magmatism episode characterized by scattering plutons across the midcontinent (Van Schmus et al., 1993; Nyma et al., 1994). The majority of these plutons were likely uplifted during the tectonic events associated with the formation of the Ancestral Rocky Mountians (Hoffman, 1989; Van Schmus et al., 1993).

Grenville Province (~900-1350 Ma)

Grenville tectonism occurred throughout Laurentia and the Gondwanan continents over a protracted period from 900 to 1300 Ma, and culminated in multiple continent-continent collisions that resulted in the amalgamation of Rodinia (Dalziel, 1997; Moores, 1991; Whitmeyer and Karlstrom, 2007). The Grenville Province encompasses the exhumed core of the Grenville orogenic belt that formed along with the final

assembly of Rodinia (Tohver et al., 2006). Approximately 4000 Km long, the Grenville Province stretches from Newfoundland to Texas and central Mexico (Mezger et al., 1993). The Grenville orogenic cycle is subdivided into the Elzervirian orogen (1220-1350 Ma), the Shawinigan orogen (1160-1190), and the Ottawan orogen (980-1090 Ma) based on the accretionary events and tectonic history of North America (Bartholomew and Hatcher, 2010; Rivers et al., 2012). The majority of Grenville age grains are associated with the recycling of older sandstones from the Appalachian forelands. However, grains with an age of ~1100 Ma may have been directly sourced from the northern Midcontinent Rift System (Craddock et al., 2013)

Neoproterozoic Province (~500-800 Ma)

Potential sources for this age range include recycled igneous plutons associated with the Iapetan syn-rift and post-rift strata of northeastern Laurentia (Thomas et al., 2004). Grains with an age of ~515-760 Ma are potentially of Appalachian origin, sourced from the Avalon (northern Appalachians), Carolina (southern Appalachians), and Suwanee terranes (Florida subsurface) that were uplifted during the Appalachian orogenic events during the Paleozoic (Dickinson and Gehrels, 2003; Murphy et al., 2004; Nance and Thompson, 1996; Opdyke et al., 1987). Minor sourcing could be from Neoproterozoic peri-Gondwanan terranes incorporated with the final suturing of Gondwana along the southern margin of Laurentia during the formation of Pangea (Murphy et al., 2004) or from recycled igneous plutons in the Wichita Igneous Province of the Southern Midcontinent (Hanson and Eschberger, 2014).

Paleozoic Province (~320-500 Ma)

Paleozoic detrital zircons identified within this study are correlated to the syn-orogenic igneous complexes of both the Taconic (440-490 Ma) and Acadian (350-420 Ma) orogenies of the Appalachian Mountains (Aleinikoff et al., 2002; Jamieson et al., 1986; Krogh et al., 1993; Miller et al., 2000; Simonetti and Doig, 2011). These grains are mostly associated with recycled sedimentary rocks that are incorporated

into both the Taconic and Acadian clastic wedges of the southern and central Appalachian forelands (Becker et al., 2005; Eriksson et al., 2003; Park et al., 2010; Thomas, 2011; Thomas et al., 2004; Thomas et al., 2017)

RESULTS OF DETRITAL ZIRCON ANALYSIS

The LA-MC-ICPMS analyses yielded 617 detrital zircon ages ranging from the Archean (3200 Ma) to the Paleozoic (370 Ma). The most dominant populations in the six samples are Grenville age zircons (~900-1300 Ma), Paleozoic age zircons (~350-500 Ma), and Midcontinental Granite-Rhyolite (~1350-1500 Ma) grains. Minor populations overlap in age with rocks from the Yavapai-Mazatzal (~1600-1800 Ma) terrane and Superior (> ~2500 Ma) Province (Aleinikoff et al., 1995; Hoffman, 1989; Ingle-Jenkins et al., 1998; Mueller et al., 1994; Van Schmus et al., 1993).

Mississippian Stanley Group

The two Mississippian Stanley samples analyzed in this study were collected from both the middle (STP-1) and uppermost sections of the group (STT-1).

Sample STP-1

Sample STP-1 (n=104) has an age range from 381 to 2822 Ma, and its age distribution shows four age peaks at ~403, ~1030, ~1150, and ~1653 Ma, respectively. The dominant population is the Grenville Province (59%), followed by the Paleozoic Province (14%), the Midcontinental Granite-Rhyolite Province (11%), and the Yavapai-Mazatzal Terranes (11%). Additionally, there are minor age populations correlated with the Neoproterozoic Terranes (2%), the Trans-Hudson/Penokean Province (2%), and the Superior Province (1%) (Figure 5).

Sample STT-1

STT-1 (n=105) has an age range from 402 Ma to 2899 Ma, and its age distribution shows five age peaks at ~420 Ma, ~1059 Ma, ~1147 Ma, ~1354 Ma, and ~1640 Ma, respectively. Similar to that of sample STP-1, the most abundant population is the Grenville Province (62%), followed by the Midcontinental Granite-Rhyolite Province (13%), and the Yavapai-Mazatzal terranes (9%). However, sample STT-1 does show a significant decrease in the Paleozoic population (5%). Additionally, there are minor age populations from the Trans-Amazonian Province (4%), the Superior Province (4%), and the Neoproterozoic Terranes (3%). Overall, despite some minor variations, the detrital zircon age distributions between the two Mississippian Stanley samples are relatively visually similar (Figure 5).

Pennsylvanian Jackfork and Johns Valley Shale

The three Pennsylvanian Jackfork samples analyzed in this study were collected from the basal (JFB-1), the middle (JFM-1), and the uppermost sections (JFT-1) of the group. The one Johns Valley Shale (JV-2) sample that was collected and analyzed is from the lowermost portion of the formation.

Sample JFB-1

JFB-1 (n=107) has an age range from 395 Ma to 2970 Ma, and its age distribution displays four major age peaks at ~411 Ma, ~480 Ma, ~1028 Ma, and ~1078 Ma, respectively. The most dominant population is the Grenville Province (58%), followed by the Midcontinental Granite-Rhyolite Province (13%), Superior Province (8%), Paleozoic Province (8%), Yavapai-Mazatzal Terranes (7%), Trans-Hudson/Penokean Province (3%), and Neoproterozoic Terranes (2%). Additionally, there was one grain with an age of 2102 Ma (1%) correlated with the Trans-Amazonian Province. In general, the detrital zircon age populations of the lowermost section of the Pennsylvanian Jackfork Group bare a strong visual resemblance to that of the uppermost section of the Mississippian Stanley Group (Figure, 5)

Sample JFM-1

JFM-1 (n=92) has an age range from 370 Ma to 2592 Ma, and its age distribution displays four age peaks at ~419 Ma, ~482 Ma, 1048 Ma, and 1119 Ma, respectively. Similar to that of previous samples, the Grenville Province remains as the most abundant age population, but it reduces significantly from 58% to 41%. As a result, there is a significant increase of the Paleozoic population (from 8% to 25%). Similar to the other samples, the remaining grains are divided more evenly into the Midcontinent Granite-Rhyolite Province (13%), and Yavapai-Mazatzal Terranes (13%), the Trans-Hudson/Penokean Province (4%), the Neoproterozoic Terranes (2%), the Trans-Amazonian Province (1%), and the Superior Province (1%) (Figure 5).

Sample JFT-1

JFT-1 (n=106) has an age range from 385 Ma to 2862 Ma, and its age distribution shows five age peaks at ~394 Ma, ~411 Ma, ~453 Ma, ~1032 Ma, and ~1068 Ma, respectively. Similar to other samples, the most dominant population is the Grenville Province (49%). In comparison to the sample JFM-1, there are notable differences with the presence of the marked enrichment of the Yavapai-Mazatzal population (17%) and the decrease in the Paleozoic population (11%). Additional detrital zircon populations are correlated to the Midcontinental Granite-Rhyolite Province (12%), the Superior Province (6%), the Neoproterozoic Terranes (3%), and the Trans-Amazonian Province (2%) (Figure 5).

Sample JV-2

JV-2 (n=104) has an age range from 394 Ma to 3279 Ma, and its age distribution displays age peaks at ~401 Ma, ~436 Ma, ~467 Ma, ~1029 Ma, and ~1116 Ma. The most dominant population is the Grenville Province (46%). Similar to sample JFT-1, there are a strong presence of the Yavapai-Mazatzal Terranes (15%) and the Paleozoic Province (13%), but with higher contribution of the Superior population (11%) and less contribution from the Midcontinental Granite-Rhyolite Province (8%). The remaining grains

include minor contributions from the Trans-Hudson/Penokean Province (3%), the Neoproterozoic Terranes (2%), and Trans-Amazonian Province (2%) (Figure 5).

INTERPRETATION

Provenance of the Mississippian Stanley Group

The relative similarity between the two Stanley samples suggests they were most likely derived from similar sources. Overall, more than 90% of zircon grains from the two samples of the Mississippian Stanley Group are comprised of the Grenville Province (61%), the Midcontinental Granite-Rhyolite Province (11%), the Paleozoic Province (10%), and the Yavapai-Mazatzal Terranes (10%). The remaining zircon grains are associated with the Trans-Amazonian Province (3%), the Neoproterozoic Terranes (2%), the Superior Province (2%), and the Trans Hudson/Penokean Province (1%). Given the fact that the majority of potential sediment sources were relatively distant from the remnant Ouachita ocean basin along the southern margin of Laurentia, it can be inferred that the transport and the recycling of pre-existing sedimentary rocks played a significant role in supplying sediment to the Southern Midcontinent region during the Mississippian.

The dominant Grenville population (up to 62%) is most likely associated with the reworking and recycling of older Paleozoic sandstones from the eastern Appalachian orogenic belt and associated forelands. The Midcontinental Granite-Rhyolite grains comprise the second most dominant age population of the Stanley Group, and are interpreted as being recycled from both the Appalachian orogenic belt and associated forelands to east, and/or the continental interior to the north. Several local sources, including reworked older sedimentary rocks from the southern Ouachita orogenic belt, and the proximal Ozark Dome, which is part of the Midcontinental Granite-Rhyolite Province, may have also contributed to the Midcontinental Granite-Rhyolite population observed in the Mississippian Stanley Group. However, the development of the shallow Kaskaskia Sea resulted in blanketing much of the Southern Midcontinent with

a thick carbonate succession during the Late Mississippian (Lane, 1978; Sloss, 1963) suggesting that the Ozark Dome itself is an unlikely active source for the remnant Ouachita ocean basin.

The Paleozoic population (up to ~14%) within the Stanley Group is mostly sourced from syn-orogenic rocks associated with the Taconic and Acadian orogens to the east, and/or the recycling and reworking of pre-existing sedimentary strata from the northern Midcontinent region. It is worth noting that the Stanley Group records a substantial peak of a Yavapai-Mazatzal population (up to 11%). Even though some of these grains can be sourced from the recycled strata of the Appalachian forelands (up to ~4%), additional sources are needed to compensate for this enrichment. These additional sources can be correlated to direct sourcing of Precambrian basement cored uplifts stemming from both the Nemaha Ridge and Cambridge Uplift of the Midcontinent to the northwest and/or the Ancestral Rocky Mountains of western Laurentia. The small amounts of grains correlated to the Superior Province, Trans-Amazonian Province, and Neoproterozoic terranes can be potentially derived by a combination of northern continental interior sources (Hoffman, 1989; Van Schmus et al., 1996) and recycled passive margin strata from northeastern Laurentia (Thomas et al., 2004).

In summary, the dominance of the Paleozoic and Grenville populations of the Stanley Group indicates they were likely derived from the eastern Appalachian orogenic belt and associated forelands. The relative enrichment of the Yavapai-Mazatzal population suggests direct contributions from the exposed Precambrian basement cored uplifts of western Laurentia. Additional contributions of recycled detritus from the northern craton interior also remain possible.

Provenance of the Early Pennsylvanian Jackfork Group and Johns Valley Shale

Overall similarity among the Pennsylvanian strata suggests that they likely reflect similar sources. The four samples from the Pennsylvanian Jackfork Group and Johns Valley Shale are comprised of age populations from the Grenville Province (48%), the Paleozoic Province (14%), the Yavapai-Mazatzal

Terranes (13%), the Midcontinental Granite-Rhyolite Province (11%), the Superior Province (8%), the Trans/Hudson Penokean Province (3%), the Neoproterozoic Terranes (2%), and the Trans-Amazonian Province (1%). The similarity between the syn-orogenic Mississippian and Pennsylvanian strata of the Ouachita Mountains indicates sediment sources were consistent throughout the Carboniferous.

Similar to that of the Mississippian strata, the dominant Grenville population (up to 58%) of the Jackfork Group and the Johns Valley Shale, is most likely derived from the reworking of older Paleozoic sandstones from the eastern Appalachian orogenic belt and associated forelands. The Paleozoic populations (up to 25%) are most likely derived from recycled detritus from eastern Appalachian orogenic sources (Acadian and Taconic). The marked enrichments of the Yavapai-Mazatzal population (up to 17%), particularly within the uppermost sections of the Jackfork Group and the Johns Valley Shale were most likely directly sourced from Precambrian cored basement uplifts, such as both the Nemaha Ridge and Cambridge Uplift of the Midcontinent, and/or from the Ancestral Rockies to the west.

The minor populations of Midcontinent Granite-Rhyolite grains within the Early Pennsylvanian strata are associated with recycled detritus derived from multiple potential sources, including the recycling of older Paleozoic sandstones from the Appalachian forelands, the Ouachita orogenic belt, and the northern cratonic interior. As previously mentioned, the vast majority of the Midcontinental Granite-Rhyolite population were derived from recycled detritus of these more regional sources. The Ozark Dome maintained a relatively low relief throughout the Early Pennsylvanian (Xie et al., 2016), which made it a non-viable, direct sediment source for the syn-orogenic Carboniferous deep-water succession of the remnant Ouachita ocean basin. Similar to potential sources for the Stanley Group, minor contributions of Neoproterozoic and Trans-Amazonian population within the Pennsylvanian strata represent possible sources in the northern continental interior (Hoffman, 1989; Van Schmus et al., 1996), from recycled passive margin strata (Thomas et al., 2004), or from the peri-Gondwana terranes.

In summary, the Early Pennsylvanian sediment was primarily supplied by Appalachian derived sources with secondary contributions from recycled sandstones of the northern Midcontinent and southern margin of Laurentia. Furthermore, the marked enrichment of the Yavapai-Mazatzal population observed in the Pennsylvanian strata indicates that additional sources in western Laurentia also supplied sediment to the remnant Ouachita ocean basin during the Carboniferous.

DISCUSSION

Proximal Orogenic vs. Distal Recycled Sources

Previous studies have suggested that deep-water turbidities of the remnant Ouachita ocean basin were either derived from distal recycled detritus from the eastern Appalachian orogenic belt (Dickinson, et al., 1988; Gleason et al., 2002; Gleason et al., 1995; Graham et al., 1975; Graham et al., 1976; Shaulis, 2010) and the northern craton interior (Danielson et al., 1988; Sharrah, 2006), or proximal orogenic detritus from the southern Ouachita orogenic belt (Hankinson, 1986; Ingersoll et al., 1995; Johnson, 1968; Mack et al., 1983; McGuire, 2017 ; Niem, 1976; Niem, 1977; Owen, 1984; Owen and Carozzi, 1986; Shaulis et al., 2012; Thomas, 1989; Thomas, 1997). The results of this study, in combination with compiled detrital zircon age data from Lower Paleozoic Laurentian sandstones (Craddock et al., 2013; Konstantinou et al., 2014; McGuire, 2017 ; Park et al., 2010), add further constraints to the ongoing debate of sediment sourcing for the remnant Ouachita ocean basin in the Carboniferous.

Given its proximal location, the tectonically derived sediments from the southern proto-Ouachita orogen have often been viewed as the primary source for syn-orogenic Carboniferous sediment in the remnant Ouachita ocean basin (Mack et al., 1983; Thomas, 1989). However, comparison of U-Pb detrital zircon age data asserts major differences in signatures between the Lower Paleozoic sedimentary rocks of the Ouachita orogenic belt (McGuire, 2017), and the syn-orogenic Carboniferous strata of the Ouachita Mountains (Figure 6). For example, there are major differences in both their Paleozoic and Midcontinental

Granite-Rhyolite populations (Figure 6). Additionally, the marked enrichment of the Superior population (up to~40%) in the Ouachita orogenic belt matches poorly with the minimal amount of Archean age grains present in the syn-orogenic Carboniferous succession of the Ouachita Mountains (Figure 6). Although similarities in Grenville signatures are observed between the two different sets of strata (Figure 6), these similarities are naturally skewed toward the high zircon fertility and the widespread distribution of the Grenville Province (Moecher and Samson, 2006). Therefore, the tectonically recycled detritus of the southern Ouachita orogenic belt played a secondary role in supplying sediment to the remnant Ouachita ocean basin in the Carboniferous.

Further comparison of the U-Pb detrital zircon age spectra reveal strong similarities of the Paleozoic and Grenville populations between the syn-orogenic Carboniferous strata of the Ouachita Mountains and the Lower Paleozoic sandstones of both the southern and central Appalachian foreland regions (Park et al., 2010) (Figure 6). Particularly, the presence of the discrete double peaks at ~1050 Ma and ~1180 Ma within the Grenville population of the syn-orogenic Carboniferous strata are strong indicators of sediment derived from recycled Appalachian orogenic sources (Alsalem et al., 2017; Becker et al., 2005; Gehrels et al., 2011; Konstantinou et al., 2014; Park et al., 2010; Thomas, 2011; Thomas et al., 2004; Thomas et al., 2017; Xie et al., 2018; Xie et al., 2016) (Figure 6). Additionally, the overlapping of the Superior Province, the Trans-Amazonian Province, the Midcontinent Granite-Rhyolite Province, and Yavapai-Mazatzal terranes between the Carboniferous syn-orogenic deep-water clastic sediments of the Ouachita Mountains, and the Lower Paleozoic sandstones of the Appalachian foreland supports the potential for Appalachian recycled orogenic detritus acting as the primary sediment source for the remnant Ouachita ocean basin in the Carboniferous (Figure 6).

Reworking and recycling of Lower Paleozoic sandstones of the northern Midcontinent region were not major sediment contributors to the remnant Ouachita ocean basin in the Carboniferous (Figure 6). This is especially evident with the lack of a Superior population and the low abundance of Paleozoic and

Yavapai-Mazatzal grains within the Lower Paleozoic sandstones of the northern Midcontinent region, further suggesting that they did not as a major source for the remnant Ouachita ocean basin in the Carboniferous(Craddock et al., 2013; Konstantinou 2014).

The marked enrichment of the Yavapai Mazatzal population within the upper sections of the Carboniferous syn-orogenic succession (up to 17%) simply cannot be attributed to recycled detritus stemming from the Appalachian forelands. This increase in the Yavapai Mazatzal population implies direct sourcing from Precambrian basement exposures, possibly from the Nemaha Ridge of Oklahoma (Gao et al., 2002; Steeples, 1982; Woelk and Hinze, 1995) and the Cambridge Uplift (Bunker and Witzke, 1988) of the Midcontinent or the Ancestral Rockies of western Laurentia (Steeples, 1982; Woelk and Hinze, 1995). Derivation from these sources would indicate a potential sediment routing network connecting western Laurentia to the deep-marine settings of the Ouachita Basin in the Carboniferous.

In summary, the comparison of the detrital zircon age spectra suggests that the Ouachita orogenic belt was a relatively minor sediment source for the syn-orogenic Carboniferous strata of the remnant Ouachita ocean basin despite its proximal location. The interpretations from this study are more consistent with those suggesting that recycled orogenic detritus from the Appalachian foreland was the primary source of sediment entering the remnant Ouachita ocean basin in the Carboniferous (Dickinson, 1988; Gleason et al., 2002; Gleason et al., 1995; Graham et al., 1975; Graham et al., 1976; Shaulis, 2010). Direct sourcing from the Nemaha Ridge and the Cambridge Uplift of the proximal Midcontinent and the Ancestral Rockies of western Laurentia may have provided auxiliary sourcing to the Southern Midcontinent region in the Carboniferous. Additionally, it remains plausible that minor sourcing could stem from the remobilization of older, pre-existing strata of the northern Midcontinent region.

Intermixed Sediment Sources

The overall lithologic similarity between the Mississippian Stanley Group and the Pennsylvanian Jackfork Group and Johns Valley Shale indicates sediment sources for the remnant Ouachita ocean basin were consistent throughout the Carboniferous. Although the Carboniferous sedimentation primarily reflects Appalachian recycled sources, the minor variations in age populations observed within the syn-orogenic Carboniferous strata of the Ouachita Mountains suggests the remnant Ouachita ocean basin along the southern margin acted as a terminus for multiple intermixed sediment sources.

Evidence for potentially intermixed sediment sources is recorded by the temporal and spatial variations in detrital signatures observed throughout the syn-orogenic Carboniferous strata of the Ouachita Mountains. Changes in signatures are present within the Paleozoic populations from both the uppermost sections of the Stanley (14% to 5%) and the basal sections of the Jackfork (8%), which can be interpreted as weaker contributions from Appalachian sources, and a stronger influence from the northern craton interior and/or the southern Ouachita orogenic belt. These stronger influences from the north or the south are also noted by the slight increases of the Midcontinental Granite-Rhyolite signatures within the uppermost sections of the Stanley (13%), and lower-middle sections of the Jackfork (13%). Additionally, the marked enrichment of the Superior population in the Lower-Middle Pennsylvanian Johns Valley Shale (up to 11%) also favors the potential for a stronger influence from the recycling of Lower Paleozoic sandstones of northern Midcontinent region and/or the southern Ouachita orogenic belt. Furthermore, the previously mentioned enriched population of the Yavapai-Mazatzal in the syn-orogenic Carboniferous strata of the Ouachita Mountains suggests auxiliary sources from both the Midcontinent and Western Laurentia were intermixed with the primary Appalachian sources, before they entered the deep-water settings of the remnant Ouachita ocean basin.

Localized differences in sourcing are also observed within the basal sections of Stanley Group. Additional data taken from McGuire (2017) show the presence of a large peri-Gondwanan population in the lowest sections of the Stanley. The drastic increase in a Neoproterozoic influence correlates to local sourcing from the encroaching peri-Gondwanan terranes associated with the Late Paleozoic Ouachita Orogeny. However, further comparison of other Stanley detrital zircon age data (Shaulis, 2010, Shaulis et al., 2012) (Figure 7) reveals no other major Neoproterozoic contributions present throughout the deposition of the Stanley. These changes in sourcing within the basal sections of the Stanley Group reveal the possibility that significant variations in sediment sourcing may have occurred throughout the remnant Ouachita ocean basin in the Carboniferous. This interpretation is further supported by the results of the MDS analysis by positioning these Stanley and Jackfork sections closer to the Lower Paleozoic sandstones of the Ouachita orogenic belt and further away from the Appalachian sources (Figure 8).

In short, the results from this study disagree with previous interpretations that the Carboniferous sedimentation of the Ouachita Mountains was controlled solely by Appalachian sources (Dickinson, 1988; Gleason et al., 2002; Gleason et al., 1995; Graham et al., 1975; Graham et al., 1976). Instead, the results of this study suggest that the primary sediment contributions from the recycled detritus of the eastern Appalachian forelands, were intermixed with sediment derived from a ranging influence of northern interior craton, southern Ouachita orogenic belt, and western Laurentian sources, prior to entering the deep-water settings of the remnant Ouachita ocean basin.

Carboniferous Sediment Dispersal in the Southern Midcontinent

The deposition of the syn-orogenic Carboniferous deep-water succession of the Ouachita Mountains, which coincides with the timing of the Ouachita Orogeny and the Taconic and Acadian orogenic events of Appalachia, allows further constraints to be placed on the sediment transport history of the Southern Midcontinent. The results of this study have been extensively complied and compared to the

detrital zircon data of coeval Mississippian and Early Pennsylvanian sandstones of surrounding areas (Becker et al., 2005; Boothroyd, 2012; Eriksson et al., 2003; Kissock et al., 2018; McGuire, 2017 ; Park et al., 2010; Shaulis, 2010; Thomas et al., 2004; Thomas et al., 2017; Wang and Bidgoli, 2019) (Figure 9). The differences and similarities observed in U-Pb detrital-zircon populations combined with paleogeographic, paleoclimate, paleotectonic, and sedimentologic data from Laurentia and previously proposed paleodrainage models (Archer and Greb, 1995; Kissock et al., 2018; Sutherland, 1988; Xie et al., 2018; Xie et al., 2016), help reconstruct sediment dispersal pathways to the Ouachita Mountains during the Carboniferous.

Early-Middle Mississippian

Strong similarities in detrital zircon age spectra signature between the Mississippian Stanley Group and coeval strata in the southern and central Appalachian foreland support the possibility of sediment routing systems transporting detritus from the Appalachian foreland to the Ouachita Mountains in the Early-Middle Mississippian (Park et al., 2010) (Figure 9). Considering that the Southern Midcontinent was still a passive margin (Arbenz et al., 1989), and was blanketed by a shallow carbonate sea following the marine transgression (Ross and Ross, 1985; Sloss, 1963) during Early-Middle Mississippian, Appalachian derived sediments were likely transported by longshore currents and marine currents facilitated by the southeasterly trade winds (Orpin et al., 1999). These systems carried recycled detritus from the southern and central Appalachian forelands and potentially the Cincinnati Arch to the southwest along the axis of the remnant Ouachita ocean basin (Figure 10). The terminal drainage of the Amazon River into the Atlantic Ocean off the eastern coast of South America is a modern analog of this proposed system, by providing evidence for the ability of marine currents transporting large volumes of sediment thousands of kilometers parallel along the eastern South American continental shelf (Nittrouer et al., 1986).

The paleogeographic location of the remnant Ouachita ocean basin during the Early Mississippian was approximately between 15°S and the paleoequator (Coleman et al., 2000) (Figure 11) with paleoclimate conditions varying from the arid subequatorial zone to the humid equatorial zone (Parrish, 1982). The occurrence of strong tropical storms is plausible under these paleoclimate conditions, therefore, and a large amount of Appalachian detritus could have been transported to the southern margin of Laurentia. The ability of cyclonic activity supplying large volumes of sediment to parallel continental shelfs is evident in the modern with the Great Barrier Reef Shelf System offshore northeastern Australia (Larcombe and Carter, 2004). Previous studies also suggest, the encroachment of Gondwana and associated island arcs throughout the Late Paleozoic may have assisted in the directing tropical storms along the southern margin of Laurentia, thus accelerating sedimentation in the area (Chapman and Laskowski, 2019).

Late Mississippian

During the Late Mississippian, the Southern Midcontinent experienced changes in both tectonics and sea level. The increase of volcanic detritus within the upper sections of the Stanley Group indicates the advancement of the southern encroaching island arc, and the progressive closure of the Iapetus Ocean along the southern margin of Laurentia (Arbenz et al., 1989) (Figure 11). Also, major changes in climate began to occur in the Late Mississippian with the Ouachita basin drifting out of the arid subequatorial zone (between 15° and 30°S) and into the humid equatorial zone (Coleman et al., 2000) (Figure 11). Higher rates of weathering associated with changes in climate and major sea level drops caused the gradient of the Arkoma Shelf to rise.

Comparison of the U-Pb age spectra confirms the similarities of the deep-water clastic deoposist of the syn-orogenic Carboniferous strata of the Ouachita Mountains with coeval Appalachian foreland strata and their strong resemblance to the Paleozoic and Grenville signatures of the northern Michigan Basin (Boothroyd, 2012). Also, the overlapping of the Midcontinent Granite-Rhyolite and Yavapai Mazatzal

populations observed in the strata of both the Ouachita Mountains and Michigan Basin suggests the plausibility of a sediment pathway from northern Laurentia to the remnant Ouachita ocean basin in the Late Mississippian-Early Pennsylvanian (Figure 9). Kissock et al. (2018) further suggest the possibility of northerly-derived sediments from the reworking and recycling of Devonian-Early Mississippian sandstones providing detritus to the Southern Midcontinent. The high degree of similarity of the detrital zircon age signatures among the western Hugoton Embayment, the northern Michigan Basin, and the eastern Appalachian foreland (Wang and Bidgoli, 2019) (Figure 9) support the interpretation that these systems were merged and intermixed in the deltaic-marine environments of the Arkoma Shelf, prior to them entering the deep-water setting of the remnant Ouachita ocean basin. Overall, this interpretation is consistent with the compilation of paleocurrent data (Gleason et al., 1995; Morris, 1974; Niem, 1976; Sutherland, 1988) and previously proposed paleographic drainage model reconstructions (Archer and Greb, 1995; Kissock et al., 2018; Sutherland, 1988; Xie et al., 2018; Xie et al., 2016).

The potential sediment pathway from the northern Michigan Basin would have flowed south across the northern Midcontinent to the Illinois Basin. Sediment transport from the north was mostly controlled by fluvio-deltaic systems that carried sediment along the Wabash Valley fault system of the most southeastern extent of the Illinois Basin (Archer and Greb, 1995; Bristol and Howard, 1974; Droste and Keller, 1989; Nelson et al., 1990) (Figure 12). Additionally, there are strong similarities of Paleozoic, Granite-Rhyolite, and Yavapai Mazatzal signatures within the syn-orogenic Carboniferous succession of the Ouachita Mountains and coeval strata of the Southern Illinois Basin (Figure 9) (Thomas et al., In Press). These similarities in detrital zircon data support the possibility of the system flowing throughout the southeastern portion of the Illinois basin. Removal of the grains derived from the Grenville Provinces (Figure 13) highlights the Paleozoic, Granite-Rhyolite, and Yavapai-Mazatzal populations that are not typical of recycled detritus from the Appalachian foreland. The presence of these grains in the Illinois Basin further strengthens the argument for a possible northern sediment dispersal system.

The presence of paleovalleys in the southeastern section of the Illinois basin shows the subaerial erosion and increased weathering of the broad carbonate platform on the Southern Midcontinent in the Late Mississippian. Sedimentologic data from both the subsurface and outcrops in the Illinois Basin suggest a southwest oriented shelf channel and deltaic systems transporting detritus to the Arkoma Shelf on the southern margin of Laurentia (Friberg, 1969; Treworgy, 1990). Paleocurrent data and previous paleogeographic reconstructions of the Arkoma Shelf further support southwest-directed subaqueous flows and currents depositing sediment into the deep-water settings of the Ouachita basin in the Chesterian. (Morris et al. 1979 ;Coleman and Anonymous, 1990; Coleman et al., 2000)

In contrast to the proposal of large fluvial systems transporting Appalachian detritus to the Ouachita Mountains during the Early-Middle Mississippian (Gehrels et al., 2011), I suggest that a large-scale longitudinal continental drainage system from the northern Michigan basin was mixing with sediment stemming from the eastern Appalachian foreland dispersal systems and local drainage networks from the Nemaha Ridge and Cambridge Uplift to the west with possible minor contributions from the Ouachita orogenic belt to the south.

Early Pennsylvanian

The deposition of Lower Pennsylvanian Jackfork Group coincided with the major lowstand of the Absaroka sequence and the occurrence of climate change in the remnant Ouachita ocean basin in the Early Pennsylvanian (Coleman et al., 2000; Ross and Ross, 1985; Sloss, 1963). Paleogeographic reconstructions suggest the remnant Ouachita ocean basin fully transitioned from a relatively arid, subequatorial environment to wet humid equatorial environment during the earliest Pennsylvanian (Coleman and Hale-Erlich, 1994; Houseknecht and Viele, 1984; McKee and Crosby, 1975; Scotese and McKerrow, 1990; Thomas, 1989; Witzke, 1990) (Figure 11). These changes in climate resulted in increased weathering and erosion throughout Laurentia. The increase of tectonics as a result of the Late Paleozoic Ouachita orogeny

further led to the closure of the Ouachita marine basin (Figure 11). The combination of climate, sea level, and tectonic changes resulted in the rapid deposition of quartz-rich, siliciclastic sediments in the deep-water environments of the Ouachita basin (Moiola and Shanmugam, 1983).

Similar to the Mississippian Stanley Group, the Early Pennsylvanian succession of the Ouachita Mountains shares great similarities in age distributions with the coeval strata in both the south and central Appalachian forelands (Becker et al., 2005; Eriksson et al., 2003; Thomas et al., 2004; Thomas et al., 2017; Thomas et al., In Press) and Michigan basin (Boothroyd, 2012) (Figure 14). However, variations in Paleozoic and Grenville zircon populations between the Caseyville Formation of the northwestern Illinois basin (Kissock et al., 2018) and the Early Pennsylvanian strata of the Ouachita Mountains suggests they were not connected via major drainage networks (Figure 14). The sediment delivery pathway from the Appalachians most likely consisted of transcontinental drainage systems from both the south and central Appalachian forelands (Figure 15). Evidence of a drainage system exiting from the Appalachian foreland includes a series of deeply incised paleovalleys along the western extent of the foreland. The bulk of the paleovalley fills is made up of quartz pebble-rich conglomerates and coarse-grained orthoquartzites, with paleocurrent data suggesting west and southwest-directed flows (Archer and Greb, 1995). Similar to the drainage systems proposed by Gehrels et al. (2011), Kissock et al. (2018), and Wang and Bidgoli (2019) these Appalachian systems consisted of extrabasinal fluvial systems that flowed westward into the southern portion of the Illinois Basin. Similar to the Late Mississippian, upon entering the southern Illinois Basin these systems continued to be intermixed with sediment transported from the northern Michigan Basin (Figure 15).

The lowstand systems and the humid-equatorial climate conditions that coincided with Jackfork deposition facilitate multiple converging fluvial systems to the Southern Midcontinent in the Early Pennsylvanian (Figure 15). Given both the location of Illinois Basin and the southern and central Appalachian forelands were close to the equator at the start of the Pennsylvanian, the regular occurrence of

monsoonal rains was common throughout both areas (Rowley et al., 1985) (Figure 15). This resulted in elevated periods of erosion and weathering, while subsequently increasing stream carrying capacity, which led to the production of quartz-rich sediment (Coleman et al., 2000; Nelson et al., 1990). The gradual increase of the drainage gradient of the Arkoma foreland resulted in the further downwrapping of the remnant Ouachita basin in the Early Pennsylvanian (Houseknecht, 1986). This increase of slope gradient further assisted these large-scale southward trending paleo-channels (Bristol and Howard, 1971, 1974) in transporting high volumes of quartz-rich sands to the Arkoma Shelf in the Early Pennsylvanian.

The dendritic and anastomosing southwest-trending paleo-valleys in the southern Illinois Basin (Bristol and Howard, 1971, 1974; Nelson et al., 1990) acted as conduits for these large-scale climate-induced fluvial systems that delivered sediment to the deltaic-marine environments of the Arkoma Shelf. Similar to the Late Mississippian, upon entering the deltaic-marine setting of the Arkoma Shelf, these sediments from the Appalachian forelands and Michigan Basin were intermixed with sediment derived from the Nemaha Ridge, the Cambridge Uplift, the Ancestral Rockies of western Laurentia (Figure 15). The similarities between in detrital age signatures of the Early Pennsylvanian strata of the Ouachita Mountains and those of the Hugoton Embayment support the potential for the intermixing of western Laurentian sources with the drainage systems stemming from both the eastern Appalachian foreland and northern Michigan Basin (Figure 15).

Lastly, nearing the end of the Early Pennsylvanian, the remnant Ouachita ocean basin experienced a major transgressive flooding event (Ross and Ross, 1985), which led to the deposition of the Johns Valley Shale over the Jackfork Group (Figure 11). This time period also coincided with decreasing precipitation and increasing tectonic activity, evident in the form of foreland basin faulting (Coleman et al., 2000). Despite these changes, the detrital zircon age signature between the samples from the Jackfork Group and the Johns Valley are nearly similar, and were most likely derived from the same drainage network as previously mentioned in this chapter.(Figures 6, 15).

Conclusions

In this study, a total of six samples from the syn-orogenic Carboniferous deep-water succession of the Ouachita Mountains were collected and processed for U-Pb detrital zircon geochronological analysis. The main conclusions from this study include:

1. Detrital zircon signatures of the syn-orogenic Carboniferous strata of the Ouachita Mountains are characterized by a predominant Grenville population (~900-1350 Ma) with secondary populations correlated to the Paleozoic Province (~320-500 Ma), the Midcontinental Granite-Rhyolite Province (~1360-1500 Ma), and the Yavapai-Mazatzal terranes (1600-1800 Ma), and minor amounts of grains associated with the Superior Province(>2500 Ma), the Neoproterozoic terranes (~500-800 Ma), the Trans-Amazonian Province (~1950-2150 Ma), and the Trans-Hudson/Penokean Province (1800-1950 Ma).

2. Overall similarity of detrital signatures suggests the syn-orogenic Carboniferous strata of the Ouachita Mountains were most likely derived from similar sources. Results of this study further constrain the provenance of the Upper Paleozoic rocks of the Ouachita Mountains by concluding they were primarily sourced from recycled detritus of the distal Appalachian orogenic belt with limited contributions from the orogenic detritus of the proximal Ouachita orogenic belt.
3. Minor variations in signatures within the Carboniferous deep-water interval of the Ouachita Mountains suggest various intermixed sediment sources used the remnant Ouachita ocean basin as a terminal sink along the southern margin of Laurentia. This interpretation is supported by temporal changes in individual age population inferring that sediment was not only derived from primarily Appalachian sources, but through mixing various sources with variable influences from the northern Midcontinent region as well as the Ouachita orogenic belt.

4. Carboniferous sediment dispersal and delivery patterns in the remnant Ouachita ocean basin were controlled by a wide array of paleogeographic, paleoclimate, and paleotectonic factors. Early-Middle Mississippian sediment delivery to Southern Midcontinent was controlled via longshore currents from the Appalachian forelands with cyclonic activity assisting in dispersing detritus. Whereas, the sediment delivery pathway to the Southern Midcontinent in the Late Mississippian-Early Pennsylvanian was controlled by both an east-west transcontinental system from the Appalachian foreland and a north-south longitudinal system flowing from the Michigan Basin through the incised valleys of the Illinois basin. Prior to entering deep-water settings of the remnant Ouachita ocean basin, these drainage systems would be intermixed with sediment sourced from western Laurentia.

REFERENCES

Aleinikoff, J. N., Horton, J. W., Jr., Drake, A. A., Jr., and Fanning, C. M., 2002, SHRIMP and conventional U-Pb ages of Ordovician granites and tonalites in the central Appalachian Piedmont; implications for Paleozoic tectonic events: American Journal of Science, v. 302, no. 1, p. 50-75.

Aleinikoff, J. N., Zartman, R. E., Walter, M., Rankin, D. W., Lyttle, P. T., and Burton, W. C., 1995, U-Pb ages of metarhyolites of the Catoctin and Mount Rogers formations, Central and Southern Appalachians; evidence for two pulses of Iapetan rifting: American Journal of Science, v. 295, no. 4, p. 428-454.

Alsalem, O. B., Fan, M., Zamora, J., Xie, X., and Griffin, W. R., 2017, Paleozoic sediment dispersal before and during the collision between Laurentia and Gondwana in the Fort Worth Basin, USA: Geosphere, v. 14, no. 1, p. 325-342.

Arbenz, J. K., Bally, A. W., and Palmer, A. R., 1989, The Ouachita system, The Geology of North America—An Overview, Volume A, Geological Society of America, The Geology of North America, p. 371-396.

-, 2008, Structural framework of the Ouachita Mountains, in Suneson, N., Arbenz, J. K., and Misch, P., eds., Stratigraphic and structural evolution of the Ouachita Mountains and Arkoma Basin, southeastern Oklahoma and west-central Arkansas: applications to petroleum exploration: Oklahoma Geological Survey Circular A, Volume 112: Norman, Oklahoma Geological Survey, p. 1-40.

Archer, A. W., and Greb, S. F., 1995, An Amazon-scale drainage system in the Early Pennsylvanian of central North America: Journal of Geology, v. 103, no. 6, p. 611-627.

Bartholomew, M. J., and Hatcher, R. D., 2010, The Grenville orogenic cycle of southern Laurentia: Unraveling sutures, rifts, and shear zones as potential piercing points for Amazonia: Journal of South American Earth Sciences, v. 29, no. 1, p. 4-20.

Becker, T. P., Thomas, W. A., Samson, S. D., and Gehrels, G. E., 2005, Detrital zircon evidence of Laurentian crustal dominance in the lower Pennsylvanian deposits of the Alleghanian clastic wedge in eastern North America: Sedimentary Geology, v. 182, no. 1, p. 59-86.

Black, L. P., Kamo, S. L., Allen, C. M., Davis, D. W., Aleinikoff, J. N., Valley, J. W., Mundil, R., Campbell, I. H., Korsch, R. J., Williams, I. S., and Foudoulis, C., 2004, Improved 206Pb/238U microprobe geochronology by the monitoring of a trace-element-related matrix effect; SHRIMP, ID-TIMS, ELA-ICP-MS and oxygen isotope documentation for a series of zircon standards: Chemical Geology, v. 205, no. 1-2, p. 115-140.

Blakey, R.C., 2013, Key Time Slices of North America 2013 Colorado Plateau Geosystems Inc.

Boothroyd, J., 2012, Carboniferous Provenance Trends from Clastic Strata of the Michigan Basin [unpublished MS thesis]: Michigan State University, East Lansing, 197 p.

Bristol, H. M., and Howard, R. H., 1971, Paleogeologic map of the sub-Pennsylvanian Chesterian (upper Mississippian) surface in the Illinois Basin: Circular - Illinois State Geological Survey, v. 458, p. 14.

-, 1974, Sub-Pennsylvanian valleys in the Chesterian surface of the Illinois Basin and related Chesterian slump blocks: Special Paper - Geological Society of America, no. 148, p. 315-335.

Bunker, B. J., and Witzke, B. J., 1988, Central Mid-continent region; United States, in Sloss, L. L ed., Sedimentary Cover-North American Craton; U.S: Boulder, CO., Geological Society of Ameirca, The Geology of North American, v. D-2.

Chapman, A. D., and Laskowski, A. K., 2019, Detrital zircon U-Pb data reveal a Mississippian sediment dispersal network originating in the Appalachian Orogen, traversing North America along its southern shelf, and reaching as far as the Southwest United States: Lithosphere, v. 11, no. 4, p. 581-587.

Cline, L. M., 1960, Stratigraphy of the late Paleozoic rocks of the Ouachita Mountains, Oklahoma: Bulletin Oklahoma Geological Survey, no. 85, 113 p.

Cline, L. M., Arbenz, K., Berry, R. M., Bowsher, A. L., and Johnson, N. L., 1968, Comparison of main geologic features of Arkoma Basin and Quachita Mountains, southeastern Oklahoma, Oklahoma City Geological Society, Oklahoma City, OK., p. 63-74.

Coleman, J. L., Jr., and Anonymous, 1990, Comparison of depositional elements of an ancient and a "modern" submarine fan complex; Early Pennsylvanian Jackfork and late Pleistocene Mississippi fans: AAPG Bulletin, v. 74, no. 5, p. 631.

-, 1993, Controls on variability of depositional style in Carboniferous submarine fan complexes of the Ouachita Basin of Oklahoma and Arkansas: Annual Meeting Expanded Abstracts - American Association of Petroleum Geologists, v. 1993, p. 86-87.

Coleman, J. L., Jr., Bouma, A. H., and Stone, C. G., 2000, Carboniferous Submarine Basin Development of the Ouachita Mountains of Arkansas and Oklahoma, Fine-Grained Turbidite Systems, Volume 72, American Association of Petroleum Geologists, p. 21-32.

Coleman, J. L., Jr., and Hale-Erlich, W. S., 1994, Annotated bibliography of selected references for the Ouachita-Appalachian structural belt, as pertains to the Black Warrior Basin of Mississippi: Mississippi Geology, v. 15, no. 2, 35 p.

Craddock, J. P., Konstantinou, A., Vervoort, J. D., Wirth, K. R., Davidson, C., Finley-Blasi, L., Juda, N. A., and Walker, E., 2013, Detrital Zircon Provenance of the Mesoproterozoic Midcontinent Rift, Lake Superior Region, U.S.A: The Journal of Geology, v. 121, no. 1, p.57-73.

Dalziel, I. W. D., 1997, Neoproterozoic-Paleozoic geography and tectonics; review, hypothesis, environmental speculation: Geological Society of America Bulletin, v. 109, no. 1, p. 16-42.

Danielson, S. E., Hankinson, P. K., Kitchings, K. D., and Thomson, A., 1988, Provenance of the Jackfork Sandstone, Ouachita Mountains, Arkansas and eastern Oklahoma: Miscellaneous Publication - Arkansas Geological Commission, 95 p.

Dickinson W.R., 1988, Provenance and Sediment Dispersal in Relation to Paleotectonics and Paleogeography of Sedimentary Basins. In: Kleinspehn K.L., Paola C. (eds) New Perspectives in Basin Analysis. Frontiers in Sedimentary Geology. Springer, New York, NY

Dickinson, W. R., and Gehrels, G. E., 2003, U–Pb ages of detrital zircons from Permian and Jurassic eolian sandstones of the Colorado Plateau, USA: paleogeographic implications: Sedimentary Geology, v. 163, no. 1, p. 29-66.

Droste, J. B., and Keller, S. J., 1989, Development of the Mississippian-Pennsylvanian unconformity in Indiana, State of Indiana, Dept. of Natural Resources, Geological Survey, Occasional Paper 55, 11 p.

Eriksson, K. A., Campbell, I. H., Palin, J. M., and Allen, C. M., 2003, Predominance of Grenvillian magmatism recorded in detrital zircons from modern Appalachian rivers: Journal of Geology, v. 111, no. 6, p. 707-717.

Flawn, P. T., Goldstein, A., Jr., King, P. B., and Weaver, C. E., 1961, The Ouachita System: Publication - University of Texas, Bureau of Economic Geology, p. 401-401, 406 sheets.

Friberg J. F, S., Siemers C.T , Straw W. T, Potter P.E, and Hrabar S. V, 1969, Bethel Sandstone (Mississippian) of western Kentucky and south-central Indiana, a submarine-channel fill: Report of Investigations - Kentucky Geological Survey, 24 p.

Gao, S. S., Liu, K. H., Cao, A., Chen, C., Hubbard, M. S., Zachary, J. A., Zhang, Y., and Anonymous, 2002, Old rifts never die; crustal thickening across the Midcontinent Rift and its possible role in post-rifting tectonics: Abstracts with Programs - Geological Society of America, v. 34, no. 6, p. 79.

Gehrels, G. E., Blakey, R., Karlstrom, K. E., Timmons, J. M., Dickinson, B., and Pecha, M., 2011, Detrital zircon U-Pb geochronology of Paleozoic strata in the Grand Canyon, Arizona: Lithosphere, v. 3, no. 3, p. 183-200.

Gleason, J. D., Finney, S. C., and Gehrels, G. E., 2002, Paleotectonic implications of a Mid- to Late-Ordovician provenance shift, as recorded in sedimentary strata of the Ouachita and southern Appalachian mountains: Journal of Geology, v. 110, no. 3, p. 291-304.

Gleason, J. D., Patchett, P. J., Dickinson, W. R., and Ruiz, J., 1995, Nd isotopic constraints on sediment sources of the Ouachita-Marathon fold belt: Geological Society of America Bulletin, v. 107, no. 10, p. 1192-1210.

Goldstein, A., Jr., and Hendricks, T. A., 1962, Late Mississippian and Pennsylvanian sediments of Ouachita facies, Oklahoma, Texas, and Arkansas: Pennsylvanian system in United States--A Symposium, p. 385-430.

Graham, S., Dickinson, W., and Ingersoll, R., 1975, Himalayan-Bengal Model for Flysch Dispersal in the Appalachian-Ouachita System: Geological Society of America Bulletin, v. 86, no. 3, p. 273-286.

Graham, S. A., Ingersoll, R. V., and Dickinson, W. R., 1976, Common provenance for lithic grains in Carboniferous sandstones from Ouachita Mountains and Black Warrior Basin: Journal of Sedimentary Petrology, v. 46, no. 3, p. 620-632.

Hankinson, P. K., 1986, Provenance of the upper Jackfork Sandstone of Arkansas and Oklahoma [unpublished MS thesis]: University of New Orleans, 125 p.

Hanson, R. E., and Eschberger, A. M., 2014, An overview of the Carlton Rhyolite Group; Cambrian A-type felsic volcanism in the Southern Oklahoma Aulacogen: Guidebook - Oklahoma Geological Survey, v. 38, p. 123-141.

Haq, B. U., and Schutter, S. R., 2008, A chronology of Paleozoic sea-level changes: Science, v. 322, no. 5898, p. 64-68.

Hartmann, L. A., 2002, The Mesoproterozoic Supercontinent Atlantica in the Brazilian Shield - Review of Geological and U-Pb Zircon and Sm-Nd Isotopic Evidence: Gondwana Research, v. 5, no. 1, p. 157-163.

Hoffman, P. F., 1989, Precambrian geology and tectonic history of North America, Geological Socitey of America, Booulder, CO., The Geology of North America; an overview, v. A, p. 447-512.

Houseknecht, D. W., 1986, Evolution from passive margin to foreland basin; the Atoka Formation of the Arkoma Basin, south-central U.S.A: Special Publication of the International Association of Sedimentologists, v. 8, p. 327-345.

Houseknecht, D. W., and Viele, G. W., 1984, Tectonic and sedimentary history of the Ouachita Foreland: Abstracts with Programs - Geological Society of America, v. 16, no. 3, p. 147.

Ingersoll, R. V., Graham, S. A., and Dickinson, W. R., 1995, Remnant ocean basin, in Busby C,J. Ingersoll R.V eds., Tectonics of Sedimentary Basins: Cambridge Massachutess, Blackwell Science, p. 363-392, Blackwell Science, Oxford.

Ingle-Jenkins, S., Mueller, P., Heatherington, A. L., Offield, T. W., and Anonymous, 1998, Age and origin of the Uwharrie Formation and Albemarle Group, Carolina slate belt; implications from U-Pb and Sm-Nd systematics: Abstracts with Programs - Geological Society of America, v. 30, no. 7, p. 239.

Jamieson, R. A., van Breemen, O., Sullivan, R. W., and Currie, K. L., 1986, The age of igneous and metamorphic events in the western Cape Breton Highlands, Nova Scotia: Canadian Journal of Earth Sciences = Revue Canadienne des Sciences de la Terre, v. 23, no. 12, p. 1891-1901.

Johnson, K. E., 1968, Sedimentary environment of Stanley Group of theOuachita Mountains of Oklahoma: Journal of Sedimentary Petrology, v. 38, no. 3, p. 723-733.

Karlstrom, K. E., Ilg, B., Williams, M., Hawkins, D., Bowring, S., Seaman, S., Beus, S., and Morales, M., 2003, Paleoproterozoic rocks of the Granite Gorges: Grand Canyon Geology, p. 9-38.

Kissock, J. K., Finzel, E. S., Malone, D. H., and Craddock, J. P., 2018, Lower-Middle Pennsylvanian strata in the North American midcontinent record the interplay between erosional unroofing of the Appalachians and eustatic sea-level rise: Geosphere (Boulder, CO), v. 14, no. 1, p. 141-161.

Konstantinou, A., Wirth, K. R., Vervoort, J. D., Malone, D. H., Davidson, C., and Craddock, J. P., 2014, Provenance of Quartz Arenites of the Early Paleozoic Midcontinent Region, USA: The Journal of Geology, v. 122, no. 2, p. 201-216.

Krogh, T. E., Kamo, S. L., Sharpton, V. L., Marin, L. E., and Hildebrand, A. R., 1993, U-Pb ages of single shocked zircons linking distal K/T ejecta to the Chicxulub crater: Nature (London), v. 366, no. 6457, p. 731-734.

Lane, H. R., 1978, The Burlington Shelf (Mississippian, North-central United States): Geologica et Palaeontologica, no. 12, p. 165-176.

Larcombe, P., and Carter, R. M., 2004, Cyclone pumping, sediment partitioning and the development of the Great Barrier Reef shelf system; a review: Quaternary Science Reviews, v. 23, no. 1-2, p. 107-135.

Link, M. H., Roberts, M. T., Stone, C. G., and Haley, B. R., 1986, Pennsylvanian paleogeography for the Ozarks, Arkoma, and Ouachita basins in east-central Arkansas: Guidebook - Arkansas Geological Commission, v. 86-3, p. 37-60.

Lowe, D. R., 1985, Ouachita Trough; part of a Cambrian failed rift system: Geology (Boulder), v. 13, no. 11, p. 790-793.

-, 1989, Stratigraphy, sedimentology, and depositional setting of pre-orogenic rocks of the Ouachita Mountains, Arkansas and Oklahoma,Geological Society of America, Boulder, CO., v. F-2, p. 575-590.

Ludwig, K., 2008, Isoplot 3.7.A Geochronological Toolkit for Microsoft Excel: Berkeley, California, USA, Berkeley Geochronology Center Special Publication, no.4, 77 p.

Mack, G. H., Thomas, W. A., and Horsey, C. A., 1983, Composition of Carboniferous sandstones and tectonic framework of southern Appalachian-Ouachita orogen: Journal of Sedimentary Petrology, v. 53, no. 3, p. 931-946.

McGuire, P. R., 2017 U-Pb Detrital Zircon Signature of the Ouachita Orogenic Belt [unpublished MS thesis]: Texas Christian University, 87 p.

McKee, E. D., and Crosby, E. J., 1975, Paleotectonic investigations of the Pennsylvanian System in the United States: U. S. Geological Survey Professional Paper, 349 p.

Mckee, E.D., and Oriel, S.S., 1967, Paleotectonic Maps of the Permain System: U.S. Geological Survey. Miscellaneous Geologic Investigations, Map I-450 164 p.

Mezger, K., Essene, E. J., van der Pluijm, B. A., and Halliday, A. N., 1993, U-Pb geochronology of the Grenville Orogen of Ontario and New York: constraints on ancient crustal tectonics: Contributions to Mineralogy and Petrology, v. 114, no. 1, p. 13-26.

Miller, C. F., Hatcher, R. D., Jr., Ayers, J. C., Coath, C. D., and Harrison, T. M., 2000, Age and zircon inheritance of eastern Blue Ridge plutons, southwestern North Carolina and northeastern Georgia, with implications for magma history and evolution of the Southern Appalachian Orogen: American Journal of Science, v. 300, no. 2, p. 142-172.

Moecher, D. P., and Samson, S. D., 2006, Differential zircon fertility of source terranes and natural bias in the detrital zircon record: Implications for sedimentary provenance analysis: Earth and Planetary Science Letters, v. 247, no. 3, p. 252-266.

Moiola, R. J., and Shanmugam, G., 1983, Submarine fan sedimentation, Ouachita Mountains, Arkansas and Oklahoma:Transactions-Gulf Coast Association of Geological Societies, v. 34 , p. 175-182.

Moores, E. M., 1991, Southwest U.S.-East Antarctic (SWEAT) connection: A hypothesis: Geology, v. 19, no. 5, p. 425-428.

Morris, R. C., 1971, Stratigraphy and sedimentology of Jackfork group, Arkansas: The American Association of Petroleum Geologists Bulletin, v. 55, no. 3, p. 387-402.

-, 1973, Sedimentary and tectonic history of Ouachita Mountains: Society of Economic Paleontologists and Mineralogists , v. 22 , p. 241-280.

Morris, R. C., 1974, Carboniferous rocks of the Ouachita Mountains, Arkansas; a study of facies patterns along the unstable slope and axis of a flysch trough: Special Paper - Geological Society of America, no. 148, p. 241-279.

Morris, R. C., 1989, Stratigraphy and sedimentary history of post-Arkansas Novaculite Carboniferous rocks of the Ouachita Mountains,Geological Society of America: The Appalachian-Ouachita Orogen in the United States, Boulder, CO., p. 591-602.

Morris, R. C., Proctor, K. E., and Koch, M. R., 1977, Petrology and diagenesis of deep-water sandstones, Ouachita Mountains, Arkansas and Oklahoma: (abstract) *in* American Association of Petroleum Geologists, Rocky Mountain sections meeting, v. 61, iss. 8, p. 1384.

-, 1979, Petrology and diagenesis of deep-water sandstones, Ouachita Mountains, Arkansas and Oklahoma: Special Publication - Society of Economic Paleontologists and Mineralogists, no. 26, p. 263-279.

Mueller, P. A., Heatherington, A. L., Wooden, J. L., Shuster, R. D., Nutman, A. P., and Williams, I. S., 1994, Precambrian zircons from the Florida basement; a Gondwanan connection: Geology (Boulder), v. 22, no. 2, p. 119-122.

Murphy, J. B., Pisarevsky, S. A., Nance, R. D., and Keppie, J. D., 2004, Neoproterozoic—Early Paleozoic evolution of peri-Gondwanan terranes: implications for Laurentia-Gondwana connections: International Journal of Earth Sciences, v. 93, no. 5, p. 659-682.

Nance, R. D., and Thompson, M. D., 1996, Avalonian and related peri-Gondwanan terranes of the circum-North Atlantic: An introduction: Geological Society of America Special Papers, v. 304, p. 1-7.

Nelson, W. J., Trask, C. B., Jacobson, R. J., Damberger, H. H., Williamson, A. D., Williams, D. A., Leighton, M. W., Kolata, D. R., Oltz, D. F., and Eidel, J. J., 1990, Absaroka Sequence: Pennsylvanian and Permian Systems, Interior Cratonic Basins, Volume 51, American Association of Petroleum Geologists, p.143-164.

Niem, A. R., 1976, Patterns of flysch deposition and deep-sea fans in the lower Stanley Group (Mississippian), Ouachita Mountains, Oklahoma and Arkansas: Journal of Sedimentary Petrology, v. 46, no. 3, p. 633-646.

Niem, A. R., 1977, Mississippian pyroclastic flow and ash-fall deposits in the deep-marine Ouachita flysch basin, Oklahoma and Arkansas: Geological Society of America Bulletin, v. 88, no. 1, p. 49-61.

Nittrouer, C. A., Curtin, T. B., and DeMaster, D. J., 1986, Concentration and flux of suspended sediment on the Amazon continental shelf: Continental Shelf Research, v. 6, no. 1, p. 151-174.

Nyman, M. W., Karlstrom, K. E., Kirby, E., and Graubard, C. M., 1994, Mesoproterozoic contractional orogeny in western North America; evidence from ca. 1.4 Ga plutons: Geology (Boulder), v. 22, no. 10, p. 901-904.

Opdyke, N. D., Jones, D. S., MacFadden, B. J., Smith, D. L., Mueller, P. A., and Shuster, R. D., 1987, Florida as an exotic terrane: Paleomagnetic and geochronologic investigation of lower Paleozoic rocks from the subsurface of Florida: Geology, v. 15, no. 10, p. 900-903.

Orpin, A., Ridd, P., and Stewart, L., 1999, Assessment of the relative importance of major sediment ‐ transport mechanisms in the central Great Barrier Reef lagoon: Australian Journal of Earth Sciences, v. 46, no. 6, p. 883-896.

Owen, M. R., 1984, Sedimentary petrology and provenance of the upper Jackfork Sandstone (Morrowan), Quachita Mountains, Arkansas, U.S.A [unpublished Disseration]: University of Illinois, Urbana-Champaign, 167 p.

Owen, M. R., and Carozzi, A. V., 1986, Southern provenance of upper Jackfork Sandstone, southern Ouachita Mountains; cathodoluminescence petrology: Geological Society of America Bulletin, v. 97, no. 1, p. 110-115.

Park, H., Barbeau, D. L., Jr., Rickenbaker, A., Bachmann-Krug, D., and Gehrels, G. E., 2010, Application of foreland basin detrital-zircon geochronology to the reconstruction of the Southern and Central Appalachian Orogen: Journal of Geology, v. 118, no. 1, p. 23-44.

Parrish, J., 1982, Upwelling and Petroleum Source Beds, with Reference to Paleozoic: ERRATUM: Aapg Bulletin - American Association of Petreloum Geologist, v. 66. no. 6, p. 750-774.

Pauli, D. A., and Anonymous, 1999, Submarine channel sandstones in the Jackfork Group; SE Oklahoma: Annual Meeting Expanded Abstracts - American Association of Petroleum Geologists, v. 1999, p. A105.

Rivers, T., Culshaw, N., Hynes, A., Indares, A., Jamieson, R., and Martignole, J., 2012, The Grenville Orogen - A post-lithoprobe perspective: Tectonic Styles in Canada: The lithoprobe perspective, v. 49, p. 97-236.

Ross, C. A., and Ross, J. R. P., 1985, Late Paleozoic depositional sequences are synchronous and worldwide: Geology, v. 13, no. 3, p. 194-197.

Rowley, D. B., Raymond, A., Parrish, J. T., Lottes, A. L., Scotese, C. R., and Ziegler, A. M., 1985, Carboniferous paleogeographic, phytogeographic, and paleoclimatic reconstructions: International Journal of Coal Geology, v. 5, no. 1-2, p. 7-42.

Schmitz, M. D., Bowring, S. A., and Ireland, T. R., 2003, Evaluation of Duluth Complex anorthositic series (AS3) zircon as a U-Pb geochronological standard; new high-precision isotope dilution thermal ionization mass spectrometry results: Geochimica et Cosmochimica Acta, v. 67, no. 19, p. 3665-3672.

Scotese, C. R., and McKerrow, W. S., 1990, Revised world maps and introduction: Memoirs of the Geological Society of London, v. 12, p. 1-21.

Sharrah, K. L., 2006, Comparative study of the sedimentology and provenance of the Atoka Formation in the Frontal Ouachita Thrust Belt, Oklahoma [unpublished Disseration]: The University of Tulsa, 252 p.

Shaulis, B., Lapen, T., Casey, J., and Reid, D., 2012, Timing and Rates of Flysch Sedimentation In the Stanley Group, Ouachita Mountains, Oklahoma and Arkansas, USA: Constraints from U-Pb Zircon Ages of Subaqueous Ash-Flow Tuffs: Journal of Sedimentary Research, v. 82, p. 833-840.

Shaulis, B. J., 2010, The Provenance of Detrital Zircons from the Ouachita Mountains of the Oklahoma and Arkansas, USA [unpublished MS thesis]: University of Houston,162 p.

Sholes, M., McBride, E. F., Briggs, G., and Moiola, R. J., 1975, A Guidebook to the Sedimentology of Paleozic Flysch and Associated Deposists, Ouachita Mountains-Arkoma Basin, Oklahoma, Dallas Geological Society Dallas, TX., p 69-87.

Simonetti, A., and Doig, R., 2011, U–Pb and Rb–Sr geochronology of Acadian plutonism in the Dunnage zone of the southeastern Quebec Appalachians: Canadian Journal of Earth Sciences, v. 27, p. 881-892.

Sloss, L. L., 1963, Sequences in the Cratonic Interior of North America: Geological Society of America Bulletin, v. 74, no. 2, p. 93-114.

Soreghan, G. S., and Soreghan, M. J., 2013, Tracing clastic delivery to the Permian Delaware Basin, U.S.A.; implications for paleogeography and circulation in westernmost equatorial Pangea: Journal of Sedimentary Research, v. 83, no. 9, p. 786-802.

Stacey, J. S., and Kramers, J. D., 1975, Approximation of terrestrial lead isotope evolution by a twostage model: Earth and Planetary Science Letters, v. 26, no. 2, p. 207-221.

Steeples, D. W., 1982, Structure of the Salina-Forest City interbasin boundary from seismic studies:University of Missouri Rolla Journal, v. 3, p. 55-81.

Stone, C. G., LeBlanc, R. J., Sr., Haley, B. R., and McFarland, J. D., III, 1979, Stop descriptions; third day: Guidebook - Oklahoma Geological Survey, no. 19, p. 39-53.

Sutherland, P. K., 1988, Late Mississippian and Pennsylvanian depositional history in the Arkoma Basin area, Oklahoma and Arkansas: Geological Society of America Bulletin, v. 100, no. 11, p. 1787-1802.

Thomas, W. A., 1976, Evolution of Ouachita-Appalachian continental margin: Journal of Geology, v. 84, no. 3, p. 323-342.

Thomas, W. A., 1985, The Appalachian-Ouachita connection; Paleozoic orogenic belt at the southern margin of North America: Annual Review of Earth and Planetary Sciences, v. 13, p. 175-199.

-, 1989, The Appalachian-Ouachita Orogen beneath the Gulf Coastal Plain between the outcrops in the Appalachian and Ouachita Mountains, Geological Society of America, Boulder, CO., p 537-553.

Thomas, W. A., 1997, Nd isotopic constraints on sediment sources of the Ouachita-Marathon fold belt: Alternative Interpretation and Reply: Geological Society of America Bulletin, v. 109, no. 6, p. 779-787.

Thomas, W. A., 2006, Tectonic inheritance at a continental margin: GSA Today, v. 16, no. 2, p. 4-11.

-, 2010, Interactions between the southern Appalachian–Ouachita orogenic belt and basement faults in the orogenic footwall and foreland, v. 206, p. 897-916.

-, 2011, Detrital-zircon geochronology and sedimentary provenance: Lithosphere, v. 3, no. 4, p. 304-308.

Thomas, W. A., Becker, T. P., Samson, S. D., and Hamilton, M. A., 2004, Detrital zircon evidence of a recycled orogenic foreland provenance for Alleghanian clastic-wedge sandstones: Journal of Geology, v. 112, no. 1, p. 23-37.

Thomas, W. A., Gehrels, G. E., Greb, S. F., Nadon, G. C., Satkoski, A. M., and Romero, M. C., 2017, Detrital zircons and sediment dispersal in the Appalachian foreland: Geosphere, v. 13, no. 6, p. 2206-2230.

Thomas, W. A., George, G. E, Sundell, K. E, Finzel, E.S, Clark, R. J, Malone, D.H, Hampton, B. A, and Romero, M. C., , In Press Detrital Zircons and Sediment Dispersal in the Eastern Midcontient of North America Geosphere.

Tohver, E., Teixeira, W., van der Pluijm, B., Geraldes, M. C., Bettencourt, J. S., and Rizzotto, G., 2006, Restored transect across the exhumed Grenville orogen of Laurentia and Amazonia, with implications for crustal architecture: Geology, v. 34, no. 8, p. 669-672.

Treworgy, J. D., 1990, Kaskaskia Sequence; Mississippian Valmeyeran and Chesterian Series: AAPG Memoir, v. 51, p. 125-142.

Van Schmus, W. R., Bickford, M. E., Condie, K. C., and Anonymous, 1993, Early Proterozoic transcontinental orogenic belts in the United States: Abstracts with Programs - Geological Society of America, v. 25, no. 1, p. 44.

Van Schmus, W. R., Bickford, M. E., and Turek, A., 1996, Proterozoic geology of the east-central Midcontinent basement: Special Paper - Geological Society of America, v. 308, p. 7-32.

Vermeesch, P., Resentini, A., and Garzanti, E., 2016, An R package for statistical provenance analysis: Sedimentary Geology, v. 336, p. 14-25.

Viele, G., and Thomas, W., 1989, Tectonic synthesis of the Ouachita orogenic belt, in Htcher, R. D., Thomas, W. A., and Viele, G. W., eds., The Appalachian-Ouachita orogen in the United States, Volume 2-F: Boulder, Colorado, Geological Society of America, p. 695-728.

Wang, W., and Bidgoli, T. S., 2019, Detrital Zircon Geochronologic Constraints on Patterns and Drivers of Continental-Scale Sediment Dispersal in the Late Mississippian: Geochemistry, Geophysics, Geosystems, v. 20, no. 11, p. 5522-5543.

Whitmeyer, S. J., and Karlstrom, K. E., 2007, Tectonic model for the Proterozoic growth of North America: Geosphere (Boulder, CO), v. 3, no. 4, p. 220-259.

Witzke, B. J., 1990, Palaeoclimatic constraints for Palaeozoic palaeolatitudes of Laurentia and Euramerica: Memoirs of the Geological Society of London, v. 12, p. 57-73.

Woelk, T. S., and Hinze, W. J., 1995, Midcontinent rift system in northeastern Kansas: Bulletin - Kansas Geological Survey, no. 237, p. 22-27.

Wooden, J. L., and Mueller, P. A., 1988, Pb, Sr, and Nd isotopic compositions of a suite of late Archean, igneous rocks, eastern Beartooth Mountains; implications for crust-mantle evolution: Earth and Planetary Science Letters, v. 87, no. 1-2, p. 59-72.

Xie, X., Buratowski, G., Manger, W. L., and Zachry, D., 2018, U-Pb detrital-zircon geochronology of the middle Bloyd Sandstone (Morrowan) of Northern Arkansas (U.S.A.); implications for early Pennsylvanian sediment dispersal in the Laurentian foreland: Journal of Sedimentary Research, v. 88, no. 7, p. 795-810.

Xie, X., Cains, W., and Manger, W. L., 2016, U/Pb detrital zircon evidence of transcontinental sediment dispersal; provenance of Late Mississippian Wedington sandstone member, NW Arkansas: International Geology Review, v. 58, no. 15-16, p. 1951-1966.

Zou, F., Slatt, R. M., Zhang, J., and Huang, T., 2017, An integrated chemo-and sequence-stratigraphic framework of the Early Pennsylvanian deepwater outcrops near Kirby, Arkansas, USA, and its implications on remnant basin tectonics: Marine and Petroleum Geology, v. 81, p. 252-277.

Figures

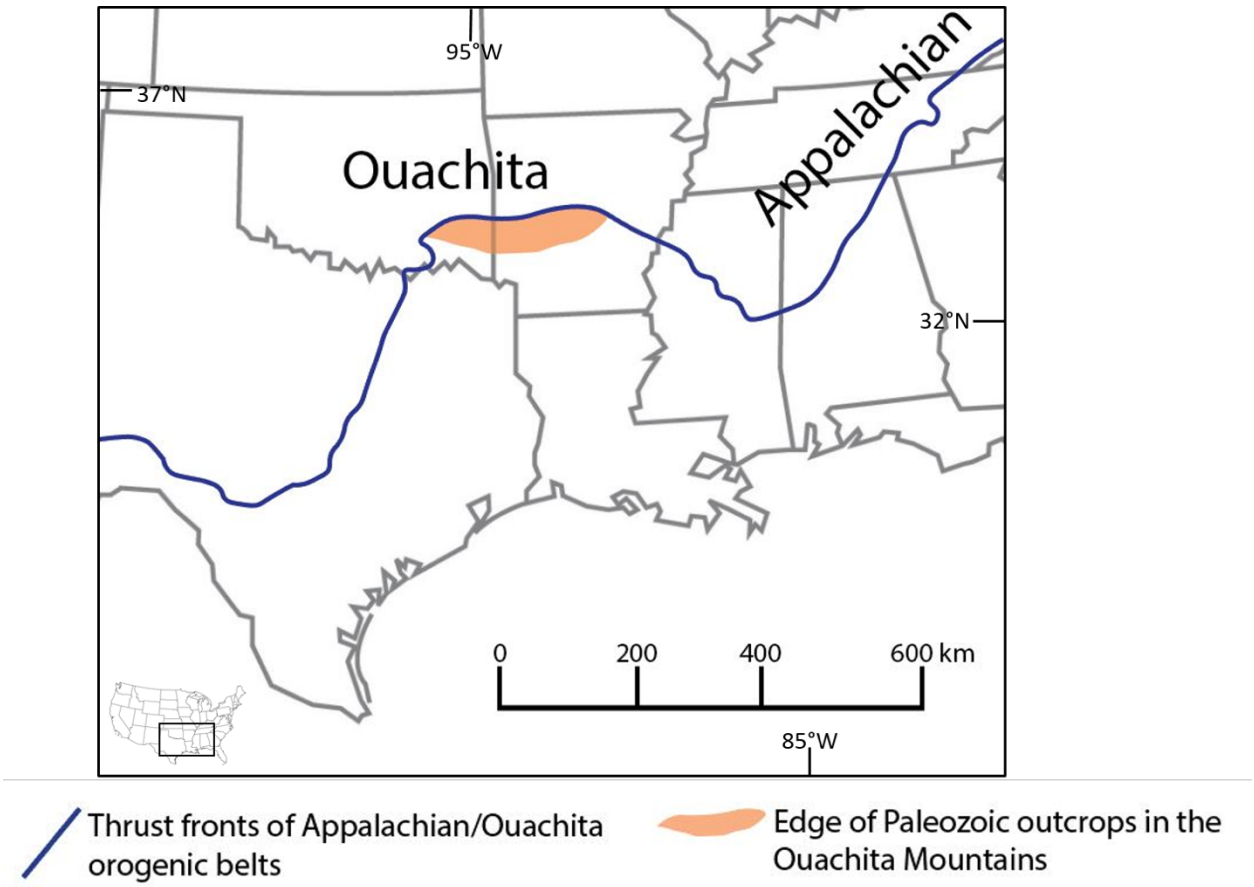

Figure 1: Map of the Ouachita and Appalachian frontal thrust belts showing the general location of the Ouachita Mountains and study area outlined by the black box (Modified from Thomas, 2010).

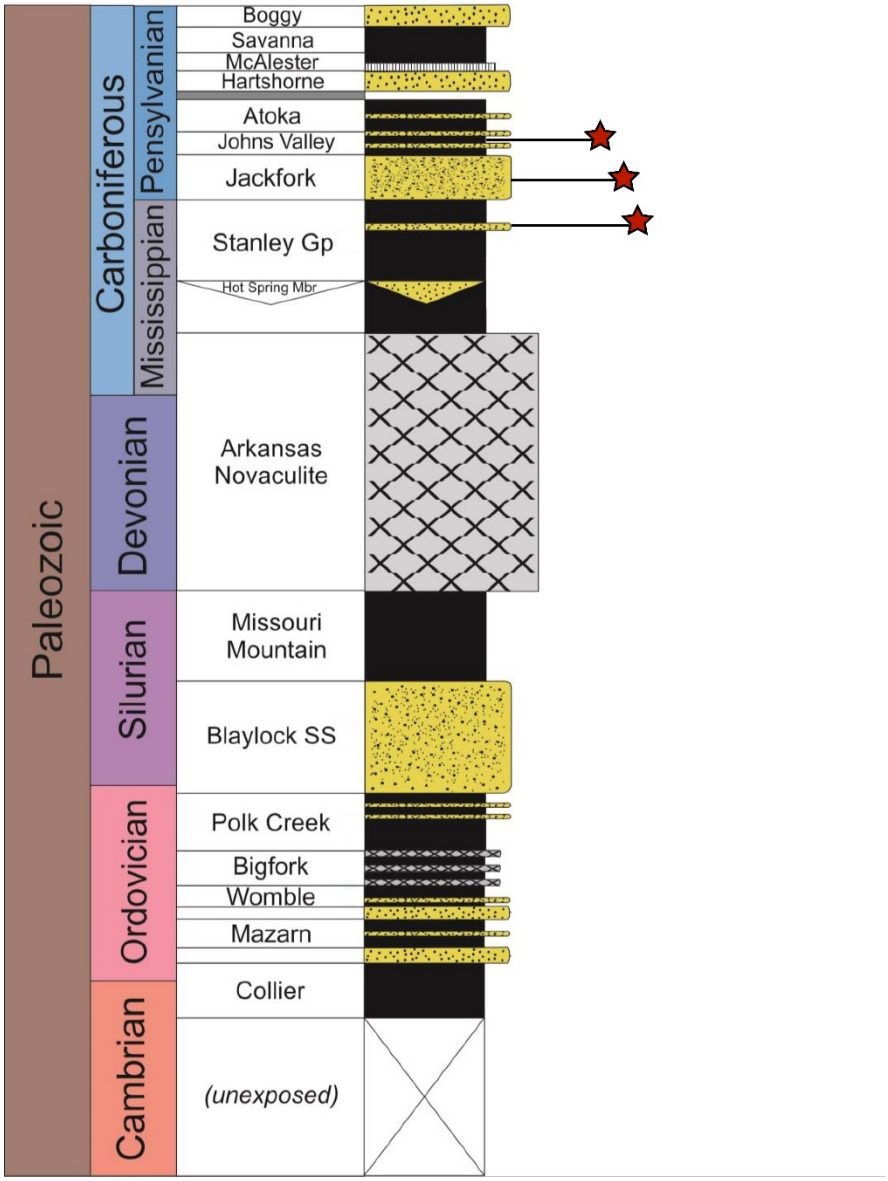

Figure 2: Paleozoic stratigraphic and lithologic column of the Paleozoic rocks in the Ouachita Mountains and Arkoma Basin. Modified from Lowe (1985). Red stars represent sampled sand and shale units. Yellow represents sandstone, black represents shale, grey represents Sub-Absaroka Unconformity, grey with (x) represents microcrystalline quartz, and the white texture is coal. *Note: Column does not represent formation thicknesses*.

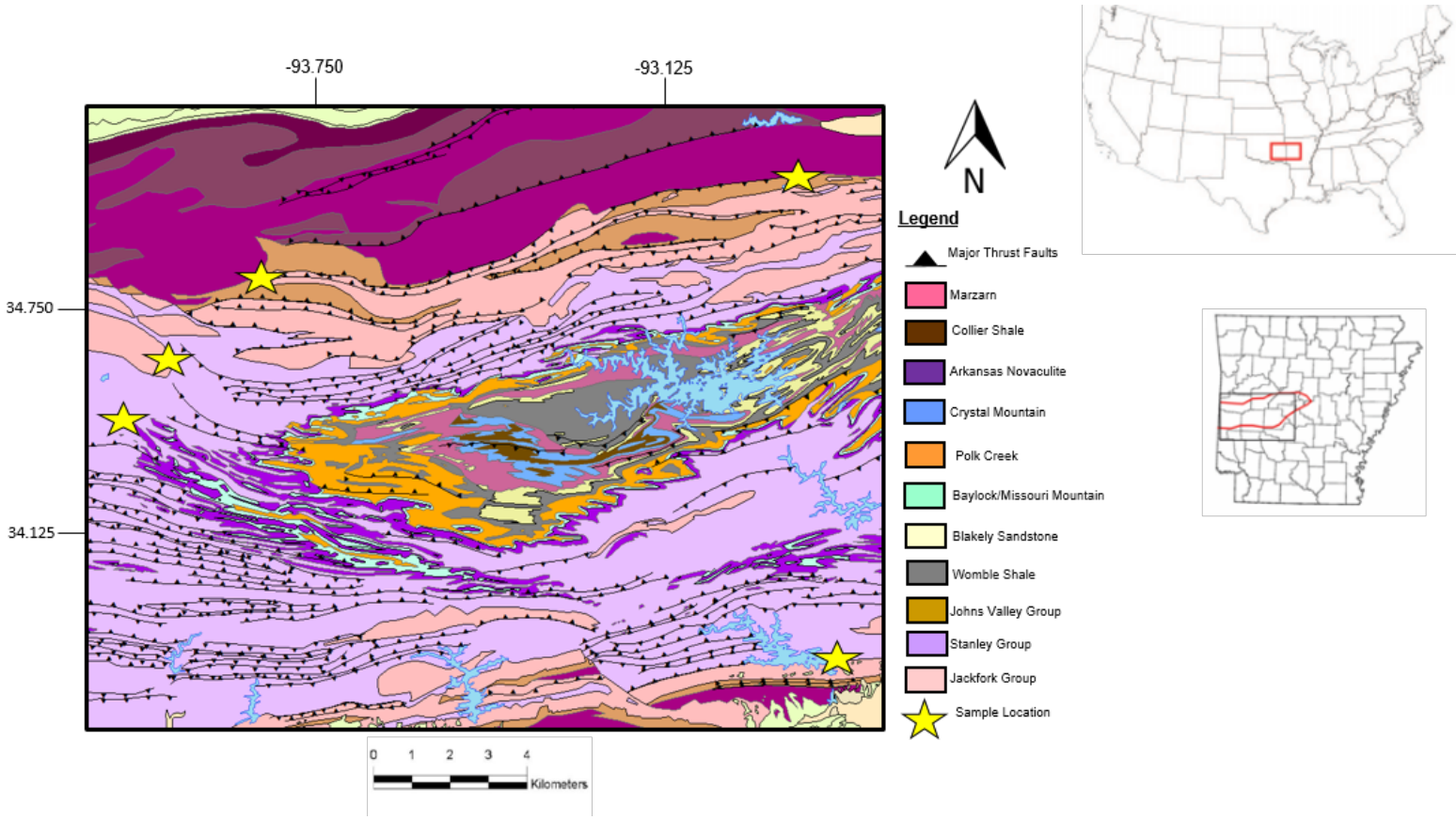

Figure 3: Geologic map of the Ouachita Mountains in Arkansas. Sample locations are displayed by gold stars with only major faults displayed. Legend shows the color of each geologic rock unit. Map source: Arkansas Geological Survey

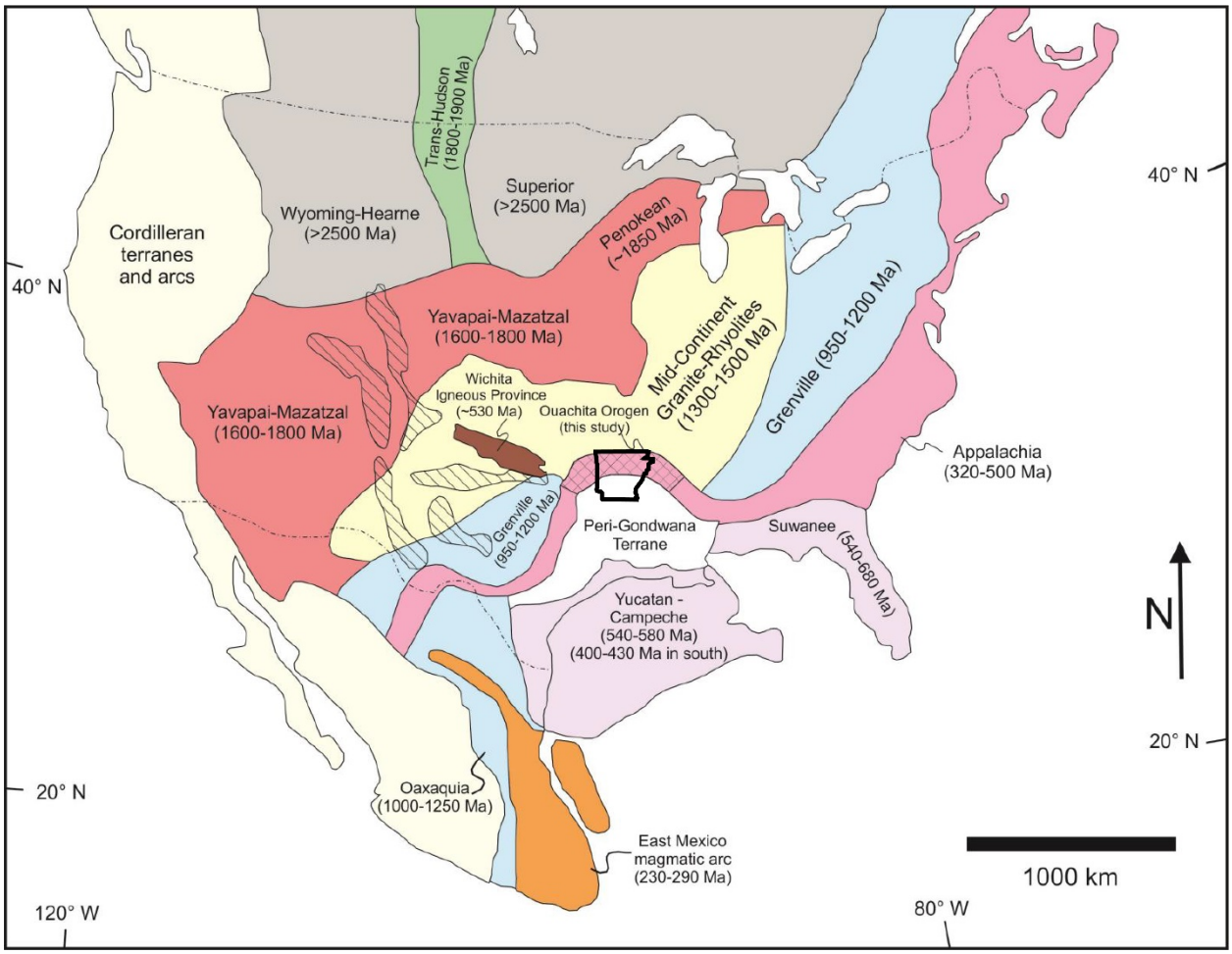

Figure 4: Major sediment terranes of North America. The State of Arkansas has been drawn in for reference. Hachured areas represent the location of the Ancestral Rockies. Modified from Gehrels et al., (2011).

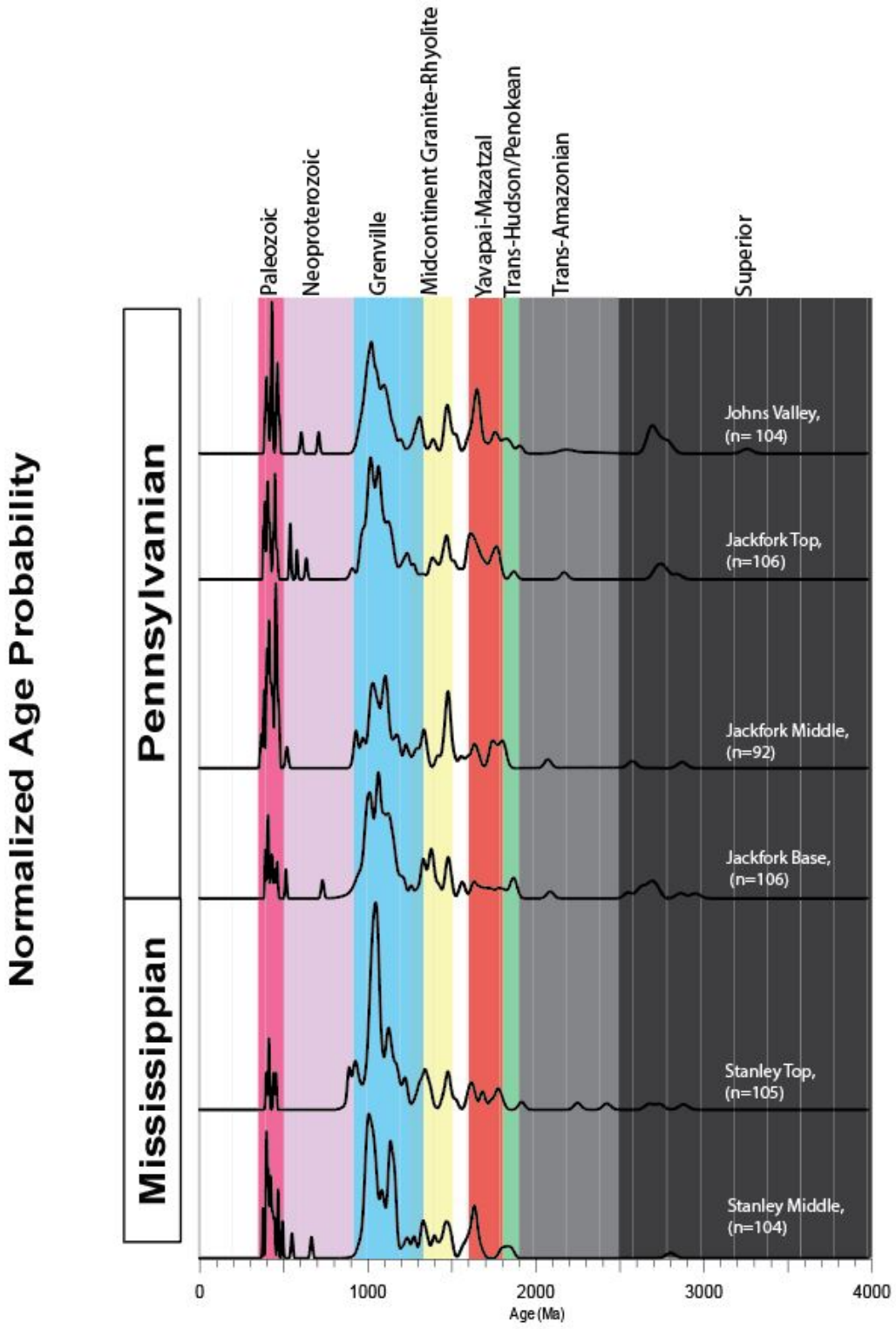

Figure 5: Normalized age probability diagram with known source terranes shaded in color.

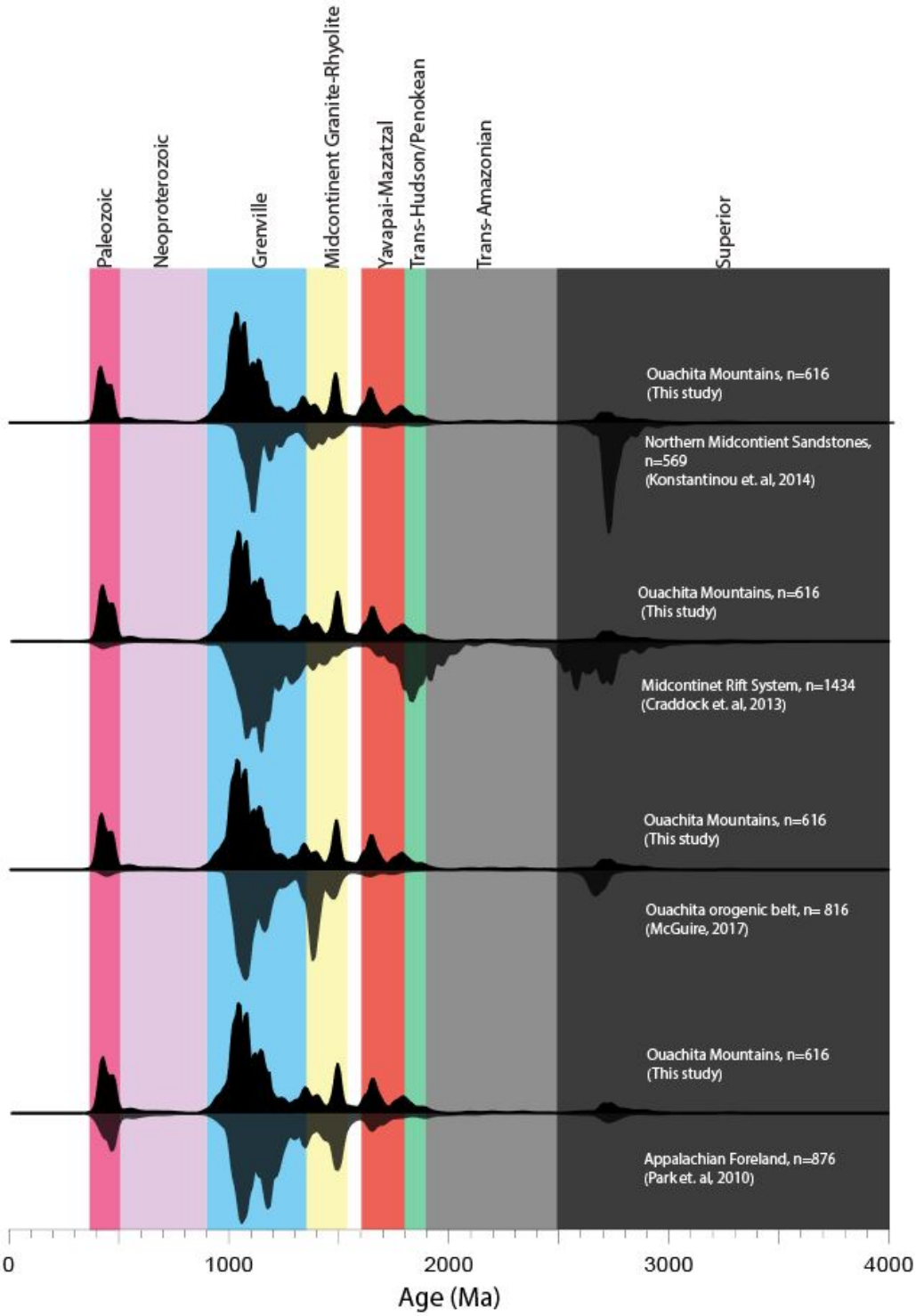

Figure 6: Comparison of detrital zircon age of syn-orogenic Carboniferous strata of the Ouachita Mountains (upward facing curves) with detrital zircon age distributions of the Appalachian foreland (Park et al., 2010), the Ouachita orogenic belt (McGuire, 2017), northern craton interior (Konstantinou et al., 2014), and the Midcontinent Rift System (Craddock et al., 2013). Known source terranes shaded in color.

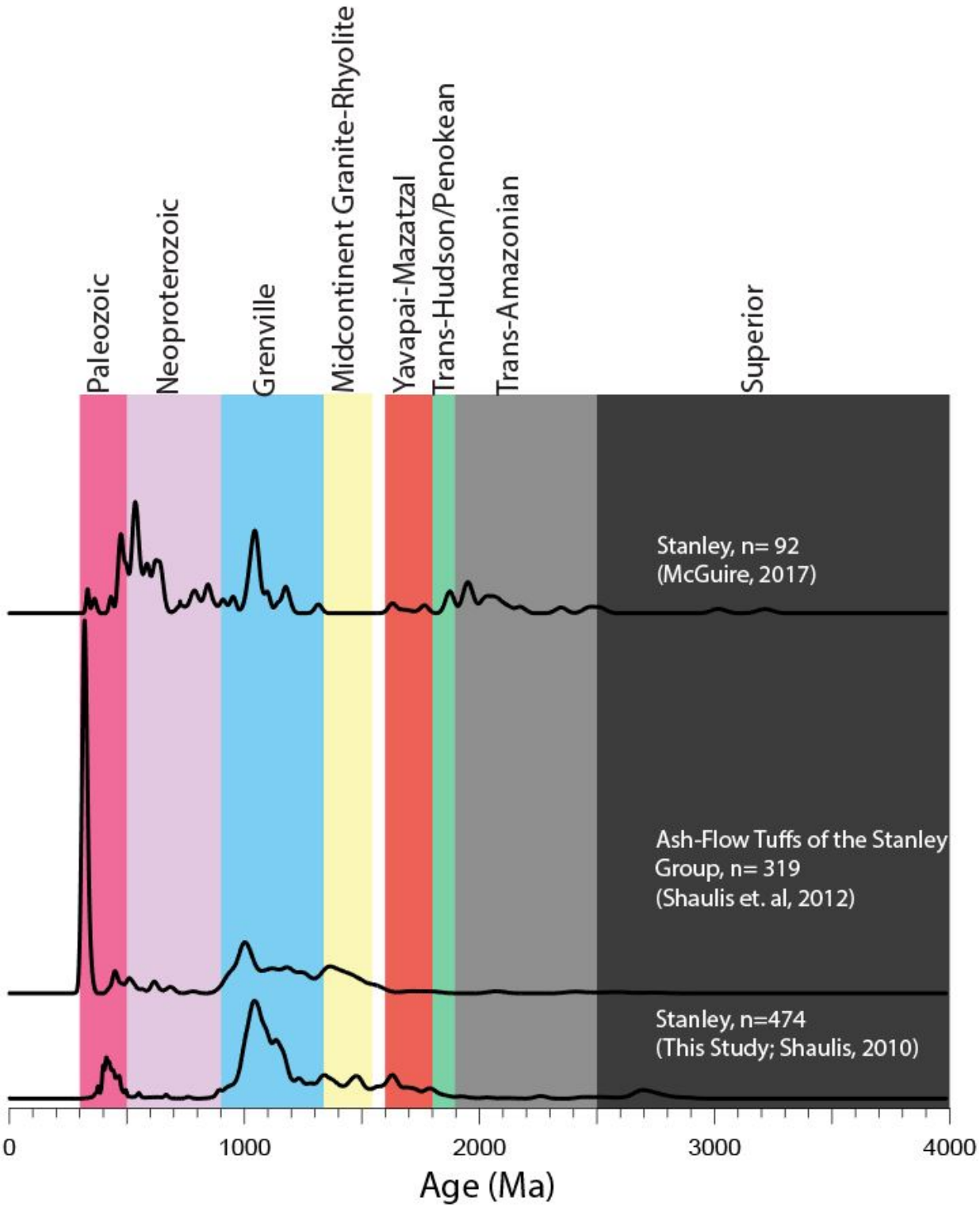

Figure 7: Normalized age probability diagrams of the Mississippian Stanley Group (McGuire, 2017; Shaulis, 2010; Shaulis et al., 2012).

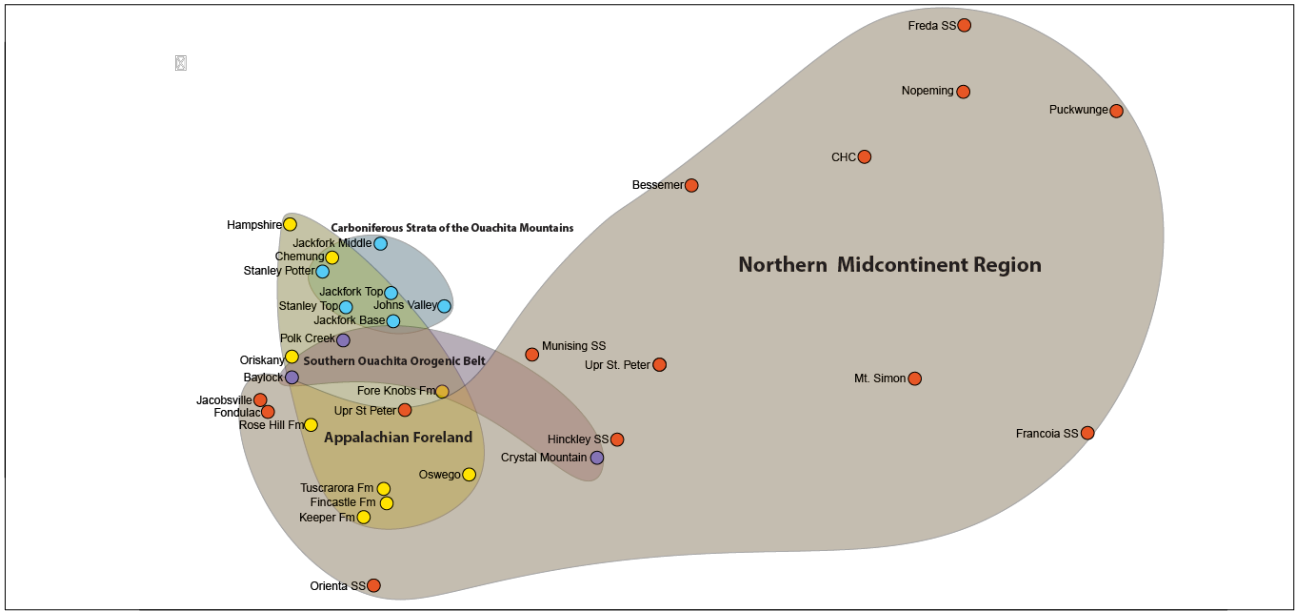

Figure 8: Results of Multidimensional scaling (MDS) analysis. Orange dots represent Lower Paleozoic strata of the northern midcontinent region, purple dots represent the Lower Paleozoic of the Ouachita orogenic belt, yellow dots represent the Lower Paleozoic strata of the Appalachian foreland, and blue represents the syn-orogenic Carboniferous strata of the Ouachita Mountains. Color fields correspond to strata found in the syn-orogenic Carboniferous strata of the Ouachita Mountains (blue), northern Midcontinent region (orange), Appalachian foreland (yellow), and southern Ouachita orogenic belt (purple).

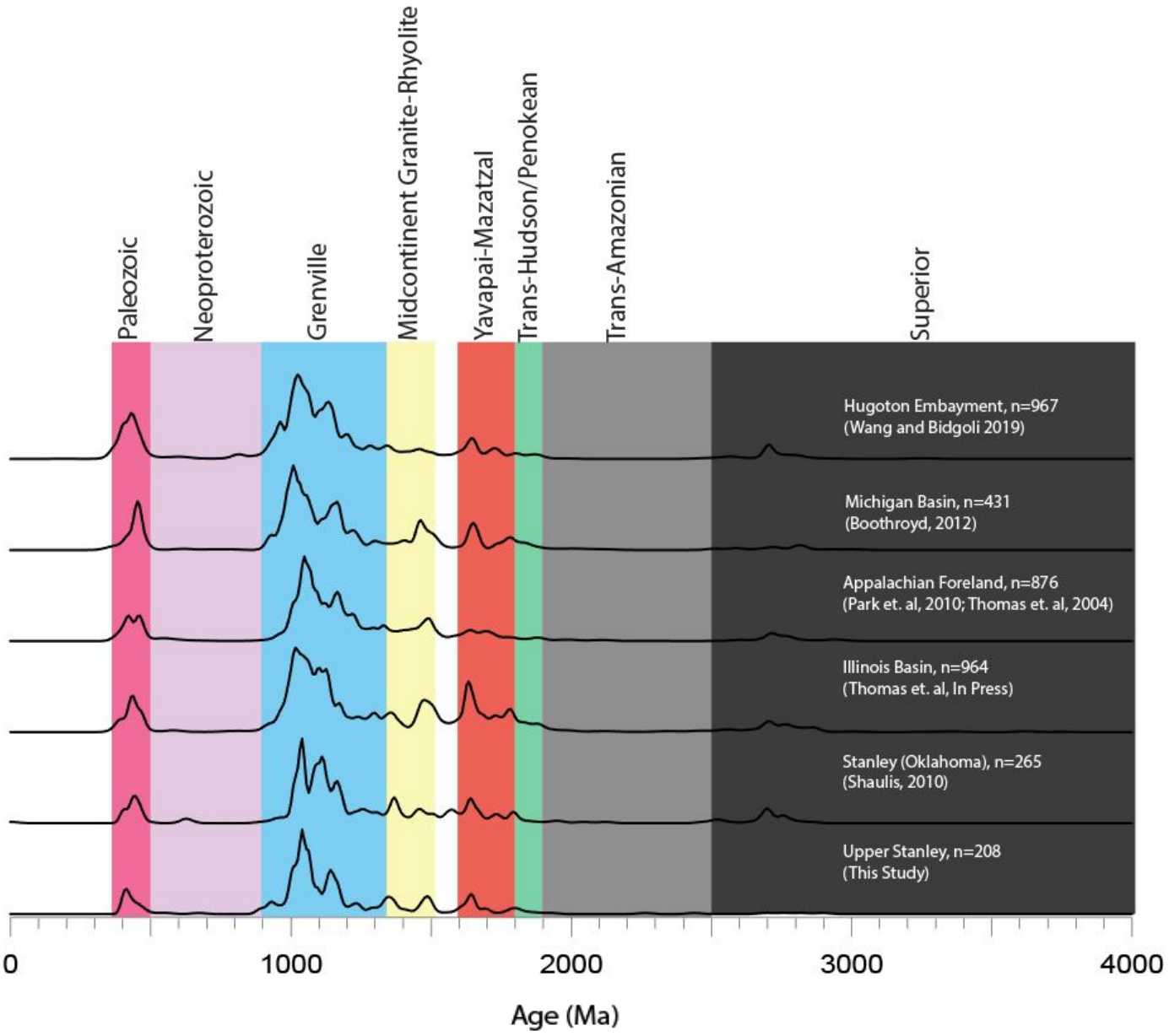

Figure 9: Detrital Age Spectra for comparison of Mississippian Stanley Group and other Mississippian sandstones from throughout Laurentia (Boothroyd, 2012; McGuire, 2017; Park et. al, 2010; Shaulis, 2010; Thomas et. al, 2004, In Press; Wang and Bidgoli, 2019). Known source terranes are shaded in color.

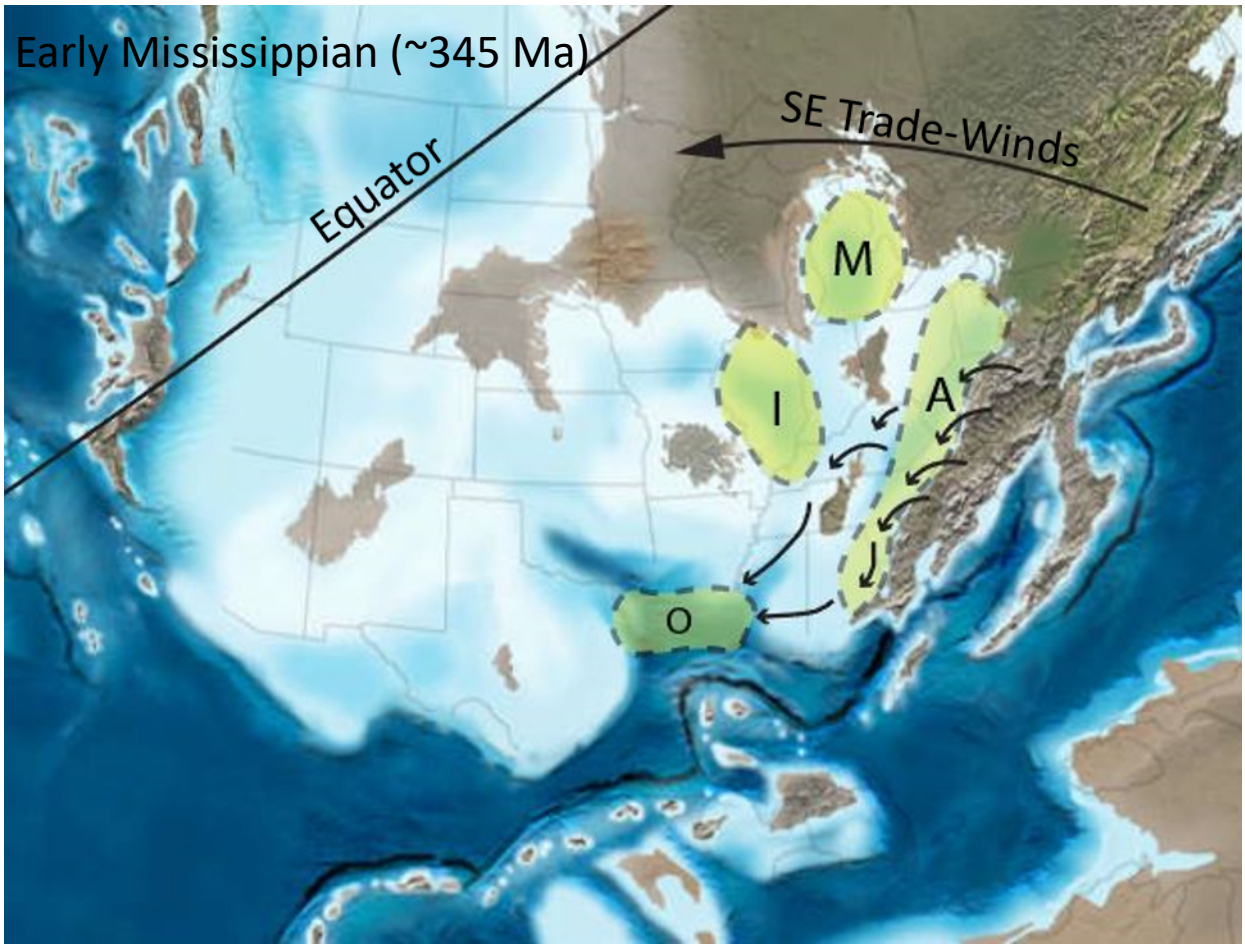

Figure 10: Sediment delivery pathway during the deposition of the deep-water clastics of the Stanley Group in the Early Mississippian (~345 Ma) (Blakely, 2013). Arrows denote proposed sediment transport network to the remnant Ouachita ocean basin. M, Michigan basin; I, Illinois basin; remnant Ouachita ocean basin; Appalachian Basin, A. Note: Texas Christian University is granted Licensee of Key Time Slices of North America 2013 Colorado Plateau Geosystem Inc

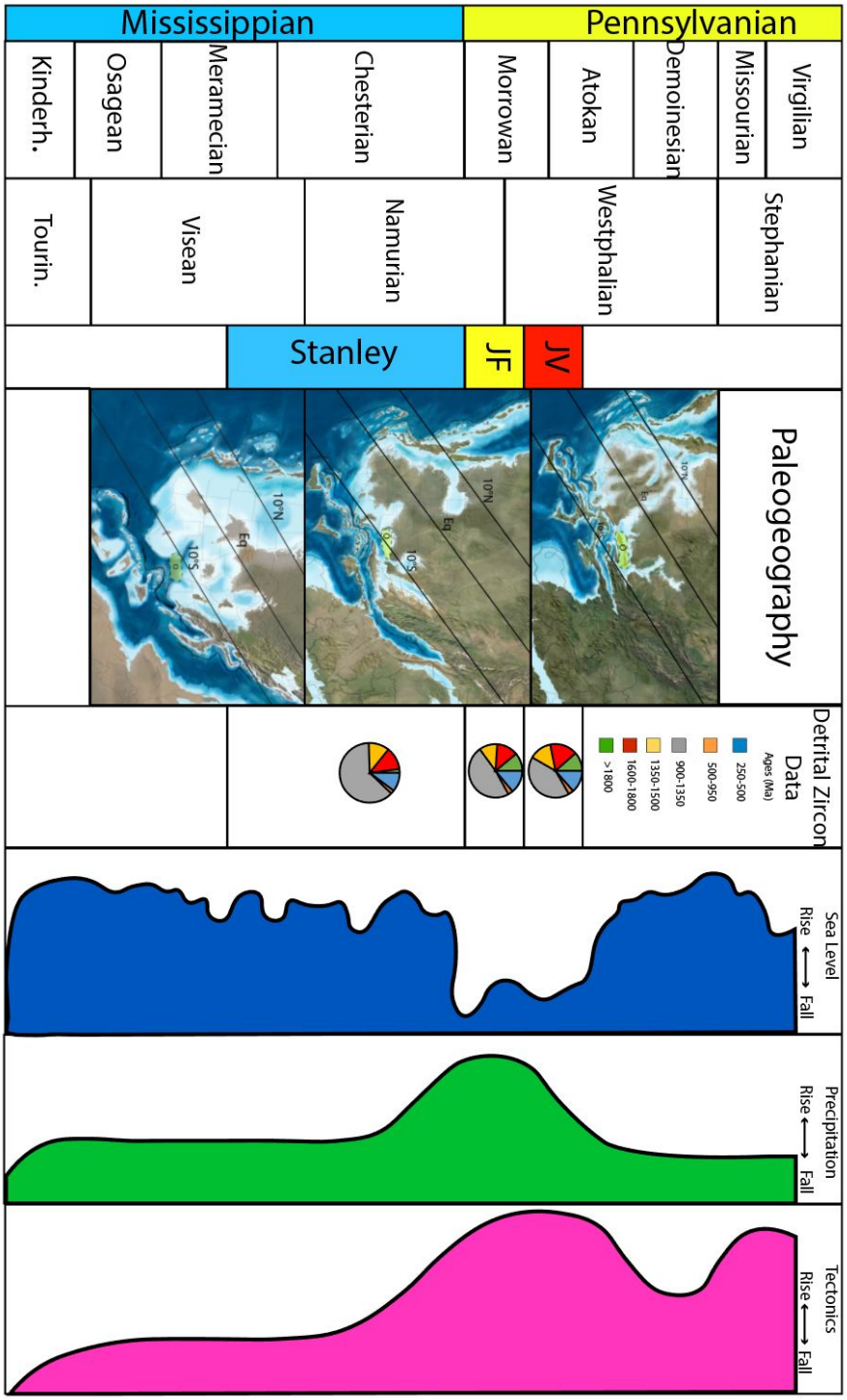

Figure 11: Paleogeographic positioning of the remnant Ouachita ocean basin throughout the Carboniferous. Detrital zircon age pie diagram, sea level, precipitation, and tectonics are also displayed. After Coleman et al. (2000).

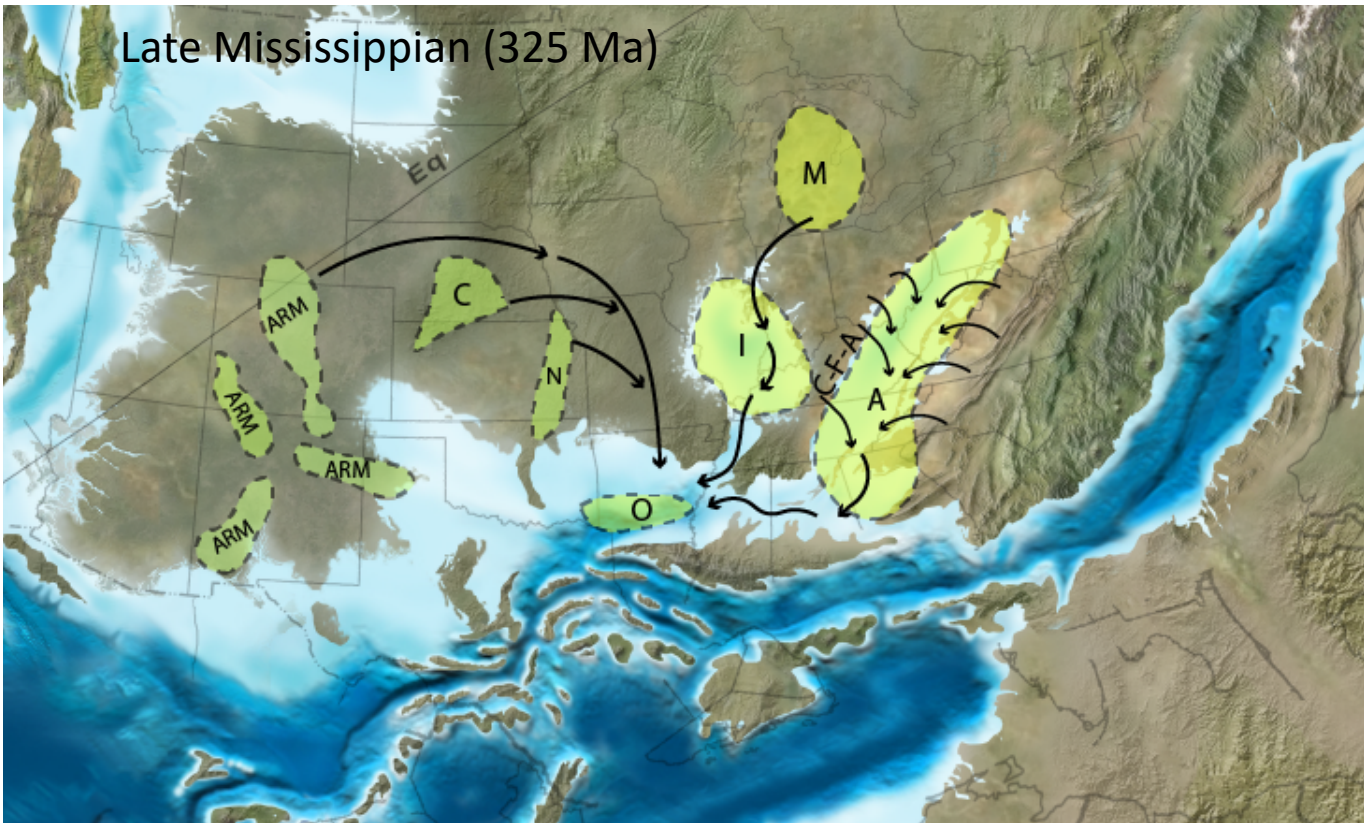

Figure 12: Sediment delivery pathway during the deposition of the deep-water clastics of the Stanley Group during the Late Mississippian (~325 Ma) (Blakey, 2013). Arrows denote proposed sediment transport network to the remnant Ouachita ocean basin. M, Michigan basin; I, Illinois basin; remnant Ouachita ocean basin; Appalachian Basin, A; C-F-A, Cincinnati Findlay-Algonquin; ARM, Ancestral Rockies Mountains; C, Cambridge Uplift; N, Nemaha Ridge; Eq, Equator. Note: Texas Christian University is granted Licensee of Key Time Slices of North America 2013 Colorado Plateau Geosystem Inc.

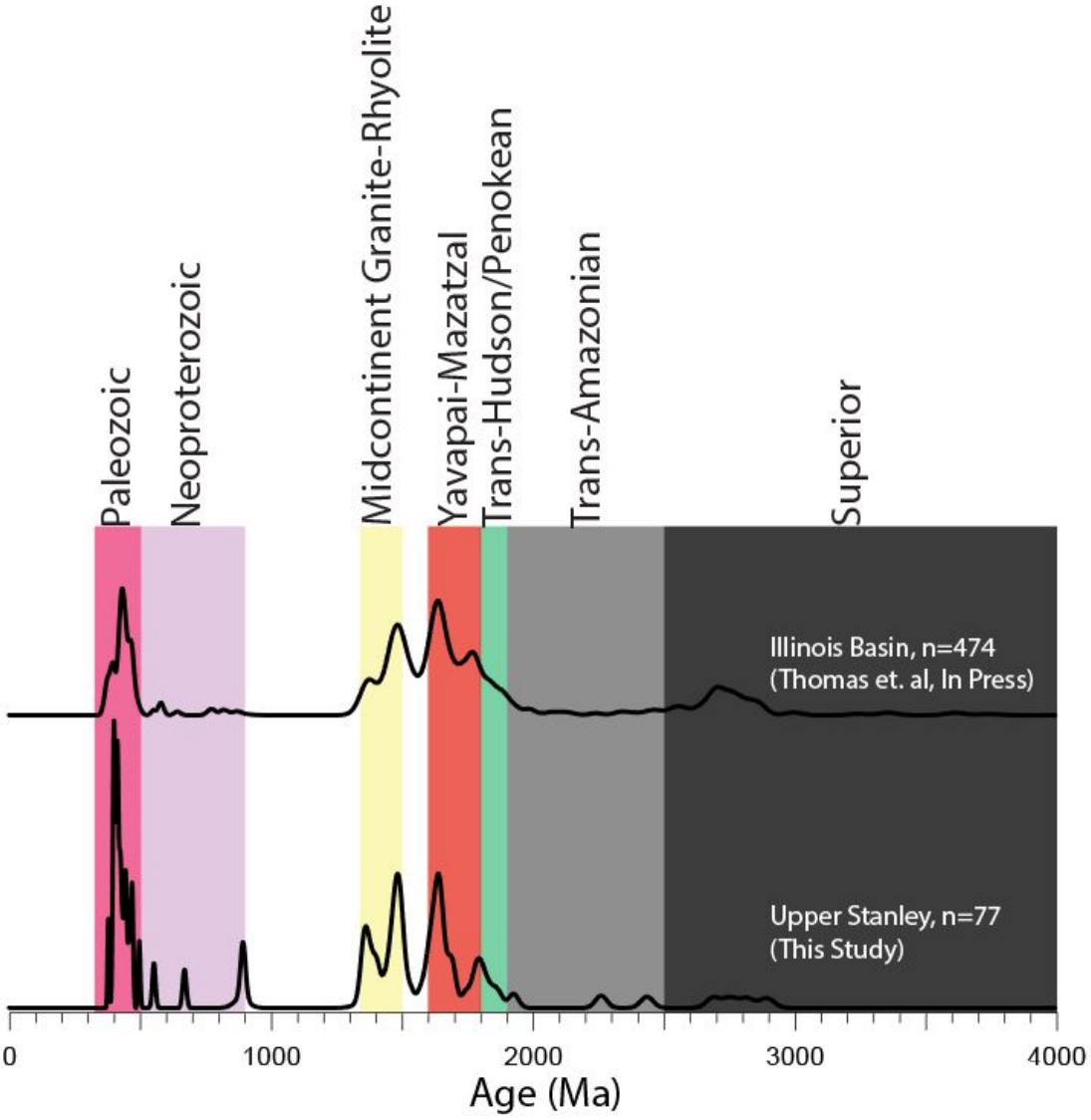

Figure 13: Normalized age probability diagram comparing the differences between the Mississippian Stanley Group and coeval strata of the Illinois basin (Thomas et al., in Press). *Note: Grenville aged grains (~900-1300 Ma) were removed to highlight similarities.*

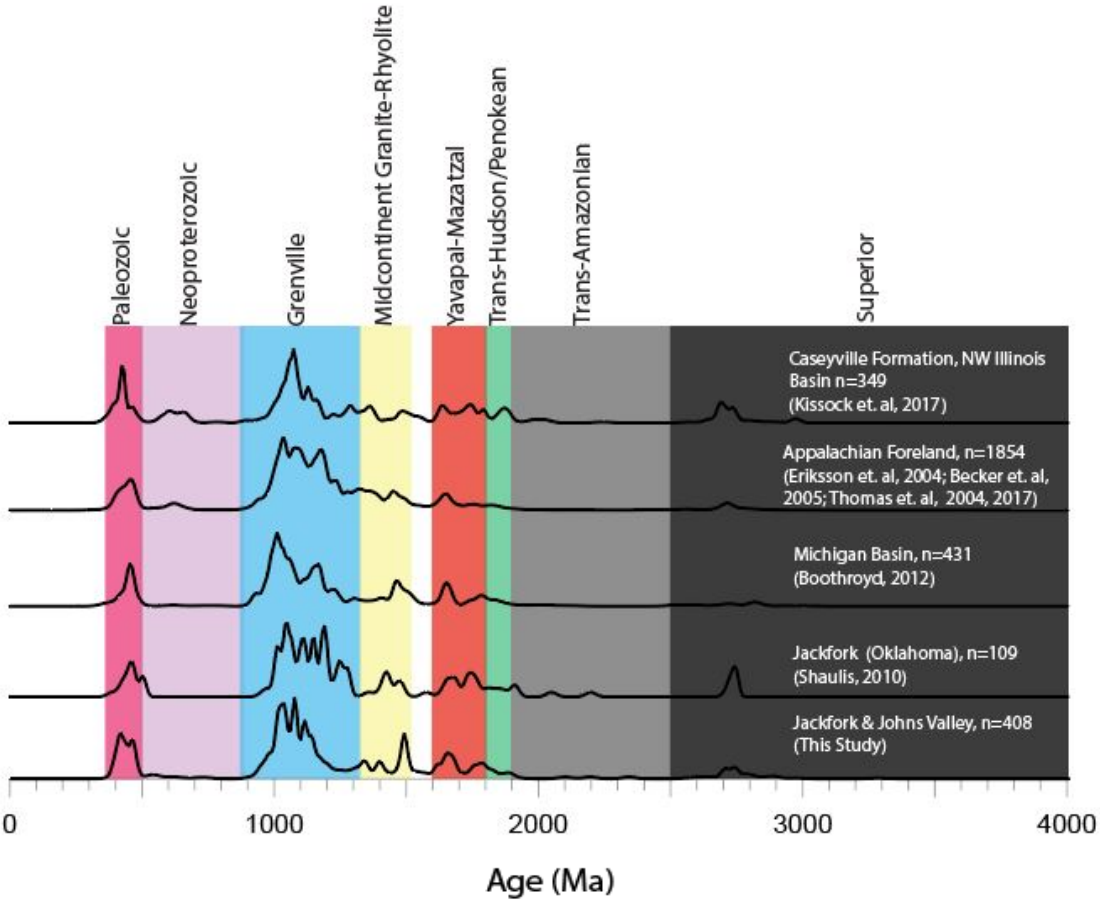

Figure 14: Detrital Age Spectra for comparison of Pennsylvanian Jackfork and Johns Valley Groups and other Lower Pennsylvanian sandstones from throughout Laurentia (Becker et al., 2005; Boothroyd, 2012; Eriksson et al., 2003; Kissock et al., 2018; Park et al., 2010; Shaulis, 2010; Thomas et al., 2004, 2017, In Press). Known source terranes are shaded in color.

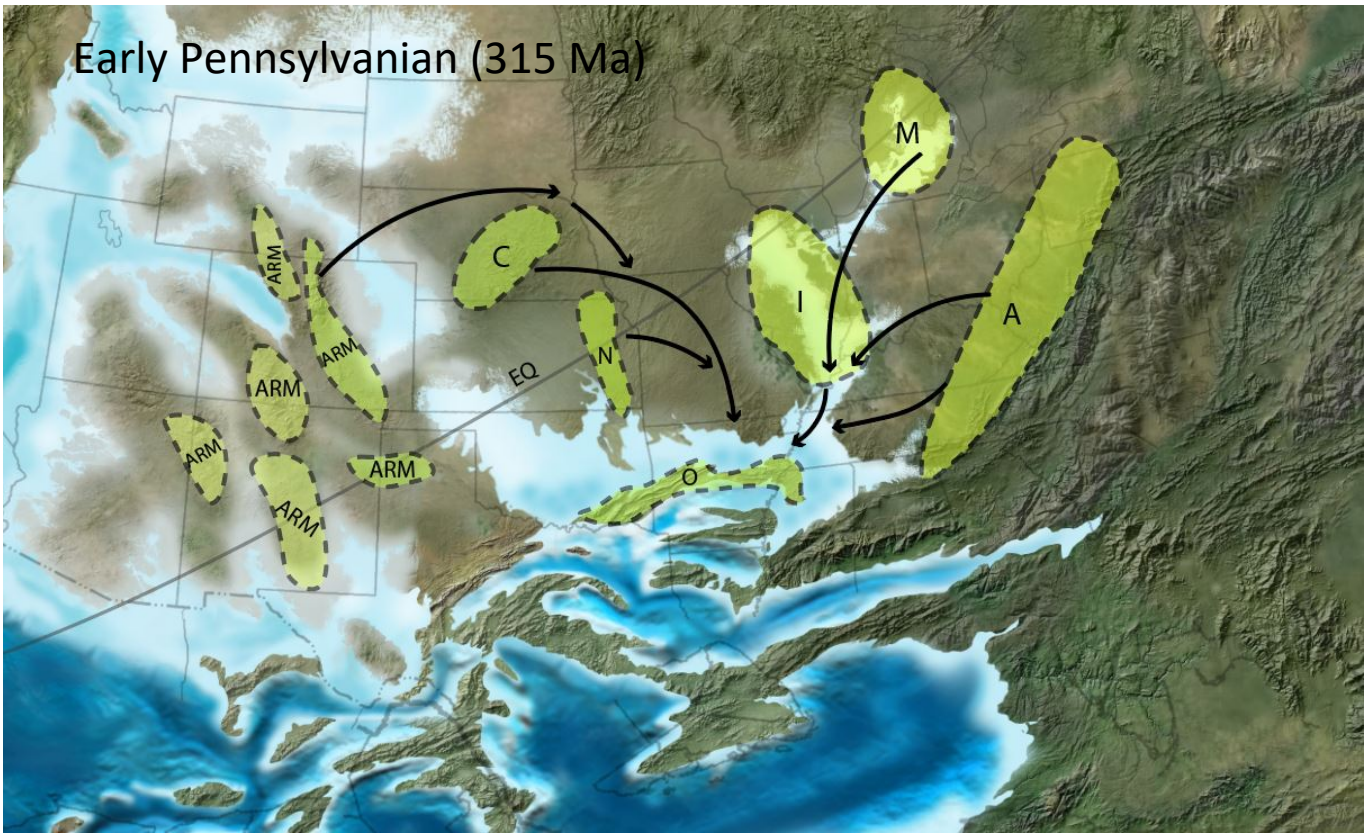

Figure 15: Sediment delivery pathway during the deposition of the deep-water clastics of the Jackfork and Johns Valley Groups during the Early Pennsylvanian (~325 Ma) (Blakely, 2013). Arrows denote proposed sediment transport network to the Ouachita Mountains (outlined in dashed lines and labeled with the O). M, Michigan basin; I, Illinois basin; Appalachian Basin; ARM, Ancestral Rockies Mountains; C, Cambridge Uplift; N, Nemaha Ridge; Eq, Equator. Note: Texas Christian University is granted Licensee of Key Time Slices of North America 2013 Colorado Plateau Geosystem Inc.

Tables:

Table 1. U-Pb detrital zircon sampling units and sample locations

Sample	Age	Group/Formation	Location
STP-1	Upper Mississippian	Stanley Group	N 34° 32' 55.89", W 94° 18' 32.79"
STT-1	Upper Mississippian	Stanley Group	N 34° 13' 56.53", W 93° 5' 59.46"
JFB-1	Lower Pennsylvanian	Jackfork Group	N 34° 13' 55.81", W 93° 5' 58.85"
JFM-1	Lower Pennsylvanian	Jackfork Group	N 34° 37' 51.09", W 94° 14' 57.06"
JFT-1	Lower Pennsylvanian	Jackfork Group	N 34° 37' 51.09", W 94° 4' 49"
JV-2	Lower Pennsylvanian	Johns Valley Shale	N 34° 52' 57.68", W 93° 9' 58.9"

APPENDIX

Tables: U-Pb Detrital Zircon Geochronology Data

Table 1. STP-1

Table_____. U-Pb geochronologic analyses.																				
						Isotope ratios						Apparent ages (Ma)								
Analysis	U	206Pb	U/Th	206Pb*	±	207Pb*	±	206Pb*	±	error	206Pb*	±	207Pb*	±	206Pb*	±	Best age	±	Conc
	(ppm)	204Pb		207Pb*	(%)	235U*	(%)	238U	(%)	corr.	238U*	(Ma)	235U	(Ma)	207Pb*	(Ma)	(Ma)	(Ma)	(%)
-Spot 1	789	22288	1.1	18.4346	0.6	0.4563	1.2	0.0610	1.0	0.83	381.9	3.6	381.7	3.7	380.3	14.4	381.9	3.6	NA
-Spot 65	466	24799	1.6	18.3936	0.7	0.4811	1.4	0.0642	1.2	0.86	401.2	4.6	398.8	4.5	385.3	15.3	401.2	4.6	104.1
-Spot 8	352	30928	15.9	17.8728	0.8	0.4980	1.1	0.0646	0.7	0.63	403.4	2.7	410.4	3.7	449.4	18.7	403.4	2.7	89.8
-Spot 108	396	34179	1.3	18.2667	0.9	0.4888	1.4	0.0648	1.0	0.76	404.6	4.0	404.1	4.5	400.8	20.0	404.6	4.0	101.0
-Spot 40	637	29102	3.2	18.2379	1.1	0.4921	2.1	0.0651	1.8	0.85	406.7	7.0	406.4	7.0	404.3	24.9	406.7	7.0	100.6
-Spot 96	318	17897	1.6	18.3022	0.8	0.4995	1.3	0.0663	1.0	0.78	414.0	4.1	411.4	4.4	396.5	18.0	414.0	4.1	104.4
-Spot 106	179	5088	1.8	19.0289	0.9	0.4810	1.4	0.0664	1.1	0.76	414.5	4.4	398.7	4.7	308.5	21.1	414.5	4.4	134.3
-Spot 88	175	14011	0.9	18.7211	1.0	0.5017	1.4	0.0681	0.9	0.65	425.0	3.7	412.8	4.7	345.5	23.5	425.0	3.7	123.0
-Spot 100	284	13869	0.8	18.3118	0.9	0.5156	1.2	0.0685	0.9	0.71	427.2	3.6	422.2	4.3	395.3	19.6	427.2	3.6	108.1
-Spot 74	320	1837620	1.0	18.0640	0.7	0.5303	1.2	0.0695	0.9	0.78	433.2	3.8	432.0	4.1	425.7	16.1	433.2	3.8	101.8
-Spot 45	137	13697	1.2	18.0872	1.2	0.5407	1.6	0.0710	1.0	0.62	441.9	4.1	438.9	5.5	422.9	27.3	441.9	4.1	104.5
-Spot 91	2257	32346	4.9	17.7004	0.6	0.5637	1.3	0.0724	1.1	0.87	450.6	4.8	453.9	4.6	470.9	13.6	450.6	4.8	95.7
-Spot 10	463	77513	0.9	17.6940	0.6	0.5898	1.1	0.0757	0.9	0.81	470.5	3.9	470.7	4.0	471.7	13.8	470.5	3.9	99.7
-Spot 7	89	5369	1.7	18.3495	1.3	0.5720	1.5	0.0762	0.8	0.53	473.2	3.7	459.3	5.7	390.7	29.1	473.2	3.7	121.1
-Spot 42	280	33303	1.3	17.8582	0.6	0.6213	1.2	0.0805	1.0	0.85	499.1	4.9	490.6	4.6	451.3	13.9	499.1	4.9	110.6
-Spot 86	146	12901	133.6	17.2452	0.9	0.7194	1.5	0.0900	1.2	0.80	555.7	6.5	550.3	6.5	528.4	20.1	555.7	6.5	105.2
-Spot 82	409	37676	0.9	16.1568	0.6	0.9384	1.3	0.1100	1.1	0.87	672.8	7.0	672.0	6.2	669.5	13.3	672.8	7.0	100.5
-Spot 4	94	32414	5.1	14.0516	0.8	1.5189	1.3	0.1549	0.9	0.74	928.2	8.0	938.0	7.7	961.3	17.3	961.3	17.3	96.5
-Spot 28	36	4737	1.2	13.9449	2.4	1.6804	2.7	0.1700	1.2	0.45	1012.2	11.2	1001.1	17.1	976.8	49.0	976.8	49.0	103.6
-Spot 29	43	8732	1.8	13.8750	1.1	1.7111	1.5	0.1723	1.0	0.66	1024.6	9.3	1012.7	9.6	987.1	22.8	987.1	22.8	103.8
-Spot 23	233	30077	4.8	13.8361	0.8	1.6611	1.3	0.1668	1.0	0.78	994.2	9.0	993.8	7.9	992.8	16.0	992.8	16.0	100.1
-Spot 64	282	395913	2.6	13.8084	0.6	1.6362	1.0	0.1639	0.8	0.81	978.6	7.5	984.3	6.4	996.9	12.0	996.9	12.0	98.2
-Spot 63	455	471790	7.4	13.8001	0.6	1.6573	1.1	0.1660	0.9	0.82	989.8	8.1	992.4	6.9	998.1	12.7	998.1	12.7	99.2
-Spot 18	244	89979	3.8	13.7711	0.6	1.6341	1.0	0.1633	0.9	0.82	975.0	7.8	983.4	6.6	1002.3	12.0	1002.3	12.0	97.3
-Spot 9	158	41878	3.0	13.7668	0.9	1.6624	1.4	0.1661	1.1	0.78	990.4	10.3	994.3	9.1	1003.0	18.3	1003.0	18.3	98.7
-Spot 60	91	33716	2.6	13.7308	0.8	1.6843	1.1	0.1678	0.8	0.70	1000.0	7.2	1002.6	7.0	1008.3	16.0	1008.3	16.0	99.2
-Spot 38	66	27252	1.3	13.7292	1.0	1.7616	1.3	0.1755	0.9	0.67	1042.3	8.5	1031.4	8.5	1008.5	19.8	1008.5	19.8	103.3
-Spot 70	208	15395	3.5	13.6988	0.7	1.6667	1.2	0.1657	0.9	0.82	988.2	8.7	995.9	7.3	1013.0	13.4	1013.0	13.4	97.5
-Spot 109	102	15952	2.7	13.6921	0.8	1.7348	1.3	0.1723	1.0	0.78	1025.0	9.5	1021.5	8.3	1014.0	16.5	1014.0	16.5	101.1
-Spot 57	362	33537	3.0	13.6879	0.5	1.7402	0.9	0.1728	0.7	0.79	1027.7	6.5	1023.5	5.6	1014.6	10.8	1014.6	10.8	101.3
-Spot 98	399	74544	2.4	13.6831	0.6	1.7523	1.1	0.1740	0.9	0.82	1034.0	8.7	1028.0	7.2	1015.3	12.9	1015.3	12.9	101.8
-Spot 105	72	9145	7.0	13.6746	0.9	1.6713	1.4	0.1658	1.1	0.78	989.1	9.7	997.7	8.6	1016.6	17.3	1016.6	17.3	97.3
-Spot 31	15	13223	3.8	13.6350	2.0	1.7465	2.2	0.1728	0.9	0.40	1027.4	8.3	1025.9	14.0	1022.5	40.1	1022.5	40.1	100.5
-Spot 43	227	88410	1.7	13.6183	0.8	1.7212	1.1	0.1701	0.8	0.73	1012.6	7.9	1016.5	7.4	1025.0	15.8	1025.0	15.8	98.8
-Spot 110	194	26197	3.5	13.6043	0.7	1.7099	1.2	0.1688	1.0	0.81	1005.4	9.0	1012.2	7.7	1027.0	14.3	1027.0	14.3	97.9
-Spot 11	266	84807	5.5	13.5889	0.7	1.6831	1.3	0.1660	1.1	0.86	989.8	10.4	1002.2	8.4	1029.3	13.7	1029.3	13.7	96.2
-Spot 50	103	45283	3.2	13.5446	0.8	1.7037	1.1	0.1674	0.8	0.71	998.0	7.2	1009.9	7.0	1035.9	15.6	1035.9	15.6	96.3
-Spot 46	61	733259	2.7	13.5378	0.7	1.7097	1.1	0.1679	0.9	0.78	1000.7	8.0	1012.2	7.1	1037.0	14.2	1037.0	14.2	96.5
-Spot 73	291	31335	2.6	13.5257	0.7	1.7524	1.2	0.1720	1.0	0.83	1023.0	9.3	1028.0	7.7	1038.7	13.3	1038.7	13.3	98.5
-Spot 75	203	146574	4.2	13.5099	0.7	1.7422	1.1	0.1708	0.9	0.77	1016.4	8.3	1024.3	7.4	1041.1	14.7	1041.1	14.7	97.6
-Spot 68	146	18726	4.8	13.4864	0.9	1.7137	1.1	0.1677	0.7	0.65	999.4	6.8	1013.7	7.3	1044.7	17.6	1044.7	17.6	95.7
-Spot 102	440	2984394	3.3	13.4730	0.6	1.8090	1.5	0.1768	1.3	0.90	1049.7	13.0	1048.7	9.7	1046.7	13.0	1046.7	13.0	100.3
-Spot 61	398	160920	5.5	13.4642	0.6	1.8000	0.9	0.1758	0.7	0.76	1044.2	6.9	1045.4	6.2	1048.0	12.5	1048.0	12.5	99.6
-Spot 27	76	8012	1.9	13.4548	1.0	1.8138	1.4	0.1771	0.9	0.65	1051.0	8.6	1050.4	8.9	1049.4	20.8	1049.4	20.8	100.1
-Spot 32	256	31870	4.1	13.3953	0.6	1.7789	1.1	0.1729	0.9	0.82	1028.0	8.3	1037.8	7.0	1058.3	12.4	1058.3	12.4	97.1
-Spot 76	331	37838	2.2	13.3696	0.5	1.8642	1.0	0.1808	0.9	0.87	1071.6	8.4	1068.5	6.5	1062.2	9.7	1062.2	9.7	100.9
-Spot 69	186	27920	3.9	13.3271	0.8	1.6958	1.2	0.1640	0.9	0.74	978.9	7.9	1007.0	7.5	1068.6	15.8	1068.6	15.8	91.6
-Spot 103	41	15465	0.8	13.3247	1.1	1.8597	1.5	0.1798	1.0	0.66	1065.9	9.6	1066.9	9.8	1068.9	22.3	1068.9	22.3	99.7
-Spot 36	26	3866	2.6	13.1841	1.7	1.9304	1.9	0.1847	1.0	0.50	1092.4	9.6	1091.7	12.9	1090.2	33.5	1090.2	33.5	100.2
-Spot 24	625	32889	34.3	13.1826	0.6	1.9722	1.3	0.1886	1.1	0.90	1114.0	11.6	1106.1	8.5	1090.4	11.2	1090.4	11.2	102.2
-Spot 52	252	88511	3.2	13.1760	0.6	1.8261	1.0	0.1746	0.8	0.79	1037.3	7.7	1054.9	6.6	1091.5	12.3	1091.5	12.3	95.0
-Spot 6	295	15333	5.8	13.1582	0.7	1.8435	1.2	0.1760	1.0	0.83	1045.1	9.2	1061.1	7.6	1094.1	13.0	1094.1	13.0	95.5
-Spot 71	115	451063	3.2	13.1123	0.9	1.9058	1.4	0.1813	1.1	0.79	1074.2	11.2	1083.1	9.5	1101.2	17.6	1101.2	17.6	97.5
-Spot 53	186	8952	4.0	13.0921	1.0	1.7630	1.4	0.1675	1.0	0.72	998.2	9.5	1032.0	9.3	1104.2	20.0	1104.2	20.0	90.4
-Spot 84	244	47460	3.7	13.0529	0.6	1.9726	0.9	0.1868	0.7	0.75	1104.1	6.9	1106.2	6.1	1110.2	11.8	1110.2	11.8	99.5
-Spot 16	155	130364	3.6	12.9193	0.9	2.0696	1.2	0.1940	0.7	0.65	1143.1	7.8	1138.8	7.9	1130.7	17.6	1130.7	17.6	101.1
-Spot 95	242	18991	3.3	12.8768	0.6	1.9880	1.1	0.1857	0.9	0.84	1098.3	9.3	1111.5	7.4	1137.3	11.8	1137.3	11.8	96.6
-Spot 3	665	1739621	6.8	12.8753	0.7	1.9725	1.5	0.1843	1.3	0.89	1090.3	13.1	1106.2	9.9	1137.5	13.4	1137.5	13.4	95.8
-Spot 34	187	12421	2.3	12.8654	0.6	2.0662	1.1	0.1929	0.9	0.83	1136.9	9.6	1137.7	7.6	1139.0	12.3	1139.0	12.3	99.8
-Spot 19	333	892824	4.6	12.8382	0.4	2.0032	1.0	0.1866	0.9	0.90	1103.0	9.1	1116.6	6.8	1143.3	8.6	1143.3	8.6	96.5
-Spot 89	163	20292	3.6	12.8331	0.6	2.0816	1.0	0.1938	0.8	0.78	1142.1	8.4	1142.7	7.0	1144.1	12.8	1144.1	12.8	99.8
-Spot 94	74	10738	2.2	12.8282	0.8	2.1151	1.2	0.1969	0.8	0.72	1158.5	8.8	1153.7	7.9	1144.8	15.9	1144.8	15.9	101.2
-Spot 5	204	52195	4.4	12.8208	0.6	2.0120	1.0	0.1872	0.8	0.81	1106.0	8.2	1119.6	6.7	1145.9	11.6	1145.9	11.6	96.5
-Spot 14	145	14988	5.5	12.7616	0.8	2.1023	1.1	0.1947	0.7	0.68	1146.6	7.8	1149.6	7.5	1155.1	15.9	1155.1	15.9	99.3
-Spot 77	151	33973	1.7	12.7531	0.6	2.0622	0.9	0.1908	0.7	0.76	1125.8	7.1	1136.3	6.2	1156.5	11.8	1156.5	11.8	97.4
-Spot 92	57	39178	3.2	12.7431	0.9	2.0899	1.3	0.1932	0.9	0.69	1138.9	9.0	1145.5	8.6	1158.0	18.1	1158.0	18.1	98.3
-Spot 67	96	19375	4.2	12.6834	0.6	2.1179	1.0	0.1949	0.8	0.80	1147.9	8.8	1154.7	7.2	1167.3	12.4	1167.3	12.4	98.3
-Spot 80	1124	410993	2.7	12.6828	0.6	2.1535	1.1	0.1982	1.0	0.85	1165.5	10.2	1166.2	7.9	1167.4	11.9	1167.4	11.9	99.8
-Spot 62	526	97558	2.9	12.6619	0.6	2.1858	1.4	0.2008	1.3	0.90	1179.7	13.6	1176.5	9.7	1170.7	11.9	1170.7	11.9	100.8
-Spot 30	272	33559	2.7	12.6609	0.6	2.1014	1.2	0.1930	1.0	0.86	1137.8	10.8	1149.3	8.3	1170.9	12.3	1170.9	12.3	97.2
-Spot 48	290	33461	1.6	12.6192	0.4	2.1502	0.8	0.1969	0.7	0.84	1158.5	7.1	1165.1	5.6	1177.4	8.7	1177.4	8.7	98.4
-Spot 79	86	15619	2.0	12.4031	0.9	2.1536	1.3	0.1938	0.9	0.70	1142.0	9.4	1166.2	8.9	1211.4	17.9	1211.4	17.9	94.3
-Spot 25	173	21293	3.1	12.2018	0.9	2.3143	1.5	0.2049	1.2	0.79	1201.6	12.7	1216.7	10.3	1243.6	17.4	1243.6	17.4	96.6
-Spot 37	55	14179	1.9	12.1771	0.8	2.3437	1.1	0.2071	0.8	0.73	1213.2	9.1	1225.6	8.0	1247.5	14.9	1247.5	14.9	97.2

-Spot 17	602	39343	2.5	11.9457	0.5	2.5234	1.0	0.2187	0.9	0.85	1275.1	10.1	1278.8	7.4	1285.0	10.5	1285.0	10.5	99.2
-Spot 104	74	20447	2.7	11.9090	0.9	2.6409	1.3	0.2282	1.0	0.75	1325.1	11.6	1312.1	9.5	1291.0	16.6	1291.0	16.6	102.6
-Spot 21	285	124911	1.2	11.6609	0.7	2.6771	1.1	0.2265	0.8	0.76	1316.2	10.0	1322.2	8.2	1331.9	13.9	1331.9	13.9	98.8
-Spot 97	679	240791	15.2	11.6390	0.5	2.5801	1.2	0.2179	1.1	0.89	1270.7	12.1	1295.0	8.7	1335.5	10.6	1335.5	10.6	95.2
-Spot 2	140	65819	2.5	11.5904	0.7	2.6563	1.0	0.2234	0.7	0.69	1299.7	8.4	1316.4	7.6	1343.6	14.4	1343.6	14.4	96.7
-Spot 58	105	18521	2.9	11.5282	0.7	2.7407	1.0	0.2293	0.8	0.73	1330.6	9.2	1339.6	7.8	1354.0	13.9	1354.0	13.9	98.3
-Spot 54	120	29230	5.6	11.4343	0.7	2.5542	1.1	0.2119	0.9	0.78	1239.0	9.8	1287.6	8.1	1369.7	13.3	1369.7	13.3	90.5
-Spot 78	283	38888	8.1	11.2243	0.6	2.7312	1.0	0.2224	0.8	0.79	1294.7	9.3	1337.0	7.5	1405.3	12.0	1405.3	12.0	92.1
-Spot 107	474	98969	4.0	11.2049	0.6	2.9629	1.4	0.2409	1.3	0.89	1391.3	16.1	1398.2	11.0	1408.6	12.4	1408.6	12.4	98.8
-Spot 12	104	10669	3.1	11.0251	0.5	3.1732	1.0	0.2538	0.9	0.87	1458.3	11.7	1450.7	7.9	1439.5	9.7	1439.5	9.7	101.3
-Spot 85	221	65518	4.9	10.8526	0.7	3.1959	1.1	0.2517	0.8	0.74	1447.0	10.4	1456.2	8.4	1469.5	13.9	1469.5	13.9	98.5
-Spot 39	362	396597	2.1	10.8511	1.5	3.4024	1.9	0.2679	1.1	0.57	1530.0	14.5	1504.9	14.7	1469.8	29.3	1469.8	29.3	104.1
-Spot 83	232	32002	1.6	10.8436	0.7	3.3170	1.0	0.2610	0.8	0.76	1494.8	10.1	1485.0	7.8	1471.1	12.4	1471.1	12.4	101.6

Table 2. STT-1

Table_____. U-Pb geochronologic analyses.																			
						Isotope ratios						Apparent ages (Ma)							
Analysis	U	206Pb	U/Th	206Pb*	±	207Pb*	±	206Pb*	±	error	206Pb*	±	207Pb*	±	206Pb*	±	Best age	±	Conc
	(ppm)	204Pb		207Pb*	(%)	235U*	(%)	238U	(%)	corr.	238U*	(Ma)	235U	(Ma)	207Pb*	(Ma)	(Ma)	(Ma)	(%)
-Spot 102	139	14307	2.6	17.6799	1.9	0.5013	2.1	0.0643	0.9	0.43	401.8	3.5	412.6	7.1	473.5	41.7	401.8	3.5	84.8
-Spot 8	521	11662	2.7	18.1635	0.7	0.5070	1.3	0.0668	1.1	0.83	416.9	4.4	416.4	4.5	413.5	16.2	416.9	4.4	100.8
-Spot 65	95	17169	2.2	18.5347	1.1	0.4989	1.4	0.0671	0.8	0.61	418.6	3.4	410.9	4.6	368.1	24.2	418.6	3.4	113.7
-Spot 58	312	17604	2.9	18.1115	0.9	0.5452	1.4	0.0716	1.1	0.75	446.0	4.6	441.8	5.1	419.9	20.9	446.0	4.6	106.2
-Spot 12	124	5720	2.2	18.4263	0.8	0.5542	1.3	0.0741	1.0	0.78	460.8	4.4	447.7	4.7	381.3	18.2	460.8	4.4	120.8
-Spot 75	49	4698	3.9	14.5492	1.4	1.4617	1.8	0.1543	1.2	0.65	925.0	10.1	914.7	10.8	889.8	27.9	889.8	27.9	104.0
-Spot 30	293	20499	1.5	14.5853	0.7	1.4089	1.3	0.1491	1.1	0.84	895.9	9.3	892.7	7.8	884.7	14.8	895.9	9.3	101.3
-Spot 71	50	9445	2.4	14.4890	1.0	1.4216	1.6	0.1494	1.3	0.78	897.9	10.7	898.0	9.7	898.4	21.0	897.9	10.7	99.9
-Spot 48	151	92338	3.3	14.2854	1.0	1.4966	1.3	0.1551	0.9	0.68	929.7	7.7	929.0	8.0	927.5	19.8	927.5	19.8	100.2
-Spot 46	189	357745	7.0	14.2800	0.8	1.4493	2.4	0.1502	2.3	0.95	901.9	19.4	909.6	14.6	928.3	16.2	928.3	16.2	97.2
-Spot 87	36	3822	2.9	14.2786	1.0	1.5620	1.6	0.1618	1.2	0.79	967.0	11.1	955.3	9.7	928.5	19.9	928.5	19.9	104.1
-Spot 33	121	15060	2.1	14.2422	0.7	1.5316	1.3	0.1583	1.0	0.80	947.2	8.9	943.1	7.7	933.7	15.3	933.7	15.3	101.4
-Spot 98	217	20926	4.0	14.2048	0.7	1.5496	1.2	0.1597	1.0	0.83	955.2	9.2	950.4	7.7	939.1	14.2	939.1	14.2	101.7
-Spot 57	138	68473	2.7	14.0681	0.9	1.5126	1.3	0.1544	1.0	0.74	925.6	8.5	935.5	8.1	958.9	18.2	958.9	18.2	96.5
-Spot 91	145	41712	2.9	14.0201	0.8	1.5315	1.5	0.1558	1.3	0.86	933.4	11.2	943.1	9.2	965.9	15.8	965.9	15.8	96.6
-Spot 13	182	34256	3.2	13.8476	0.9	1.6735	1.3	0.1681	0.9	0.71	1001.9	8.3	998.5	8.0	991.1	18.0	991.1	18.0	101.1
-Spot 100	101	17163	3.3	13.7644	0.8	1.7683	1.4	0.1766	1.2	0.82	1048.4	11.5	1033.9	9.4	1003.3	16.8	1003.3	16.8	104.5
-Spot 64	194	23349	1.9	13.7477	0.9	1.6260	1.7	0.1622	1.5	0.86	969.0	13.4	980.3	10.9	1005.8	17.9	1005.8	17.9	96.3
-Spot 82	53	9333	2.8	13.6859	1.1	1.6925	1.5	0.1681	1.0	0.67	1001.5	9.0	1005.7	9.3	1014.9	21.9	1014.9	21.9	98.7
-Spot 37	105	14229	3.2	13.6303	0.7	1.7528	1.2	0.1733	1.0	0.84	1030.5	10.0	1028.2	8.1	1023.2	13.7	1023.2	13.7	100.7
-Spot 10	143	25481	3.2	13.6262	0.5	1.7529	1.1	0.1733	1.0	0.87	1030.3	9.3	1028.2	7.2	1023.8	11.0	1023.8	11.0	100.6
-Spot 108	68	11700	1.7	13.6002	1.0	1.7568	1.4	0.1734	1.0	0.71	1030.6	9.4	1029.7	9.0	1027.6	20.0	1027.6	20.0	100.3
-Spot 94	121	363911	1.9	13.5806	0.8	1.7728	1.2	0.1747	0.9	0.76	1037.9	8.8	1035.6	7.8	1030.6	15.7	1030.6	15.7	100.7
-Spot 1	79	7714	1.4	13.5725	1.0	1.7471	1.4	0.1721	1.0	0.70	1023.4	9.0	1026.1	8.8	1031.8	19.8	1031.8	19.8	99.2
-Spot 85	140	68171	2.7	13.5385	0.6	1.7822	1.3	0.1751	1.1	0.86	1040.0	10.6	1039.0	8.3	1036.8	13.1	1036.8	13.1	100.3
-Spot 34	107	15234	3.4	13.5331	0.8	1.7824	1.3	0.1750	1.0	0.78	1039.7	9.9	1039.1	8.7	1037.6	16.9	1037.6	16.9	100.2
-Spot 3	121	72713	4.0	13.5303	0.8	1.7100	1.2	0.1679	0.9	0.75	1000.4	8.4	1012.3	7.7	1038.1	16.2	1038.1	16.2	96.4
-Spot 40	234	192786	3.5	13.5298	0.7	1.8099	1.3	0.1777	1.0	0.80	1054.3	9.8	1049.0	8.2	1038.1	15.1	1038.1	15.1	101.6
-Spot 50	138	32702	1.5	13.5263	0.8	1.7844	1.2	0.1751	0.9	0.75	1040.3	8.8	1039.8	8.0	1038.7	16.3	1038.7	16.3	100.2
-Spot 60	66	32923	1.9	13.5064	1.0	1.7310	1.3	0.1696	0.9	0.69	1010.1	8.4	1020.1	8.5	1041.6	19.4	1041.6	19.4	97.0
-Spot 84	90	17446	1.6	13.4995	1.1	1.6984	1.3	0.1664	0.8	0.57	992.0	7.0	1007.9	8.4	1042.7	21.8	1042.7	21.8	95.1
-Spot 78	199	70917	3.4	13.4992	0.8	1.7263	1.3	0.1691	1.0	0.81	1007.1	9.8	1018.4	8.3	1042.7	15.2	1042.7	15.2	96.6
-Spot 23	87	110783	1.3	13.4931	0.9	1.7635	1.2	0.1727	0.9	0.72	1026.7	8.6	1032.1	8.1	1043.7	17.4	1043.7	17.4	98.4
-Spot 26	191	71628	2.6	13.4665	0.7	1.7121	1.4	0.1673	1.2	0.85	997.2	11.3	1013.1	9.2	1047.6	15.1	1047.6	15.1	95.2
-Spot 70	180	33365	2.9	13.4575	0.6	1.7487	1.1	0.1708	0.9	0.83	1016.3	8.8	1026.7	7.3	1049.0	12.9	1049.0	12.9	96.9
-Spot 92	156	39850	4.4	13.4433	0.8	1.7845	1.4	0.1741	1.1	0.80	1034.5	10.6	1039.8	9.0	1051.1	16.8	1051.1	16.8	98.4
-Spot 2	409	25100	3.5	13.4254	0.7	1.7821	1.3	0.1736	1.1	0.85	1031.9	10.7	1039.0	8.6	1053.8	14.1	1053.8	14.1	97.9
-Spot 36	137	234488	3.4	13.4174	0.9	1.7412	1.3	0.1695	0.9	0.72	1009.4	8.9	1023.9	8.4	1055.0	18.2	1055.0	18.2	95.7
-Spot 43	329	30263	4.9	13.3994	0.8	1.8757	1.6	0.1824	1.3	0.86	1079.9	13.3	1072.6	10.3	1057.7	15.8	1057.7	15.8	102.1
-Spot 49	75	14153	3.1	13.3920	0.9	1.7944	1.3	0.1744	0.9	0.72	1036.1	8.8	1043.4	8.3	1058.8	17.6	1058.8	17.6	97.9
-Spot 9	200	22657	4.7	13.3860	0.7	1.7739	1.3	0.1723	1.1	0.83	1024.7	10.0	1035.9	8.2	1059.7	14.1	1059.7	14.1	96.7
-Spot 55	238	39899	1.8	13.3762	0.9	1.8566	1.2	0.1802	0.8	0.65	1068.0	7.5	1065.8	7.8	1061.2	18.3	1061.2	18.3	100.6
-Spot 52	607	41693	26.0	13.3670	0.7	1.7377	1.4	0.1685	1.2	0.86	1004.0	10.9	1022.6	8.8	1062.6	13.9	1062.6	13.9	94.5
-Spot 97	53	23250	3.5	13.3473	0.7	1.7675	1.2	0.1712	1.0	0.81	1018.6	9.4	1033.6	8.0	1065.5	14.5	1065.5	14.5	95.6
-Spot 27	215	36178	2.9	13.3449	0.8	1.8145	1.3	0.1757	1.0	0.78	1043.4	9.5	1050.7	8.2	1065.9	15.6	1065.9	15.6	97.9
-Spot 38	124	11277	2.5	13.3413	0.6	1.8905	1.2	0.1830	1.1	0.87	1083.4	10.8	1077.8	8.3	1066.5	12.3	1066.5	12.3	101.6
-Spot 95	602	169562	7.4	13.3233	0.6	1.8767	1.3	0.1814	1.2	0.90	1074.8	11.7	1072.9	8.7	1069.2	11.7	1069.2	11.7	100.5
-Spot 29	139	821899	1.1	13.3094	0.6	1.7896	1.1	0.1728	0.9	0.86	1027.6	9.0	1041.7	7.2	1071.3	11.4	1071.3	11.4	95.9
-Spot 7	35	10657	1.1	13.3085	1.1	1.8092	1.6	0.1747	1.2	0.76	1038.0	11.8	1048.8	10.6	1071.4	21.1	1071.4	21.1	96.9
-Spot 72	459	40820	9.6	13.2989	0.7	1.9314	1.8	0.1864	1.6	0.92	1101.7	16.3	1092.0	11.8	1072.8	14.2	1072.8	14.2	102.7
-Spot 22	322	31641	3.6	13.2747	0.8	1.8618	1.3	0.1793	1.0	0.81	1063.3	10.1	1067.6	8.4	1076.5	15.1	1076.5	15.1	98.8
-Spot 35	173	20962	2.8	13.2619	0.7	1.8938	1.3	0.1822	1.1	0.84	1079.2	11.1	1078.9	8.8	1078.4	14.2	1078.4	14.2	100.1
-Spot 28	100	43643	2.9	13.2213	1.1	1.7767	1.7	0.1704	1.3	0.77	1014.6	12.1	1037.0	10.9	1084.6	21.2	1084.6	21.2	93.5
-Spot 54	399	60484	5.6	13.1454	0.6	1.9724	1.4	0.1881	1.3	0.91	1111.2	13.1	1106.1	9.5	1096.1	11.9	1096.1	11.9	101.4
-Spot 17	206	27010	5.5	13.0943	0.9	1.9502	1.4	0.1853	1.0	0.74	1095.8	10.1	1098.5	9.1	1103.9	18.4	1103.9	18.4	99.3
-Spot 45	72	996899	4.0	13.0006	1.2	1.9452	1.5	0.1835	1.0	0.64	1086.0	9.7	1096.8	10.2	1118.3	23.3	1118.3	23.3	97.1
-Spot 51	28	5426	3.6	12.9871	1.1	2.0692	1.5	0.1950	1.0	0.69	1148.3	10.8	1138.7	10.3	1120.3	21.7	1120.3	21.7	102.5
-Spot 107	74	17382	2.3	12.9682	0.8	2.0612	1.2	0.1940	0.9	0.72	1142.8	9.0	1136.0	8.3	1123.2	16.8	1123.2	16.8	101.7
-Spot 89	99	37369	3.8	12.9399	0.6	2.0553	1.3	0.1930	1.2	0.88	1137.4	12.0	1134.0	9.0	1127.5	12.6	1127.5	12.6	100.9
-Spot 20	86	16860	2.1	12.9282	0.7	2.0081	1.4	0.1884	1.1	0.84	1112.5	11.6	1118.2	9.2	1129.4	14.6	1129.4	14.6	98.5
-Spot 24	73	7511	3.4	12.9037	0.8	2.0786	1.2	0.1946	0.9	0.77	1146.3	9.6	1141.8	8.1	1133.1	15.1	1133.1	15.1	101.2
-Spot 109	248	42343	14.8	12.8868	0.7	2.1446	1.1	0.2005	0.9	0.77	1178.2	9.5	1163.3	7.9	1135.8	14.5	1135.8	14.5	103.7
-Spot 63	81	32493	3.4	12.8128	0.7	2.0511	1.0	0.1907	0.8	0.75	1125.1	8.1	1132.7	7.1	1147.2	13.8	1147.2	13.8	98.1
-Spot 74	427	38579	3.9	12.8058	0.8	2.1037	1.8	0.1955	1.6	0.89	1150.9	16.4	1150.0	12.1	1148.3	16.2	1148.3	16.2	100.2
-Spot 104	367	378894	3.7	12.7576	0.8	2.0394	1.9	0.1888	1.7	0.91	1114.8	17.4	1128.7	12.8	1155.8	15.6	1155.8	15.6	96.5
-Spot 14	24	16688	1.5	12.7318	1.1	1.9894	1.5	0.1838	1.1	0.69	1087.6	10.7	1111.9	10.4	1159.8	22.0	1159.8	22.0	93.8
-Spot 105	214	30761	8.2	12.6839	0.8	2.1064	1.5	0.1939	1.3	0.85	1142.2	13.3	1150.9	10.3	1167.2	15.8	1167.2	15.8	97.9

-Spot 86	261	74347	2.8	12.6211	0.7	2.1511	1.1	0.1970	0.8	0.78	1159.1	8.8	1165.4	7.4	1177.1	13.4	1177.1	13.4	98.5
-Spot 88	219	33892	2.8	12.5581	0.7	2.1779	1.1	0.1984	0.8	0.77	1167.0	9.0	1174.0	7.6	1187.0	13.9	1187.0	13.9	98.3
-Spot 32	63	27859	1.4	12.5209	0.8	2.3232	1.5	0.2111	1.3	0.85	1234.5	14.6	1219.4	10.8	1192.8	15.6	1192.8	15.6	103.5
-Spot 68	164	9830	2.3	12.3805	1.1	1.9812	1.6	0.1780	1.1	0.70	1055.9	10.5	1109.1	10.5	1215.0	22.0	1215.0	22.0	86.9
-Spot 81	101	16356	3.1	12.3107	0.7	2.2772	1.2	0.2034	1.0	0.84	1193.6	11.1	1205.3	8.6	1226.1	13.0	1226.1	13.0	97.3
-Spot 6	21	13834	3.0	12.2714	1.2	2.4571	1.8	0.2188	1.4	0.76	1275.4	15.9	1259.5	13.1	1232.5	23.2	1232.5	23.2	103.5
-Spot 73	111	69501	2.8	12.2249	0.6	2.3843	1.1	0.2115	0.9	0.81	1236.8	9.9	1237.9	7.8	1239.9	12.6	1239.9	12.6	99.7
-Spot 19	82	33533	4.2	11.8944	0.9	2.4767	1.5	0.2137	1.2	0.79	1248.8	13.2	1265.2	10.7	1293.4	17.6	1293.4	17.6	96.5
-Spot 16	78	23883	4.1	11.7537	0.8	2.6999	1.4	0.2303	1.2	0.85	1335.8	14.7	1328.4	10.6	1316.5	14.6	1316.5	14.6	101.5
-Spot 79	171	63849	2.7	11.7030	0.7	2.6765	1.2	0.2273	0.9	0.77	1320.2	10.8	1322.0	8.7	1324.9	14.5	1324.9	14.5	99.6
-Spot 106	106	33761	3.0	11.5818	0.8	2.8025	1.1	0.2355	0.8	0.70	1363.3	9.5	1356.2	8.3	1345.0	15.3	1345.0	15.3	101.4
-Spot 41	62	18632	1.5	11.5599	0.7	2.8187	1.3	0.2364	1.0	0.83	1368.1	12.8	1360.5	9.4	1348.6	13.6	1348.6	13.6	101.4
-Spot 25	119	32448	3.2	11.4876	0.8	2.7745	1.3	0.2313	1.0	0.80	1341.1	12.4	1348.7	9.6	1360.8	14.9	1360.8	14.9	98.6
-Spot 61	92	115254	2.6	11.4465	1.0	2.8227	1.4	0.2344	1.0	0.71	1357.7	12.1	1361.6	10.4	1367.7	18.8	1367.7	18.8	99.3
-Spot 21	76	6993	1.5	11.4447	1.9	2.4604	2.1	0.2043	1.0	0.46	1198.4	10.7	1260.5	15.3	1368.0	36.1	1368.0	36.1	87.6
-Spot 42	110	70321	3.3	11.3447	0.7	2.7983	1.1	0.2303	0.9	0.79	1336.3	10.4	1355.1	8.2	1384.8	13.0	1384.8	13.0	96.5
-Spot 44	57	28464	1.5	10.9078	0.6	3.0473	1.2	0.2412	1.0	0.85	1392.8	12.6	1419.5	9.0	1459.9	11.7	1459.9	11.7	95.4
-Spot 90	176	77361	3.4	10.7632	0.8	3.2957	1.2	0.2574	1.0	0.78	1476.4	12.8	1480.0	9.7	1485.2	14.9	1485.2	14.9	99.4
-Spot 62	131	32190	3.3	10.7535	0.6	3.3622	1.2	0.2623	1.0	0.83	1501.8	12.8	1495.6	9.0	1486.9	12.2	1486.9	12.2	101.0
-Spot 69	274	1424853	3.1	10.7256	0.9	3.1045	1.6	0.2416	1.3	0.84	1395.0	16.7	1433.8	12.1	1491.8	16.2	1491.8	16.2	93.5

Table 3. JFB-1

Table_____. U-Pb geochronologic analyses.																			
						Isotope ratios					Apparent ages (Ma)								
Analysis	U	206Pb	U/Th	206Pb*	±	207Pb*	±	206Pb*	±	error	206Pb*	±	207Pb*	±	206Pb*	±	Best age	±	Conc
	(ppm)	204Pb		207Pb*	(%)	235U*	(%)	238U	(%)	corr.	238U*	(Ma)	235U	(Ma)	207Pb*	(Ma)	(Ma)	(Ma)	(%)
-Spot 80	78	3134	1.2	18.3181	1.2	0.4759	1.5	0.0633	1.0	0.64	395.4	3.7	395.3	5.0	394.5	26.1	395.4	3.7	NA
-Spot 12	73	23044	3.1	18.2272	1.0	0.4938	1.4	0.0653	1.0	0.70	407.8	4.0	407.5	4.8	405.6	22.6	407.8	4.0	100.5
-Spot 106	169	74028	1.1	17.8576	0.8	0.5114	1.2	0.0663	0.9	0.74	413.6	3.5	419.4	4.1	451.3	18.1	413.6	3.5	91.6
-Spot 95	218	73500	1.2	17.9292	0.9	0.5103	1.3	0.0664	0.9	0.71	414.3	3.8	418.7	4.5	442.4	20.8	414.3	3.8	93.7
-Spot 75	198	17992	1.8	17.9951	0.8	0.5276	1.4	0.0689	1.1	0.81	429.4	4.7	430.2	4.8	434.3	17.9	429.4	4.7	98.9
-Spot 4	101	3237	1.4	18.7013	0.9	0.5175	1.4	0.0702	1.0	0.74	437.5	4.3	423.5	4.7	347.9	20.4	437.5	4.3	125.8
-Spot 105	48	6708	0.8	18.1820	1.7	0.5508	2.0	0.0727	1.2	0.57	452.2	5.1	445.5	7.3	411.2	37.1	452.2	5.1	110.0
-Spot 67	293	35477	1.3	17.7041	0.7	0.5853	1.3	0.0752	1.1	0.84	467.3	4.8	467.8	4.8	470.5	15.6	467.3	4.8	99.3
-Spot 66	106	15300	3.6	16.4691	0.8	0.7023	1.3	0.0839	1.1	0.81	519.5	5.3	540.2	5.6	628.4	16.8	519.5	5.3	82.7
-Spot 41	478	154582	2.5	15.5494	0.6	1.0762	1.3	0.1214	1.2	0.89	738.7	8.3	741.8	7.1	750.9	13.2	738.7	8.3	98.4
-Spot 22	11	2278	1.5	14.4338	2.8	1.5115	3.0	0.1583	0.9	0.29	947.3	7.7	935.0	18.1	906.2	58.4	906.2	58.4	104.5
-Spot 94	19	4945	1.3	14.1316	1.6	1.5314	2.1	0.1570	1.3	0.62	940.2	11.3	943.1	12.7	949.7	33.1	949.7	33.1	99.0
-Spot 92	24	6826	1.8	14.1221	1.2	1.5511	1.7	0.1589	1.2	0.70	950.9	10.6	950.9	10.6	951.1	25.2	951.1	25.2	100.0
-Spot 72	11	4800	6.0	14.0859	2.6	1.6165	2.8	0.1652	1.0	0.36	985.7	9.3	976.6	17.5	956.3	53.2	956.3	53.2	103.1
-Spot 64	72	30491	5.2	14.0290	1.0	1.5922	1.5	0.1621	1.1	0.72	968.3	9.7	967.2	9.2	964.6	20.8	964.6	20.8	100.4
-Spot 56	29	7153	2.0	13.8388	1.6	1.6804	1.8	0.1687	0.9	0.48	1005.1	8.1	1001.1	11.5	992.4	32.1	992.4	32.1	101.3
-Spot 97	457	36950	4.7	13.8100	0.6	1.6868	1.3	0.1690	1.2	0.88	1006.7	10.9	1003.6	8.4	996.6	12.6	996.6	12.6	101.0
-Spot 47	49	8065	2.2	13.7852	0.9	1.7003	1.6	0.1701	1.3	0.81	1012.5	12.0	1008.7	10.2	1000.3	19.1	1000.3	19.1	101.2
-Spot 88	36	17366	2.4	13.7798	0.9	1.6034	1.3	0.1603	1.0	0.76	958.5	9.0	971.5	8.3	1001.1	17.5	1001.1	17.5	95.8
-Spot 9	63	20325	3.0	13.7760	0.8	1.7477	1.2	0.1747	0.8	0.71	1037.9	8.1	1026.3	7.7	1001.6	17.0	1001.6	17.0	103.6
-Spot 79	37	5479	2.9	13.7314	2.0	1.7390	2.2	0.1733	1.0	0.46	1030.1	9.8	1023.1	14.3	1008.2	39.8	1008.2	39.8	102.2
-Spot 13	49	12983	1.7	13.7082	1.0	1.6346	1.5	0.1626	1.1	0.72	971.1	9.6	983.6	9.3	1011.6	20.7	1011.6	20.7	96.0
-Spot 61	136	18715	9.7	13.7008	0.7	1.7276	1.4	0.1717	1.2	0.85	1021.7	11.1	1018.8	8.9	1012.7	14.6	1012.7	14.6	100.9
-Spot 62	50	75999	0.6	13.6969	0.8	1.7223	1.3	0.1712	1.0	0.78	1018.5	9.3	1016.9	8.2	1013.3	16.1	1013.3	16.1	100.5
-Spot 30	323	189580	3.5	13.6956	0.8	1.7176	1.4	0.1707	1.1	0.83	1015.9	10.7	1015.1	8.8	1013.5	15.5	1013.5	15.5	100.2
-Spot 14	90	33468	1.2	13.6458	0.8	1.6969	1.4	0.1680	1.1	0.81	1001.2	10.6	1007.4	9.0	1020.9	16.8	1020.9	16.8	98.1
-Spot 87	52	61812	3.0	13.6435	1.0	1.7303	1.5	0.1713	1.1	0.75	1019.2	10.3	1019.8	9.4	1021.2	19.5	1021.2	19.5	99.8
-Spot 77	119	33361	3.8	13.6086	0.8	1.7494	1.1	0.1727	0.8	0.74	1027.2	7.9	1027.0	7.3	1026.4	15.6	1026.4	15.6	100.1
-Spot 108	220	134990	2.9	13.5886	0.5	1.7358	1.2	0.1711	1.0	0.89	1018.4	9.7	1021.9	7.5	1029.4	10.9	1029.4	10.9	98.9
-Spot 107	89	13465	1.5	13.5327	0.9	1.8381	1.4	0.1805	1.0	0.74	1069.6	10.0	1059.2	9.0	1037.7	18.8	1037.7	18.8	103.1
-Spot 100	115	4602286	2.9	13.5166	0.9	1.7000	1.4	0.1667	1.0	0.77	994.0	9.5	1008.5	8.7	1040.1	17.6	1040.1	17.6	95.6
-Spot 93	63	16680	1.3	13.5023	0.9	1.8571	1.4	0.1819	1.1	0.77	1077.6	10.9	1066.0	9.4	1042.3	18.3	1042.3	18.3	103.4
-Spot 37	231	24089	4.2	13.4473	0.8	1.7115	1.3	0.1670	1.1	0.81	995.5	9.8	1012.8	8.4	1050.5	15.3	1050.5	15.3	94.8
-Spot 48	126	15251	1.3	13.4093	0.6	1.7772	1.2	0.1729	1.0	0.85	1028.2	9.4	1037.2	7.6	1056.2	12.2	1056.2	12.2	97.3
-Spot 68	156	36706	2.7	13.3336	0.8	1.8492	1.1	0.1789	0.8	0.68	1061.0	7.5	1063.2	7.5	1067.6	16.8	1067.6	16.8	99.4
-Spot 53	223	58552	2.5	13.3310	0.6	1.8205	1.1	0.1761	0.9	0.82	1045.6	8.9	1052.9	7.4	1068.0	12.8	1068.0	12.8	97.9
-Spot 69	92	115837	2.5	13.3089	0.7	1.8556	1.1	0.1792	0.9	0.81	1062.6	8.8	1065.4	7.4	1071.3	13.2	1071.3	13.2	99.2
-Spot 98	261	71303	1.9	13.3055	0.7	1.8394	1.5	0.1776	1.3	0.89	1053.7	12.8	1059.6	9.8	1071.8	13.7	1071.8	13.7	98.3
-Spot 33	105	843823	2.2	13.2906	0.7	1.8661	1.1	0.1800	0.8	0.78	1066.7	8.0	1069.2	7.0	1074.1	13.3	1074.1	13.3	99.3
-Spot 2	42	6859	3.5	13.2774	0.8	1.8943	1.1	0.1825	0.8	0.74	1080.6	8.2	1079.1	7.4	1076.1	15.1	1076.1	15.1	100.4
-Spot 89	175	148229	2.9	13.2696	0.6	1.8683	1.1	0.1799	0.9	0.80	1066.4	8.5	1069.9	7.2	1077.2	13.0	1077.2	13.0	99.0
-Spot 102	110	18908	2.0	13.2631	0.7	1.8307	1.3	0.1762	1.0	0.82	1046.0	10.0	1056.5	8.3	1078.3	14.3	1078.3	14.3	97.0
-Spot 50	52	15609	1.7	13.2602	0.9	1.8273	1.5	0.1758	1.1	0.78	1044.1	11.1	1055.3	9.7	1078.7	18.6	1078.7	18.6	96.8
-Spot 109	43	15904	1.1	13.2593	1.1	1.8275	1.4	0.1758	1.0	0.67	1044.1	9.2	1055.4	9.4	1078.8	21.4	1078.8	21.4	96.8
-Spot 81	115	43675	1.2	13.2505	0.6	1.9110	1.1	0.1837	0.9	0.80	1087.3	8.5	1084.9	7.1	1080.1	12.7	1080.1	12.7	100.7
-Spot 60	181	8416219	2.8	13.0966	0.6	1.9813	1.0	0.1883	0.9	0.82	1112.0	8.7	1109.1	7.0	1103.5	11.9	1103.5	11.9	100.8
-Spot 90	60	11276	3.0	13.0938	0.8	1.9609	1.3	0.1863	1.1	0.82	1101.3	11.2	1102.2	9.0	1104.0	15.3	1104.0	15.3	99.8
-Spot 7	101	23654	2.1	13.0686	0.7	1.9575	1.2	0.1856	1.0	0.80	1097.6	9.7	1101.0	8.1	1107.8	14.4	1107.8	14.4	99.1
-Spot 27	22	13460	4.1	13.0640	1.3	2.0282	1.7	0.1923	1.1	0.65	1133.6	11.9	1125.0	11.9	1108.5	26.5	1108.5	26.5	102.3
-Spot 16	85	107444	1.7	13.0490	0.9	2.0145	1.4	0.1907	1.0	0.75	1125.4	10.8	1120.4	9.5	1110.8	18.5	1110.8	18.5	101.3
-Spot 34	98	330584	2.9	13.0452	0.9	1.8936	1.3	0.1792	0.9	0.74	1062.8	9.2	1078.9	8.5	1111.4	17.2	1111.4	17.2	95.6
-Spot 19	156	82584	1.9	13.0361	0.8	1.9226	1.2	0.1818	0.8	0.70	1077.1	8.0	1089.0	7.8	1112.8	16.7	1112.8	16.7	96.8
-Spot 31	74	15044	1.3	12.9335	0.8	2.0063	1.3	0.1883	1.0	0.79	1112.0	10.0	1117.6	8.5	1128.5	15.4	1128.5	15.4	98.5
-Spot 10	143	28018	3.0	12.9117	0.8	2.1238	1.3	0.1990	1.1	0.82	1169.8	11.6	1156.6	9.2	1131.9	15.3	1131.9	15.3	103.3
-Spot 52	95	17078	2.7	12.8913	0.7	2.0198	1.1	0.1889	0.8	0.74	1115.5	8.1	1122.2	7.3	1135.1	14.4	1135.1	14.4	98.3
-Spot 20	114	13110	2.9	12.8831	0.9	2.0755	1.3	0.1940	1.0	0.75	1143.1	10.2	1140.8	8.9	1136.3	17.2	1136.3	17.2	100.6
-Spot 35	99	11192	2.6	12.8561	0.8	2.0141	1.3	0.1879	1.1	0.79	1109.8	10.9	1120.3	9.2	1140.5	16.3	1140.5	16.3	97.3
-Spot 104	135	29136	2.4	12.8450	0.8	2.0730	1.3	0.1932	1.0	0.77	1138.7	10.5	1139.9	8.9	1142.2	16.5	1142.2	16.5	99.7
-Spot 58	109	34928	1.8	12.8300	0.8	2.1025	1.1	0.1957	0.8	0.68	1152.3	8.1	1149.6	7.8	1144.6	16.4	1144.6	16.4	100.7
-Spot 73	429	45976	3.2	12.7707	0.7	2.1623	1.5	0.2004	1.4	0.89	1177.3	14.8	1169.0	10.7	1153.7	14.3	1153.7	14.3	102.0

-Spot 57	68	110259	3.3	12.6961	0.7	2.0989	1.2	0.1934	1.0	0.84	1139.5	10.8	1148.5	8.5	1165.3	13.4	1165.3	13.4	97.8
-Spot 71	91	62830	2.2	12.6667	0.7	2.0889	1.2	0.1920	1.0	0.81	1132.1	10.4	1145.2	8.4	1170.0	14.2	1170.0	14.2	96.8
-Spot 70	55	58135	2.6	12.6638	0.8	2.0597	1.2	0.1893	0.8	0.70	1117.4	8.5	1135.5	8.0	1170.4	16.6	1170.4	16.6	95.5
-Spot 86	102	10591	3.0	12.5941	1.4	2.1179	1.7	0.1935	1.0	0.59	1140.5	10.7	1154.6	12.0	1181.3	27.9	1181.3	27.9	96.5
-Spot 84	111	91301	3.8	12.5056	0.8	2.1854	1.3	0.1983	1.0	0.80	1166.2	11.1	1176.4	9.1	1195.3	15.5	1195.3	15.5	97.6
-Spot 54	120	88741	2.4	12.3787	0.8	2.2617	1.3	0.2031	1.0	0.77	1192.2	10.6	1200.4	9.0	1215.4	16.2	1215.4	16.2	98.1
-Spot 55	140	344143	2.4	12.2951	0.7	2.2988	1.2	0.2051	1.0	0.80	1202.6	10.8	1211.9	8.7	1228.7	14.6	1228.7	14.6	97.9
-Spot 18	125	50516	2.7	12.0496	0.6	2.4263	1.1	0.2121	0.9	0.84	1240.1	10.0	1250.4	7.6	1268.1	11.2	1268.1	11.2	97.8
-Spot 38	53	115269	3.2	11.8236	0.9	2.4826	1.3	0.2130	0.9	0.73	1244.7	10.5	1267.0	9.2	1305.0	16.8	1305.0	16.8	95.4
-Spot 11	146	421805	3.3	11.6388	0.7	2.6019	1.3	0.2197	1.1	0.86	1280.4	13.3	1301.2	9.8	1335.5	13.2	1335.5	13.2	95.9
-Spot 59	57	82780	1.5	11.6086	0.6	2.6481	1.1	0.2230	0.9	0.82	1298.0	10.2	1314.1	7.8	1340.5	11.8	1340.5	11.8	96.8
-Spot 17	139	71066	1.2	11.5906	0.7	2.6191	1.2	0.2203	0.9	0.80	1283.3	10.7	1306.0	8.5	1343.5	13.3	1343.5	13.3	95.5
-Spot 49	18	7898	0.6	11.4993	0.9	2.7795	1.3	0.2319	0.9	0.72	1344.5	11.5	1350.0	9.9	1358.8	17.9	1358.8	17.9	98.9
-Spot 23	66	33936	3.1	11.4056	0.9	2.8349	1.4	0.2346	1.1	0.75	1358.6	12.9	1364.8	10.6	1374.5	18.0	1374.5	18.0	98.8
-Spot 24	193	31462	1.7	11.3592	0.7	2.7360	1.2	0.2255	1.0	0.81	1310.9	11.3	1338.3	8.8	1382.4	13.4	1382.4	13.4	94.8
-Spot 63	28	6702	2.3	11.3006	0.8	2.9272	1.4	0.2400	1.1	0.81	1386.8	14.0	1389.0	10.5	1392.3	15.7	1392.3	15.7	99.6
-Spot 91	84	15832	2.6	11.2942	0.7	2.8691	1.2	0.2351	0.9	0.78	1361.3	11.5	1373.8	9.0	1393.4	14.2	1393.4	14.2	97.7
-Spot 99	202	100073	2.7	11.2876	0.8	2.8437	1.2	0.2329	1.0	0.79	1349.7	12.0	1367.1	9.4	1394.5	14.6	1394.5	14.6	96.8
-Spot 43	179	21128	2.8	11.1824	1.0	2.9579	1.4	0.2400	1.0	0.71	1386.7	12.2	1396.9	10.4	1412.5	18.6	1412.5	18.6	98.2
-Spot 46	65	36883	2.4	11.0405	0.7	3.2308	1.1	0.2588	0.8	0.75	1483.8	10.6	1464.6	8.3	1436.8	13.6	1436.8	13.6	103.3
-Spot 76	303	73425	3.2	10.8117	0.5	3.3356	1.2	0.2617	1.1	0.92	1498.4	14.8	1489.4	9.4	1476.7	9.1	1476.7	9.1	101.5
-Spot 44	74	411513	2.3	10.7559	0.7	3.2333	1.1	0.2523	0.8	0.79	1450.5	11.0	1465.2	8.3	1486.5	12.5	1486.5	12.5	97.6
-Spot 83	84	38388	2.1	10.7413	0.6	3.2619	1.0	0.2542	0.8	0.78	1460.2	10.4	1472.0	7.9	1489.0	12.1	1489.0	12.1	98.1
-Spot 28	134	67620	3.1	10.6746	0.7	3.3207	1.3	0.2572	1.0	0.82	1475.5	13.7	1485.9	9.9	1500.8	13.8	1500.8	13.8	98.3
-Spot 103	172	158074	3.2	10.6647	0.6	3.0950	1.2	0.2395	1.0	0.85	1384.1	12.5	1431.5	9.1	1502.6	11.9	1502.6	11.9	92.1
-Spot 26	159	42248	2.3	10.3062	0.8	3.6902	1.2	0.2760	0.9	0.76	1571.0	12.8	1569.2	9.6	1566.9	14.7	1566.9	14.7	100.3
-Spot 39	170	152648	1.6	10.2174	0.6	3.7300	1.1	0.2765	0.9	0.84	1573.8	12.5	1577.8	8.5	1583.1	10.8	1583.1	10.8	99.4

Table 4. JFM-1

Analysis	U	206Pb	U/Th	206Pb*	±	207Pb*	±	206Pb*	±	error	206Pb*	±	207Pb*	±	206Pb*	±	Best age	±	Conc
	(ppm)	204Pb		207Pb*	(%)	235U*	(%)	238U	(%)	corr.	238U*	(Ma)	235U	(Ma)	207Pb*	(Ma)	(Ma)	(Ma)	(%)
-SAMPLE 1 Spot 5	616	20562	0.6	18.2942	0.6	0.4692	1.1	0.0623	0.9	0.81	389.5	3.2	390.7	3.4	397.4	13.8	389.5	3.2	99.7
-SAMPLE 1 Spot 22	315	14253	1.5	18.2954	0.9	0.4856	1.3	0.0645	0.9	0.68	402.7	3.4	401.9	4.2	397.3	20.9	402.7	3.4	101.4
-SAMPLE 1 Spot 21	2283	30493	4.1	17.7199	0.6	0.5060	1.2	0.0651	1.0	0.85	406.3	3.9	415.7	4.0	468.5	13.8	406.3	3.9	86.7
-SAMPLE 1 Spot 11	240	3008	0.7	18.4070	1.4	0.4966	1.7	0.0663	0.9	0.54	414.0	3.7	409.4	5.8	383.6	32.3	414.0	3.7	107.9
-SAMPLE 1 Spot 17	411	14902	1.2	17.8110	0.9	0.5489	1.4	0.0709	1.1	0.76	441.8	4.5	444.3	5.0	457.1	20.0	441.8	4.5	96.6
-SAMPLE 1 Spot 48	1085	28634	5.0	17.4252	0.7	0.5778	1.3	0.0731	1.1	0.85	454.5	4.7	463.0	4.7	505.5	14.9	454.5	4.7	89.9
-SAMPLE 1 Spot 30	320	13910	2.5	18.1480	0.8	0.5598	1.2	0.0737	0.9	0.75	458.5	3.9	451.4	4.2	415.4	17.2	458.5	3.9	110.4
-SAMPLE 1 Spot 38	33	2322	2.4	18.2031	2.7	0.5647	2.9	0.0746	1.2	0.41	463.7	5.4	454.6	10.7	408.6	59.7	463.7	5.4	113.5
-SAMPLE 1 Spot 23	350	15020	1.2	17.2912	0.8	0.6158	1.0	0.0773	0.6	0.62	479.8	3.0	487.2	4.0	522.5	17.9	479.8	3.0	91.8
-SAMPLE 1 Spot 26	484	2413	1.0	13.0580	6.2	0.8967	6.4	0.0850	1.6	0.25	525.6	8.0	649.9	30.6	1109.4	123.3	525.6	8.0	47.4
-SAMPLE 1 Spot 32	97	6526	1.5	14.2088	0.9	1.5784	1.3	0.1627	0.9	0.72	971.9	8.3	961.7	7.9	938.6	18.2	938.6	18.2	103.6
-SAMPLE 1 Spot 36	742	51504	1.9	14.2073	0.5	1.5229	1.1	0.1570	1.0	0.89	940.1	8.7	939.7	6.9	938.8	10.6	938.8	10.6	100.1
-SAMPLE 1 Spot 29	1350	113502	2.1	13.9428	0.7	1.6401	1.3	0.1659	1.2	0.87	989.6	10.7	985.7	8.4	977.1	13.4	977.1	13.4	101.3
-SAMPLE 1 Spot 12	55	25562	0.3	13.7217	0.9	1.6926	1.3	0.1685	0.9	0.72	1004.0	8.5	1005.8	8.0	1009.6	17.6	1009.6	17.6	99.4
-SAMPLE 1 Spot 8	145	10582	1.9	13.6469	1.0	1.7814	1.3	0.1764	0.8	0.63	1047.2	7.7	1038.7	8.2	1020.7	20.0	1020.7	20.0	102.6
-SAMPLE 1 Spot 4	151	22304	2.2	13.5977	0.6	1.8254	1.1	0.1801	0.9	0.81	1067.5	8.5	1054.6	7.0	1028.0	12.8	1028.0	12.8	103.8
-SAMPLE 1 Spot 20	204	21719	1.0	13.4951	1.2	1.7133	1.5	0.1678	0.9	0.61	999.8	8.6	1013.5	9.8	1043.4	24.5	1043.4	24.5	95.8
-SAMPLE 1 Spot 42	49	2955	2.3	13.3563	2.0	1.7896	2.2	0.1734	1.0	0.44	1031.0	9.1	1041.7	14.2	1064.2	39.4	1064.2	39.4	96.9
-SAMPLE 1 Spot 16	101	36959	2.0	13.3162	0.8	1.9252	1.3	0.1860	0.9	0.74	1099.7	9.4	1089.9	8.4	1070.2	16.9	1070.2	16.9	102.8
-SAMPLE 1 Spot 18	363	14638	2.2	13.3139	0.5	1.8311	1.0	0.1769	0.8	0.85	1049.9	8.0	1056.7	6.4	1070.6	10.4	1070.6	10.4	98.1
-SAMPLE 1 Spot 47	126	11730	1.0	13.1379	0.9	1.9128	1.3	0.1823	0.9	0.71	1079.8	8.8	1085.6	8.3	1097.2	17.7	1097.2	17.7	98.4
-SAMPLE 1 Spot 9	445	80665	2.8	13.0932	0.6	1.9331	1.1	0.1836	0.9	0.81	1086.9	9.1	1092.6	7.5	1104.1	12.9	1104.1	12.9	98.4
-SAMPLE 1 Spot 39	326	17561	2.2	13.0407	0.6	1.9782	0.9	0.1872	0.7	0.75	1106.1	7.1	1108.1	6.3	1112.1	12.5	1112.1	12.5	99.5
-SAMPLE 1 Spot 46	118	22559	1.4	13.0002	0.8	1.8887	1.8	0.1782	1.6	0.90	1056.9	15.9	1077.1	12.1	1118.3	15.9	1118.3	15.9	94.5
-SAMPLE 1 Spot 33	325	59274	2.8	12.9694	0.6	2.0212	1.1	0.1902	1.0	0.87	1122.5	10.0	1122.7	7.6	1123.0	11.1	1123.0	11.1	100.0
-SAMPLE 1 Spot 24	84	27535	18.4	12.1695	0.9	2.2703	1.5	0.2005	1.2	0.80	1177.8	12.7	1203.1	10.3	1248.8	17.1	1248.8	17.1	94.3
-SAMPLE 1 Spot 45	41	18272	1.7	11.9379	1.2	2.2006	1.6	0.1906	1.1	0.66	1124.7	11.1	1181.2	11.3	1286.3	23.5	1286.3	23.5	87.4
-SAMPLE 1 Spot 27	130	38123	3.4	11.8434	0.8	2.5681	1.4	0.2207	1.1	0.82	1285.5	13.2	1291.6	10.1	1301.7	15.2	1301.7	15.2	98.8
-SAMPLE 1 Spot 10	1654	11809	8.1	11.6710	1.0	2.2555	1.4	0.1910	1.1	0.75	1126.8	11.1	1198.5	10.1	1330.2	18.4	1330.2	18.4	84.7
-SAMPLE 1 Spot 37	171	18053	2.3	11.4898	0.8	2.7909	1.3	0.2327	1.1	0.80	1348.5	12.9	1353.1	10.0	1360.4	15.6	1360.4	15.6	99.1
-SAMPLE 1 Spot 34	115	486900	2.0	10.8874	0.8	3.1880	1.3	0.2518	1.0	0.78	1448.0	13.1	1454.3	10.0	1463.4	15.5	1463.4	15.5	98.9
-SAMPLE 1 Spot 1	495	35947	11.0	10.8357	0.6	3.1408	1.0	0.2469	0.8	0.77	1422.6	9.9	1442.7	7.8	1472.5	12.2	1472.5	12.2	96.6
-SAMPLE 1 Spot 35	193	52267	1.0	10.7752	0.6	3.3374	1.1	0.2609	1.0	0.85	1494.6	12.8	1489.8	8.8	1483.1	11.4	1483.1	11.4	100.8
-SAMPLE 1 Spot 50	343	45152	2.5	10.7347	0.6	3.3119	1.0	0.2580	0.8	0.79	1479.4	10.3	1483.9	7.7	1490.2	11.4	1490.2	11.4	99.3
-SAMPLE 1 Spot 28	454	45792	3.6	10.7329	0.6	3.3194	1.0	0.2585	0.8	0.82	1482.2	11.2	1485.6	8.0	1490.5	11.0	1490.5	11.0	99.4
-SAMPLE 1 Spot 6	794	73225	1.6	10.6881	0.4	3.3714	1.1	0.2615	1.0	0.93	1497.3	13.1	1497.8	8.3	1498.5	7.5	1498.5	7.5	99.9
-SAMPLE 1 Spot 2	446	355907	1.9	10.5415	0.5	3.4255	0.8	0.2620	0.7	0.82	1500.1	8.9	1510.3	6.3	1524.5	8.6	1524.5	8.6	98.4
-SAMPLE 1 Spot 43	2097	11800464	1.5	10.3007	0.6	3.4044	1.3	0.2544	1.2	0.88	1461.4	15.2	1505.4	10.4	1568.0	11.9	1568.0	11.9	93.2
-SAMPLE 1 Spot 49	335	46369	1.4	9.7379	0.6	4.2062	1.0	0.2972	0.8	0.81	1677.4	11.9	1675.2	8.2	1672.5	11.0	1672.5	11.0	100.3
-SAMPLE 1 Spot 13	1294	28608	1.3	9.2465	0.7	4.4457	1.2	0.2983	1.0	0.84	1682.7	15.4	1720.9	10.2	1767.7	12.1	1767.7	12.1	95.2
-SAMPLE 1 Spot 25	79	6304	0.7	9.0306	0.9	5.1840	1.3	0.3397	0.9	0.70	1885.1	15.1	1850.0	11.2	1810.7	17.1	1810.7	17.1	104.1
-SAMPLE 1 Spot 3	1970	16262	8.5	8.9969	0.7	4.2765	1.2	0.2792	1.0	0.83	1587.2	14.3	1688.8	10.1	1817.5	12.6	1817.5	12.6	87.3
-SAMPLE 1 Spot 15	536	628566	9.0	8.9307	0.7	4.9647	1.7	0.3217	1.5	0.90	1798.1	23.5	1813.3	14.1	1830.9	13.2	1830.9	13.2	98.2
-SAMPLE 1 Spot 14	219	32279	2.0	7.7337	0.6	6.3065	1.0	0.3539	0.8	0.82	1953.1	13.8	2019.4	8.8	2087.7	10.0	2087.7	10.0	93.6
-SAMPLE 1 Spot 41	167	351	1.2	6.6777	18.0	1.6851	18.6	0.0816	4.7	0.25	505.9	22.8	1002.9	118.9	2342.3	310.3	2342.3	310.3	21.6
-SAMPLE 1 Spot 44	229	53900	3.5	5.7573	1.3	11.4938	2.5	0.4801	2.2	0.85	2527.9	45.1	2564.1	23.7	2592.8	22.4	2592.8	22.4	97.5
Analysis	U	206Pb	U/Th	206Pb*	±	207Pb*	±	206Pb*	±	error	206Pb*	±	207Pb*	±	206Pb*	±	Best age	±	Conc
	(ppm)	204Pb		207Pb*	(%)	235U*	(%)	238U	(%)	corr.	238U*	(Ma)	235U	(Ma)	207Pb*	(Ma)	(Ma)	(Ma)	(%)
-SAMPLE 1 Spot 5	616	20562	0.6	18.2942	0.6	0.4692	1.1	0.0623	0.9	0.81	389.5	3.2	390.7	3.4	397.4	13.8	389.5	3.2	99.7
-SAMPLE 1 Spot 22	315	14253	1.5	18.2954	0.9	0.4856	1.3	0.0645	0.9	0.68	402.7	3.4	401.9	4.2	397.3	20.9	402.7	3.4	101.4

-SAMPLE 1 Spot 21	2283	30493	4.1	17.7199	0.6	0.5060	1.2	0.0651	1.0	0.85	406.3	3.9	415.7	4.0	468.5	13.8	406.3	3.9	86.7
-SAMPLE 1 Spot 11	240	3008	0.7	18.4070	1.4	0.4966	1.7	0.0663	0.9	0.54	414.0	3.7	409.4	5.8	383.6	32.3	414.0	3.7	107.9
-SAMPLE 1 Spot 17	411	14902	1.2	17.8110	0.9	0.5489	1.4	0.0709	1.1	0.76	441.8	4.5	444.3	5.0	457.1	20.0	441.8	4.5	96.6
-SAMPLE 1 Spot 48	1085	28634	5.0	17.4252	0.7	0.5778	1.3	0.0731	1.1	0.85	454.5	4.7	463.0	4.7	505.5	14.9	454.5	4.7	89.9
-SAMPLE 1 Spot 30	320	13910	2.5	18.1480	0.8	0.5598	1.2	0.0737	0.9	0.75	458.5	3.9	451.4	4.2	415.4	17.2	458.5	3.9	110.4
-SAMPLE 1 Spot 38	33	2322	2.4	18.2031	2.7	0.5647	2.9	0.0746	1.2	0.41	463.7	5.4	454.6	10.7	408.6	59.7	463.7	5.4	113.5
-SAMPLE 1 Spot 23	350	15020	1.2	17.2912	0.8	0.6158	1.0	0.0773	0.6	0.62	479.8	3.0	487.2	4.0	522.5	17.9	479.8	3.0	91.8
-SAMPLE 1 Spot 26	484	2413	1.0	13.0580	6.2	0.8967	6.4	0.0850	1.6	0.25	525.6	8.0	649.9	30.6	1109.4	123.3	525.6	8.0	47.4
-SAMPLE 1 Spot 32	97	6526	1.5	14.2088	0.9	1.5784	1.3	0.1627	0.9	0.72	971.9	8.3	961.7	7.9	938.6	18.2	938.6	18.2	103.6
-SAMPLE 1 Spot 36	742	51504	1.9	14.2073	0.5	1.5229	1.1	0.1570	1.0	0.89	940.1	8.7	939.7	6.9	938.8	10.6	938.8	10.6	100.1
-SAMPLE 1 Spot 29	1350	113502	2.1	13.9428	0.7	1.6401	1.3	0.1659	1.2	0.87	989.6	10.7	985.7	8.4	977.1	13.4	977.1	13.4	101.3
-SAMPLE 1 Spot 12	55	25562	0.3	13.7217	0.9	1.6926	1.3	0.1685	0.9	0.72	1004.0	8.5	1005.8	8.0	1009.6	17.6	1009.6	17.6	99.4
-SAMPLE 1 Spot 8	145	10582	1.9	13.6469	1.0	1.7814	1.3	0.1764	0.8	0.63	1047.2	7.7	1038.7	8.2	1020.7	20.0	1020.7	20.0	102.6
-SAMPLE 1 Spot 4	151	22304	2.2	13.5977	0.6	1.8254	1.1	0.1801	0.9	0.81	1067.5	8.5	1054.6	7.0	1028.0	12.8	1028.0	12.8	103.8
-SAMPLE 1 Spot 20	204	21719	1.0	13.4951	1.2	1.7133	1.5	0.1678	0.9	0.61	999.8	8.6	1013.5	9.8	1043.4	24.5	1043.4	24.5	95.8
-SAMPLE 1 Spot 42	49	2955	2.3	13.3563	2.0	1.7896	2.2	0.1734	1.0	0.44	1031.0	9.1	1041.7	14.2	1064.2	39.4	1064.2	39.4	96.9
-SAMPLE 1 Spot 16	101	36959	2.0	13.3162	0.8	1.9252	1.3	0.1860	0.9	0.74	1099.7	9.4	1089.9	8.4	1070.2	16.9	1070.2	16.9	102.8
-SAMPLE 1 Spot 18	363	14638	2.2	13.3139	0.5	1.8311	1.0	0.1769	0.8	0.85	1049.9	8.0	1056.7	6.4	1070.6	10.4	1070.6	10.4	98.1
-SAMPLE 1 Spot 47	126	11730	1.0	13.1379	0.9	1.9128	1.3	0.1823	0.9	0.71	1079.8	8.8	1085.6	8.3	1097.2	17.7	1097.2	17.7	98.4
-SAMPLE 1 Spot 9	445	80665	2.8	13.0932	0.6	1.9331	1.1	0.1836	0.9	0.81	1086.9	9.1	1092.6	7.5	1104.1	12.9	1104.1	12.9	98.4
-SAMPLE 1 Spot 39	326	17561	2.2	13.0407	0.6	1.9782	0.9	0.1872	0.7	0.75	1106.1	7.1	1108.1	6.3	1112.1	12.5	1112.1	12.5	99.5
-SAMPLE 1 Spot 46	118	22559	1.4	13.0002	0.8	1.8887	1.8	0.1782	1.6	0.90	1056.9	15.9	1077.1	12.1	1118.3	15.9	1118.3	15.9	94.5
-SAMPLE 1 Spot 33	325	59274	2.8	12.9694	0.6	2.0212	1.1	0.1902	1.0	0.87	1122.5	10.0	1122.7	7.6	1123.0	11.1	1123.0	11.1	100.0
-SAMPLE 1 Spot 24	84	27535	18.4	12.1695	0.9	2.2703	1.5	0.2005	1.2	0.80	1177.8	12.7	1203.1	10.3	1248.8	17.1	1248.8	17.1	94.3
-SAMPLE 1 Spot 45	41	18272	1.7	11.9379	1.2	2.2006	1.6	0.1906	1.1	0.66	1124.7	11.1	1181.2	11.3	1286.3	23.5	1286.3	23.5	87.4
-SAMPLE 1 Spot 27	130	38123	3.4	11.8434	0.8	2.5681	1.4	0.2207	1.1	0.82	1285.5	13.2	1291.6	10.1	1301.7	15.2	1301.7	15.2	98.8
-SAMPLE 1 Spot 10	1654	11809	8.1	11.6710	1.0	2.2555	1.4	0.1910	1.1	0.75	1126.8	11.1	1198.5	10.1	1330.2	18.4	1330.2	18.4	84.7
-SAMPLE 1 Spot 37	171	18053	2.3	11.4898	0.8	2.7909	1.3	0.2327	1.1	0.80	1348.5	12.9	1353.1	10.0	1360.4	15.6	1360.4	15.6	99.1
-SAMPLE 1 Spot 34	115	486900	2.0	10.8874	0.8	3.1880	1.3	0.2518	1.0	0.78	1448.0	13.1	1454.3	10.0	1463.4	15.5	1463.4	15.5	98.9
-SAMPLE 1 Spot 1	495	35947	11.0	10.8357	0.6	3.1408	1.0	0.2469	0.8	0.77	1422.6	9.9	1442.7	7.8	1472.5	12.2	1472.5	12.2	96.6
-SAMPLE 1 Spot 35	193	52267	1.0	10.7752	0.6	3.3374	1.1	0.2609	1.0	0.85	1494.6	12.8	1489.8	8.8	1483.1	11.4	1483.1	11.4	100.8
-SAMPLE 1 Spot 50	343	45152	2.5	10.7347	0.6	3.3119	1.0	0.2580	0.8	0.79	1479.4	10.3	1483.9	7.7	1490.2	11.4	1490.2	11.4	99.3
-SAMPLE 1 Spot 28	454	45792	3.6	10.7329	0.6	3.3194	1.0	0.2585	0.8	0.82	1482.2	11.2	1485.6	8.0	1490.5	11.0	1490.5	11.0	99.4
-SAMPLE 1 Spot 6	794	73225	1.6	10.6881	0.4	3.3714	1.1	0.2615	1.0	0.93	1497.3	13.1	1497.8	8.3	1498.5	7.5	1498.5	7.5	99.9
-SAMPLE 1 Spot 2	446	355907	1.9	10.5415	0.5	3.4255	0.8	0.2620	0.7	0.82	1500.1	8.9	1510.3	6.3	1524.5	8.6	1524.5	8.6	98.4
-SAMPLE 1 Spot 43	2097	11800464	1.5	10.3007	0.6	3.4044	1.3	0.2544	1.2	0.88	1461.4	15.2	1505.4	10.4	1568.0	11.9	1568.0	11.9	93.2
-SAMPLE 1 Spot 49	335	46369	1.4	9.7379	0.6	4.2062	1.0	0.2972	0.8	0.81	1677.4	11.9	1675.2	8.2	1672.5	11.0	1672.5	11.0	100.3
-SAMPLE 1 Spot 13	1294	28608	1.3	9.2465	0.7	4.4457	1.2	0.2983	1.0	0.84	1682.7	15.4	1720.9	10.2	1767.7	12.1	1767.7	12.1	95.2
-SAMPLE 1 Spot 25	79	6304	0.7	9.0306	0.9	5.1840	1.3	0.3397	0.9	0.70	1885.1	15.1	1850.0	11.2	1810.7	17.1	1810.7	17.1	104.1
-SAMPLE 1 Spot 3	1970	16262	8.5	8.9969	0.7	4.2765	1.2	0.2792	1.0	0.83	1587.2	14.3	1688.8	10.1	1817.5	12.6	1817.5	12.6	87.3
-SAMPLE 1 Spot 15	536	628566	9.0	8.9307	0.7	4.9647	1.7	0.3217	1.5	0.90	1798.1	23.5	1813.3	14.1	1830.9	13.2	1830.9	13.2	98.2
-SAMPLE 1 Spot 14	219	32279	2.0	7.7337	0.6	6.3065	1.0	0.3539	0.8	0.82	1953.1	13.8	2019.4	8.8	2087.7	10.0	2087.7	10.0	93.6
-SAMPLE 1 Spot 41	167	351	1.2	6.6777	18.0	1.6851	18.6	0.0816	4.7	0.25	505.9	22.8	1002.9	118.9	2342.3	310.3	2342.3	310.3	21.6
-SAMPLE 1 Spot 44	229	53900	3.5	5.7573	1.3	11.4938	2.5	0.4801	2.2	0.85	2527.9	45.1	2564.1	23.7	2592.8	22.4	2592.8	22.4	97.5

Table 5. JFT-1

Table_____. U-Pb geochronologic analyses.																			
						Isotope ratios						Apparent ages (Ma)							
Analysis	U	206Pb	U/Th	206Pb*	±	207Pb*	±	206Pb*	±	error	206Pb*	±	207Pb*	±	206Pb*	±	Best age	±	Conc
	(ppm)	204Pb		207Pb*	(%)	235U*	(%)	238U	(%)	corr.	238U*	(Ma)	235U	(Ma)	207Pb*	(Ma)	(Ma)	(Ma)	(%)
-Spot 55	67	10269	1.3	18.3965	1.9	0.4609	2.1	0.0615	1.0	0.48	384.9	3.8	384.9	6.8	384.9	42.0	384.9	3.8	100.0
-Spot 100	84	8117	2.6	18.0098	1.2	0.4814	1.5	0.0629	1.0	0.65	393.3	3.8	399.1	5.0	432.4	26.0	393.3	3.8	98.6
-Spot 73	485	10720	2.5	18.4069	0.8	0.4722	1.6	0.0631	1.4	0.87	394.3	5.2	392.7	5.1	383.7	17.7	394.3	5.2	100.4
-Spot 58	185	92880	1.1	17.7342	0.9	0.5097	1.4	0.0656	1.0	0.74	409.5	3.9	418.3	4.6	466.7	20.3	409.5	3.9	87.7
-Spot 86	268	9181	1.6	18.4119	0.9	0.4942	1.3	0.0660	1.0	0.75	412.1	4.0	407.7	4.5	383.0	19.8	412.1	4.0	107.6
-Spot 50	326	7416	1.9	18.3927	1.7	0.5033	2.1	0.0672	1.2	0.57	419.1	4.9	413.9	7.2	385.4	39.0	419.1	4.9	108.7
-Spot 14	209	12626	1.3	17.9353	1.1	0.5238	1.4	0.0682	0.9	0.64	425.1	3.7	427.7	5.0	441.7	24.5	425.1	3.7	96.3
-Spot 24	342	59902	1.6	16.5794	0.9	0.5900	1.3	0.0710	0.9	0.72	442.0	4.0	470.9	4.9	614.0	19.4	442.0	4.0	72.0
-Spot 23	214	196848	1.6	16.8847	0.9	0.5930	1.4	0.0727	1.0	0.78	452.1	4.6	472.8	5.1	574.5	18.5	452.1	4.6	78.7
-Spot 15	137	30990	2.4	17.3542	1.0	0.5784	1.3	0.0728	0.9	0.67	453.2	3.9	463.4	4.9	514.5	21.5	453.2	3.9	88.1
-Spot 46	379	33546	1.6	17.5920	0.9	0.5732	1.2	0.0732	0.8	0.68	455.2	3.6	460.1	4.5	484.5	19.8	455.2	3.6	94.0
-Spot 107	76	7998	1.7	17.9429	1.3	0.5768	1.8	0.0751	1.1	0.65	466.8	5.1	462.4	6.5	440.7	29.6	466.8	5.1	105.9
-Spot 85	136	11058	2.1	17.1221	1.0	0.7083	1.4	0.0880	1.0	0.70	543.7	5.1	543.7	5.8	544.0	21.6	543.7	5.1	99.9
-Spot 67	68	9370	2.4	16.9109	1.1	0.7211	1.6	0.0885	1.1	0.71	546.5	5.9	551.3	6.7	571.1	24.1	546.5	5.9	95.7
-Spot 108	187	113730	1.9	16.5614	0.8	0.7914	1.2	0.0951	0.9	0.78	585.6	5.2	592.0	5.4	616.3	16.2	585.6	5.2	95.0
-Spot 91	906	144985	3.4	16.4058	0.7	0.8784	1.3	0.1046	1.1	0.87	641.1	7.0	640.1	6.3	636.7	14.3	641.1	7.0	100.7
-Spot 56	210	839252	3.5	14.3648	0.7	1.4607	1.2	0.1522	0.9	0.79	913.5	8.0	914.3	7.1	916.1	14.8	916.1	14.8	99.7
-Spot 57	591	199632	2.6	13.9866	0.7	1.6108	1.6	0.1635	1.4	0.91	976.0	13.1	974.4	10.0	970.8	13.5	970.8	13.5	100.5
-Spot 70	263	35699	6.1	13.9843	0.8	1.5857	1.3	0.1609	1.1	0.81	961.8	9.4	964.6	8.1	971.1	15.6	971.1	15.6	99.0
-Spot 102	97	39461	0.8	13.9104	0.9	1.5924	1.4	0.1607	1.0	0.75	960.8	9.2	967.2	8.6	981.9	18.7	981.9	18.7	97.9
-Spot 34	76	43491	2.5	13.9063	1.0	1.5899	1.5	0.1604	1.2	0.77	959.1	10.6	966.2	9.6	982.5	19.8	982.5	19.8	97.6
-Spot 82	59	47503	3.3	13.8879	0.9	1.6140	1.5	0.1626	1.2	0.78	971.4	10.4	975.7	9.2	985.2	18.6	985.2	18.6	98.6
-Spot 17	62	8427	2.8	13.7603	0.9	1.7128	1.3	0.1710	1.0	0.71	1017.7	9.1	1013.3	8.6	1003.9	19.1	1003.9	19.1	101.4
-Spot 106	112	78039	4.2	13.7310	0.9	1.5708	1.3	0.1565	0.9	0.71	937.3	7.9	958.7	7.9	1008.3	18.0	1008.3	18.0	93.0
-Spot 90	65	8748	0.8	13.7083	0.9	1.6893	1.4	0.1680	1.0	0.76	1001.3	9.6	1004.5	8.6	1011.6	17.7	1011.6	17.7	99.0
-Spot 40	232	32083	4.6	13.6990	0.7	1.6654	1.1	0.1655	0.8	0.75	987.5	7.5	995.4	7.0	1013.0	14.8	1013.0	14.8	97.5
-Spot 7	344	25688	2.1	13.6693	0.6	1.7430	1.1	0.1729	0.9	0.83	1027.9	9.0	1024.6	7.3	1017.4	12.7	1017.4	12.7	101.0
-Spot 3	301	29372	2.4	13.6567	0.7	1.7308	1.0	0.1715	0.8	0.73	1020.4	7.2	1020.1	6.7	1019.3	14.3	1019.3	14.3	100.1

-Spot 12	29	2994	1.3	13.6524	3.5	1.7187	3.6	0.1703	1.0	0.27	1013.5	9.0	1015.5	23.2	1019.9	70.6	1019.9	70.6	99.4
-Spot 76	616	188881	4.5	13.6391	0.6	1.7260	1.3	0.1708	1.2	0.88	1016.6	11.1	1018.3	8.6	1021.9	12.7	1021.9	12.7	99.5
-Spot 9	74	32605	1.8	13.5829	0.9	1.7220	1.3	0.1697	0.9	0.71	1010.5	8.7	1016.8	8.4	1030.2	18.5	1030.2	18.5	98.1
-Spot 27	182	39436	3.3	13.5715	0.8	1.7293	1.3	0.1703	1.1	0.80	1013.7	9.9	1019.5	8.4	1031.9	15.9	1031.9	15.9	98.2
-Spot 81	168	36437	3.7	13.5627	0.6	1.7607	1.0	0.1733	0.8	0.79	1030.1	7.7	1031.1	6.6	1033.2	12.7	1033.2	12.7	99.7
-Spot 45	82	25771	3.4	13.5579	0.8	1.6926	1.3	0.1665	1.0	0.78	992.8	9.2	1005.7	8.2	1034.0	16.3	1034.0	16.3	96.0
-Spot 20	90	9243	4.5	13.5556	0.8	1.7904	1.2	0.1761	0.9	0.77	1045.6	9.1	1042.0	7.9	1034.3	15.7	1034.3	15.7	101.1
-Spot 84	91	44277	2.5	13.5513	0.9	1.8345	1.2	0.1804	0.8	0.69	1069.0	8.3	1057.9	8.1	1034.9	18.1	1034.9	18.1	103.3
-Spot 26	89	8152	1.5	13.5179	0.9	1.8136	1.3	0.1779	0.9	0.73	1055.4	9.1	1050.4	8.4	1039.9	17.7	1039.9	17.7	101.5
-Spot 61	130	38806	2.8	13.4805	0.8	1.7707	1.2	0.1732	0.9	0.77	1029.7	8.8	1034.8	7.7	1045.5	15.3	1045.5	15.3	98.5
-Spot 38	78	15115	3.6	13.4663	0.9	1.7542	1.3	0.1714	1.0	0.73	1019.8	9.0	1028.7	8.5	1047.7	18.4	1047.7	18.4	97.3
-Spot 11	113	8313	1.6	13.3878	0.8	1.8491	1.2	0.1796	1.0	0.78	1064.9	9.5	1063.1	8.2	1059.5	15.6	1059.5	15.6	100.5
-Spot 36	655	63980	2.3	13.3553	0.7	1.9330	1.4	0.1873	1.2	0.85	1106.8	12.3	1092.6	9.4	1064.3	14.7	1064.3	14.7	104.0
-Spot 83	136	59845	1.4	13.3128	0.7	1.7520	1.1	0.1692	0.9	0.81	1007.9	8.4	1027.9	7.2	1070.7	13.2	1070.7	13.2	94.1
-Spot 99	51	32537	3.2	13.3116	0.8	1.7854	1.2	0.1724	1.0	0.79	1025.6	9.2	1040.1	8.0	1070.9	15.2	1070.9	15.2	95.8
-Spot 48	83	145981	1.5	13.2849	0.7	1.7963	1.2	0.1732	0.9	0.79	1029.5	8.8	1044.1	7.7	1075.0	14.4	1075.0	14.4	95.8
-Spot 80	292	73802	1.0	13.2843	0.6	1.8564	0.9	0.1789	0.7	0.76	1061.2	7.0	1065.7	6.2	1075.0	12.4	1075.0	12.4	98.7
-Spot 22	116	11788	1.6	13.2763	0.7	1.8498	1.1	0.1782	0.8	0.72	1057.1	7.4	1063.4	7.0	1076.2	14.7	1076.2	14.7	98.2
-Spot 10	285	120783	1.7	13.2564	0.7	1.8454	1.2	0.1775	0.9	0.76	1053.3	8.5	1061.8	7.6	1079.3	15.0	1079.3	15.0	97.6
-Spot 101	52	20092	2.1	13.2559	1.0	1.8440	1.4	0.1774	1.1	0.75	1052.5	10.4	1061.3	9.4	1079.3	19.1	1079.3	19.1	97.5
-Spot 72	526	34932	3.4	13.2529	0.6	1.9473	1.4	0.1873	1.2	0.90	1106.5	12.6	1097.5	9.2	1079.8	12.2	1079.8	12.2	102.5
-Spot 35	34	8732	2.0	13.1782	1.2	1.8299	1.5	0.1750	0.9	0.58	1039.5	8.3	1056.3	9.7	1091.1	24.2	1091.1	24.2	95.3
-Spot 66	209	294841	1.9	13.1289	0.7	1.7419	1.2	0.1659	1.0	0.80	989.7	8.8	1024.2	7.8	1098.6	14.6	1098.6	14.6	90.1
-Spot 8	198	56279	2.1	13.1226	0.6	1.8892	1.2	0.1799	1.0	0.85	1066.3	10.2	1077.3	8.1	1099.6	12.7	1099.6	12.7	97.0
-Spot 94	184	34602	2.6	13.0797	0.8	1.8486	1.1	0.1754	0.7	0.67	1042.0	7.0	1062.9	7.2	1106.1	16.1	1106.1	16.1	94.2
-Spot 110	315	393395	3.7	13.0174	0.6	1.9945	1.2	0.1884	1.0	0.85	1112.6	10.1	1113.7	7.9	1115.7	12.4	1115.7	12.4	99.7
-Spot 16	188	105231	3.1	12.9654	0.7	1.8923	1.1	0.1780	0.9	0.79	1056.1	8.8	1078.4	7.6	1123.6	14.1	1123.6	14.1	94.0
-Spot 37	249	148658	2.4	12.9099	0.7	2.0331	1.2	0.1904	1.0	0.83	1123.8	10.4	1126.7	8.3	1132.2	13.6	1132.2	13.6	99.3
-Spot 69	135	14716	3.4	12.8761	0.8	1.9536	1.2	0.1825	1.0	0.78	1080.7	9.5	1099.7	8.2	1137.4	15.1	1137.4	15.1	95.0
-Spot 52	345	115574	3.5	12.8707	0.6	2.0466	1.1	0.1911	0.9	0.81	1127.5	8.9	1131.2	7.2	1138.3	12.2	1138.3	12.2	99.1
-Spot 88	67	19716	3.1	12.7674	0.8	2.1268	1.2	0.1970	0.9	0.72	1159.3	9.1	1157.5	8.2	1154.2	16.3	1154.2	16.3	100.4
-Spot 4	128	129176	2.3	12.7540	0.7	2.1207	1.1	0.1963	0.9	0.77	1155.2	9.1	1155.6	7.7	1156.3	14.1	1156.3	14.1	99.9
-Spot 105	86	36668	2.7	12.7105	0.9	2.0262	1.3	0.1869	1.0	0.76	1104.4	10.2	1124.3	9.0	1163.1	16.9	1163.1	16.9	95.0
-Spot 74	510	5943	1.8	12.4778	2.8	1.8938	3.0	0.1715	1.1	0.37	1020.1	10.5	1078.9	19.9	1199.7	54.8	1199.7	54.8	85.0
-Spot 109	46	14560	5.0	12.4541	1.1	2.1754	1.6	0.1966	1.2	0.75	1156.9	12.6	1173.2	11.1	1203.4	20.8	1203.4	20.8	96.1
-Spot 95	105	29252	1.1	12.3140	0.7	2.2656	1.2	0.2024	0.9	0.78	1188.4	9.9	1201.7	8.2	1225.6	14.3	1225.6	14.3	97.0
-Spot 42	234	59311	3.5	12.1906	0.5	2.3202	1.1	0.2052	1.0	0.88	1203.3	10.7	1218.5	7.9	1245.4	10.4	1245.4	10.4	96.6
-Spot 2	108	137912	4.4	12.1191	0.8	2.3891	1.2	0.2101	0.9	0.76	1229.3	10.1	1239.3	8.4	1256.9	14.9	1256.9	14.9	97.8
-Spot 49	204	176291	3.6	11.9434	0.6	2.5606	1.0	0.2219	0.9	0.83	1291.9	10.1	1289.5	7.6	1285.4	11.5	1285.4	11.5	100.5
-Spot 60	37	9478	7.5	11.6428	1.4	2.7295	1.6	0.2306	0.8	0.48	1337.6	9.3	1336.5	12.0	1334.8	27.6	1334.8	27.6	100.2
-Spot 6	375	274982	2.0	11.3230	0.6	2.8970	1.0	0.2380	0.7	0.76	1376.4	9.2	1381.1	7.4	1388.5	12.3	1388.5	12.3	99.1
-Spot 62	367	90176	3.1	11.2542	0.6	2.8680	1.1	0.2342	0.9	0.84	1356.5	11.3	1373.6	8.3	1400.2	11.5	1400.2	11.5	96.9
-Spot 19	411	165706	6.8	11.1306	0.6	3.0270	1.6	0.2445	1.5	0.93	1409.9	18.9	1414.5	12.2	1421.3	11.0	1421.3	11.0	99.2
-Spot 78	31	5603	0.8	10.9623	1.0	3.1299	1.6	0.2490	1.3	0.80	1433.1	16.3	1440.1	12.2	1450.4	18.2	1450.4	18.2	98.8
-Spot 75	678	55481	2.9	10.9104	0.6	3.2510	1.3	0.2574	1.1	0.87	1476.3	14.7	1469.4	9.9	1459.4	11.9	1459.4	11.9	101.2
-Spot 98	138	20003	2.2	10.8149	0.6	3.2275	1.2	0.2533	1.0	0.84	1455.3	12.8	1463.8	9.1	1476.1	12.1	1476.1	12.1	98.6
-Spot 97	255	39693	1.4	10.7889	0.6	3.2191	1.2	0.2520	1.1	0.89	1448.8	14.3	1461.8	9.6	1480.7	10.7	1480.7	10.7	97.8
-Spot 71	521	396994	2.6	10.7520	0.5	3.3757	1.1	0.2634	1.0	0.90	1507.0	13.7	1498.8	8.9	1487.2	9.4	1487.2	9.4	101.3
-Spot 96	785	125748	5.4	10.7393	0.6	3.4175	1.2	0.2663	1.1	0.88	1522.0	14.3	1508.4	9.5	1489.4	11.0	1489.4	11.0	102.2
-Spot 1	140	379460	1.3	10.5783	0.5	3.4534	1.0	0.2651	0.9	0.89	1515.7	12.6	1516.6	8.2	1518.0	9.0	1518.0	9.0	99.8
-Spot 44	229	105726	1.8	10.5025	0.8	3.3860	1.2	0.2580	0.8	0.73	1479.7	11.1	1501.2	9.0	1531.5	14.9	1531.5	14.9	96.6
-Spot 51	383	63839	5.3	10.3079	0.7	3.6464	1.5	0.2727	1.3	0.89	1554.6	18.6	1559.7	12.0	1566.6	12.6	1566.6	12.6	99.2
-Spot 77	419	75963	1.9	10.0716	0.6	3.9106	1.2	0.2858	1.1	0.86	1620.4	15.4	1615.9	10.1	1610.0	11.8	1610.0	11.8	100.6
-Spot 89	113	95190	1.9	10.0705	0.5	3.7567	1.2	0.2745	1.1	0.90	1563.6	15.5	1583.6	9.9	1610.2	10.1	1610.2	10.1	97.1
-Spot 63	484	62700	3.2	10.0570	0.6	3.8556	1.4	0.2814	1.3	0.91	1598.2	18.1	1604.4	11.4	1612.7	11.0	1612.7	11.0	99.1
-Spot 54	223	182210	1.1	9.9966	0.5	3.8505	1.0	0.2793	0.9	0.87	1587.8	12.5	1603.4	8.2	1623.9	9.3	1623.9	9.3	97.8
-Spot 64	432	687293	2.6	9.9421	0.5	4.1097	1.4	0.2965	1.3	0.93	1673.7	19.7	1656.2	11.8	1634.1	10.1	1634.1	10.1	102.4
-Spot 28	238	29577	1.5	9.9105	0.6	3.8996	1.0	0.2804	0.8	0.81	1593.5	11.5	1613.6	8.1	1640.0	10.8	1640.0	10.8	97.2
-Spot 5	48	18740	1.1	9.8651	0.7	4.0184	1.2	0.2876	1.0	0.84	1629.7	14.8	1637.9	10.0	1648.5	12.4	1648.5	12.4	98.9
-Spot 93	73	20011	1.3	9.8289	0.7	4.0917	1.1	0.2918	0.9	0.79	1650.6	13.2	1652.6	9.4	1655.3	13.1	1655.3	13.1	99.7
-Spot 25	67	32845	1.4	9.7338	0.8	4.1123	1.4	0.2904	1.1	0.83	1643.7	16.7	1656.8	11.3	1673.3	14.3	1673.3	14.3	98.2
-Spot 30	148	81596	1.5	9.7262	0.6	4.1496	1.2	0.2928	1.1	0.86	1655.7	15.4	1664.1	10.0	1674.7	11.5	1674.7	11.5	98.9
-Spot 79	113	14179	2.0	9.6001	0.5	4.0921	0.9	0.2850	0.8	0.82	1616.7	11.0	1652.7	7.7	1698.8	10.1	1698.8	10.1	95.2
-Spot 65	107	173810	2.0	9.5181	0.7	4.4449	0.9	0.3070	0.6	0.68	1725.8	9.7	1720.8	7.8	1714.6	12.6	1714.6	12.6	100.7
-Spot 92	144	53741	2.3	9.3607	0.6	4.3874	1.0	0.2980	0.8	0.79	1681.3	11.4	1710.0	8.1	1745.2	11.1	1745.2	11.1	96.3
-Spot 104	142	37905	3.7	9.3081	0.7	4.6646	1.1	0.3150	0.8	0.78	1765.5	13.1	1760.9	9.1	1755.5	12.5	1755.5	12.5	100.6
-Spot 39	493	388325	2.8	9.2213	0.7	4.7510	1.7	0.3179	1.5	0.91	1779.4	23.5	1776.3	13.9	1772.7	12.5	1772.7	12.5	100.4
-Spot 18	287	91204	4.9	9.1744	0.6	4.7861	0.8	0.3186	0.6	0.70	1782.9	9.2	1782.5	7.0	1781.9	10.8	1781.9	10.8	100.1
-Spot 31	116	176487	2.7	9.1360	0.6	4.7195	1.0	0.3129	0.8	0.82	1754.7	13.0	1770.7	8.7	1789.6	11.0	1789.6	11.0	98.1
-Spot 68	160	53032	3.2	9.1016	0.6	4.8773	1.1	0.3221	0.9	0.84	1800.0	14.0	1798.3	8.9	1796.4	10.4	1796.4	10.4	100.2
-Spot 47	43	320341	1.5	8.6739	0.7	5.3046	1.4	0.3339	1.2	0.86	1857.0	18.9	1869.6	11.6	1883.6	12.6	1883.6	12.6	98.6
-Spot 33	52	12567	2.2	7.3150	0.8	6.6100	1.5	0.3508	1.2	0.85	1938.6	20.7	2060.7	12.9	2185.1	13.5	2185.1	13.5	88.7
-Spot 103	340	76199	0.7	5.2656	0.8	13.4322	1.6	0.5132	1.4	0.87	2670.3	31.4	2710.5	15.6	2740.7	13.3	2740.7	13.3	97.4
-Spot 87	195	48821	1.6	5.2629	0.6	13.2733	1.2	0.5069	1.0	0.86	2643.2	22.5	2699.3	11.4	2741.5	10.3	2741.5	10.3	96.4
-Spot 41	133	631576	3.5	5.1277	0.5	14.1962	0.9	0.5282	0.7	0.80	2733.8	15.8	2762.9	8.4	2784.2	8.7	2784.2	8.7	98.2
-Spot 32	178	59141	2.2	5.1229	0.7	14.6246	1.3	0.5436	1.1	0.85	2798.6	25.2	2791.1	12.4	2785.8	11.1	2785.8	11.1	100.5
-Spot 21	85	57643	2.1	4.8875	0.7	15.7089	1.2	0.5571	1.0	0.80	2854.6	22.5	2859.3	11.6	2862.6	11.8	2862.6	11.8	99.7
-Spot 53	76	5721	2.9	18.8438	1.7	0.4770	1.9	0.0652	0.8	0.45	407.3	3.3	396.0	6.1	330.7	37.7	407.3	3.3	123.1

Table 6. JV-1

Table_____. U-Pb geochronologic analyses.																				
						Isotope ratios						Apparent ages (Ma)								
Analysis	U	206Pb	U/Th	206Pb*	±	207Pb*	±	206Pb*	±	error	206Pb*	±	207Pb*	±	206Pb*	±	Best age	±	Conc
	(ppm)	204Pb		207Pb*	(%)	235U*	(%)	238U	(%)	corr.	238U*	(Ma)	235U	(Ma)	207Pb*	(Ma)	(Ma)	(Ma)	(%)
-Spot 30	183	32168	1.1	17.9869	0.8	0.4839	1.3	0.0632	1.1	0.81	394.8	4.1	400.7	4.4	435.3	17.7	394.8	4.1	98.5
-Spot 38	178	148572	1.3	17.9206	1.2	0.4957	1.5	0.0645	1.0	0.63	402.7	3.8	408.8	5.1	443.5	26.3	402.7	3.8	98.5
-Spot 100	1734	7540	1.2	16.5076	1.4	0.5408	1.7	0.0648	1.1	0.62	404.6	4.1	439.0	6.1	623.3	29.1	404.6	4.1	92.2
-Spot 89	116	7966	2.0	18.0807	1.4	0.5053	1.7	0.0663	0.9	0.57	413.8	3.8	415.3	5.6	423.7	30.3	413.8	3.8	99.6
-Spot 78	376	23554	2.2	17.8093	0.8	0.5325	1.5	0.0688	1.3	0.86	429.0	5.4	433.5	5.3	457.4	16.8	429.0	5.4	99.0
-Spot 46	1220	23306	72.5	17.1972	1.0	0.5581	1.4	0.0696	0.9	0.69	434.0	3.9	450.3	4.9	534.4	21.7	434.0	3.9	96.4
-Spot 51	596	114463	1.5	17.9856	0.5	0.5343	1.2	0.0697	1.1	0.90	434.5	4.5	434.6	4.2	435.4	11.9	434.5	4.5	100.0
-Spot 103	121	16163	0.9	18.1373	1.0	0.5337	1.5	0.0702	1.1	0.72	437.6	4.5	434.3	5.2	416.7	22.6	437.6	4.5	100.8
-Spot 22	114	436347	0.6	17.6529	1.1	0.5487	1.6	0.0703	1.1	0.72	437.9	4.8	444.2	5.6	476.9	23.8	437.9	4.8	98.6
-Spot 44	495	284334	1.6	17.6943	0.7	0.5808	1.3	0.0746	1.1	0.87	463.6	5.0	465.0	4.9	471.7	14.4	463.6	5.0	99.7
-Spot 106	170	59593	1.7	17.4001	1.2	0.5984	1.6	0.0756	1.1	0.66	469.5	4.8	476.2	6.1	508.7	26.5	469.5	4.8	98.6
-Spot 20	186	170183	1.7	17.3606	0.7	0.6001	1.2	0.0756	0.9	0.81	469.8	4.3	477.3	4.4	513.7	14.9	469.8	4.3	98.4
-Spot 97	403	34027	1.8	15.3584	1.2	0.6944	1.6	0.0774	1.0	0.62	480.5	4.6	535.4	6.6	777.0	26.3	480.5	4.6	89.7
-Spot 18	576	47775	1.7	16.4101	0.6	0.8351	1.4	0.0994	1.2	0.90	611.1	7.1	616.4	6.2	636.1	12.4	611.1	7.1	99.1
-Spot 73	154	13216	10.7	15.7077	0.9	1.0301	1.4	0.1174	1.2	0.80	715.6	7.8	719.0	7.4	729.6	18.2	715.6	7.8	99.5
-Spot 74	79	16930	3.5	14.1352	0.9	1.5348	1.3	0.1574	1.0	0.75	942.4	8.8	944.4	8.2	949.2	18.2	949.2	18.2	99.8
-Spot 6	68	19041	2.4	14.0395	0.7	1.5401	1.3	0.1569	1.1	0.83	939.5	9.3	946.6	7.9	963.1	14.7	963.1	14.7	99.3
-Spot 49	30	3648	1.1	13.9532	1.3	1.6647	1.7	0.1685	1.1	0.67	1004.1	10.5	995.2	10.7	975.7	25.5	975.7	25.5	100.9
-Spot 25	241	38517	6.8	13.9217	0.7	1.5575	1.2	0.1573	1.0	0.79	941.9	8.4	953.5	7.5	980.3	15.0	980.3	15.0	98.8
-Spot 107	113	279345	1.2	13.9062	0.7	1.6323	1.2	0.1647	1.0	0.81	982.8	8.9	982.7	7.6	982.5	14.4	982.5	14.4	100.0
-Spot 85	119	32188	0.7	13.7850	0.7	1.6686	1.1	0.1669	0.8	0.76	995.0	7.7	996.6	6.9	1000.3	14.4	1000.3	14.4	99.8
-Spot 87	117	12604	4.8	13.7658	0.8	1.7442	1.4	0.1742	1.1	0.80	1035.3	10.8	1025.0	9.1	1003.1	17.0	1003.1	17.0	101.0
-Spot 57	584	61866	1.9	13.7423	0.8	1.7397	1.5	0.1735	1.3	0.86	1031.2	12.3	1023.3	9.6	1006.6	15.4	1006.6	15.4	100.8
-Spot 65	100	11920	2.4	13.7357	0.7	1.7668	1.0	0.1761	0.7	0.69	1045.6	6.5	1033.3	6.3	1007.6	14.3	1007.6	14.3	101.2
-Spot 32	75	34706	1.5	13.7169	0.8	1.6351	1.3	0.1627	1.0	0.77	972.0	9.3	983.8	8.4	1010.4	17.2	1010.4	17.2	98.8
-Spot 21	160	24960	3.2	13.7164	0.9	1.7401	1.3	0.1732	0.9	0.71	1029.6	8.6	1023.5	8.1	1010.4	17.9	1010.4	17.9	100.6
-Spot 94	49	13483	0.8	13.6993	1.0	1.6764	1.4	0.1666	1.0	0.72	993.5	9.2	999.6	8.9	1013.0	19.7	1013.0	19.7	99.4
-Spot 8	186	72410	1.8	13.6543	0.7	1.7028	1.1	0.1687	0.9	0.79	1004.9	8.4	1009.6	7.3	1019.6	14.1	1019.6	14.1	99.5
-Spot 37	331	73924	29.4	13.6139	0.7	1.7101	1.3	0.1689	1.1	0.86	1006.2	10.6	1012.3	8.5	1025.6	13.5	1025.6	13.5	99.4
-Spot 63	187	39065	3.8	13.5814	0.6	1.7707	1.1	0.1745	0.9	0.82	1036.8	8.3	1034.8	6.8	1030.5	12.0	1030.5	12.0	100.2
-Spot 104	407	71474	4.4	13.5750	0.6	1.7810	1.3	0.1754	1.2	0.88	1041.9	11.4	1038.5	8.8	1031.4	12.8	1031.4	12.8	100.3
-Spot 55	115	41488	2.5	13.5695	0.8	1.7797	1.1	0.1752	0.8	0.71	1040.8	7.8	1038.1	7.4	1032.2	16.3	1032.2	16.3	100.3
-Spot 1	226	141082	2.6	13.5410	0.4	1.7060	1.0	0.1676	0.9	0.93	999.0	8.3	1010.8	6.2	1036.5	7.2	1036.5	7.2	98.8
-Spot 81	79	8598	2.8	13.5337	1.0	1.8353	1.5	0.1802	1.1	0.72	1068.2	10.6	1058.2	9.8	1037.6	21.1	1037.6	21.1	100.9
-Spot 27	660	87410	10.5	13.5066	0.7	1.8036	1.3	0.1768	1.1	0.85	1049.2	10.7	1046.8	8.5	1041.6	13.8	1041.6	13.8	100.2
-Spot 4	106	105570	1.6	13.4317	0.7	1.7755	1.0	0.1730	0.7	0.69	1028.8	6.6	1036.5	6.5	1052.9	14.7	1052.9	14.7	99.3
-Spot 34	376	135402	3.7	13.3977	0.7	1.8077	1.3	0.1757	1.2	0.87	1043.6	11.3	1048.2	8.8	1058.0	13.3	1058.0	13.3	99.6
-Spot 2	111	33198	2.5	13.3845	0.7	1.8003	1.2	0.1748	0.9	0.78	1038.7	8.8	1045.6	7.7	1059.9	14.9	1059.9	14.9	99.3
-Spot 28	140	23448	4.5	13.3845	0.7	1.7695	1.1	0.1718	0.8	0.75	1022.3	7.5	1034.3	6.9	1059.9	14.2	1059.9	14.2	98.8
-Spot 14	165	15473	2.5	13.3685	1.0	1.7769	1.4	0.1724	1.0	0.74	1025.1	9.9	1037.0	9.2	1062.4	19.2	1062.4	19.2	98.8
-Spot 66	191	31132	2.3	13.3361	0.5	1.9096	0.9	0.1848	0.7	0.80	1093.0	7.5	1084.4	6.1	1067.2	11.0	1067.2	11.0	100.8
-Spot 80	240	23876	1.9	13.2699	0.8	1.9524	1.2	0.1880	0.9	0.74	1110.4	9.1	1099.3	8.0	1077.2	16.1	1077.2	16.1	101.0
-Spot 86	34	37005	1.6	13.2352	0.9	1.8547	1.4	0.1781	1.1	0.79	1056.6	10.8	1065.1	9.3	1082.5	17.5	1082.5	17.5	99.2
-Spot 79	105	19207	2.8	13.1978	0.6	1.9137	1.0	0.1833	0.8	0.82	1084.7	8.3	1085.9	6.8	1088.1	11.6	1088.1	11.6	99.9
-Spot 45	132	12887	1.5	13.1782	0.8	1.8881	1.2	0.1805	0.9	0.76	1069.9	9.3	1076.9	8.2	1091.1	16.0	1091.1	16.0	99.3
-Spot 41	92	13249	3.7	13.1038	0.7	1.9723	1.2	0.1875	1.0	0.83	1108.0	10.3	1106.1	8.2	1102.4	13.4	1102.4	13.4	100.2
-Spot 109	96	15401	2.2	13.0692	0.7	2.0072	1.3	0.1903	1.0	0.82	1123.2	10.7	1117.9	8.5	1107.7	14.4	1107.7	14.4	100.5
-Spot 48	169	34032	3.1	13.0420	0.6	1.9714	0.9	0.1866	0.7	0.74	1102.7	6.8	1105.8	6.1	1111.9	12.1	1111.9	12.1	99.7
-Spot 95	52	12090	3.8	13.0263	1.0	1.9113	1.3	0.1807	0.8	0.66	1070.5	8.3	1085.0	8.6	1114.3	19.4	1114.3	19.4	98.7
-Spot 76	110	19956	3.4	13.0095	0.8	1.9285	1.2	0.1820	0.9	0.77	1078.1	9.1	1091.0	8.0	1116.9	15.3	1116.9	15.3	98.8
-Spot 19	172	419426	3.3	12.9333	0.7	2.0020	1.2	0.1879	0.9	0.79	1109.8	9.4	1116.2	7.9	1128.6	14.1	1128.6	14.1	99.4
-Spot 61	147	46111	3.1	12.9006	0.6	2.0272	1.1	0.1898	0.9	0.81	1120.0	9.2	1124.7	7.5	1133.6	12.8	1133.6	12.8	99.6
-Spot 62	45	7407	2.1	12.8280	1.1	2.0245	1.5	0.1884	1.1	0.73	1112.9	11.6	1123.8	10.5	1144.9	20.9	1144.9	20.9	99.0
-Spot 83	70	13029	2.1	12.8157	0.8	2.0873	1.3	0.1941	1.0	0.80	1143.5	10.6	1144.6	8.8	1146.8	15.4	1146.8	15.4	99.9
-Spot 101	249	120859	2.7	12.6921	0.7	2.1234	1.1	0.1956	0.9	0.82	1151.4	9.7	1156.5	7.8	1166.0	12.9	1166.0	12.9	99.6
-Spot 33	86	8221	1.5	12.6088	1.3	2.1253	1.6	0.1944	0.9	0.57	1145.4	9.4	1157.1	10.9	1179.0	25.7	1179.0	25.7	99.0
-Spot 75	42	11485	3.2	12.4294	0.7	2.2508	1.2	0.2030	1.0	0.81	1191.4	10.9	1197.0	8.7	1207.3	14.3	1207.3	14.3	99.5
-Spot 35	643	95976	12.7	12.0491	1.4	2.4438	2.1	0.2137	1.5	0.72	1248.2	17.1	1255.6	15.0	1268.2	28.1	1268.2	28.1	99.4
-Spot 56	211	34503	1.4	11.8954	0.8	2.4153	2.3	0.2085	2.2	0.94	1220.6	24.5	1247.2	16.8	1293.2	15.5	1293.2	15.5	97.9
-Spot 43	9	2813	1.3	11.7756	1.8	2.0719	2.2	0.1770	1.3	0.58	1050.7	12.3	1139.6	15.0	1312.9	34.8	1312.9	34.8	92.2
-Spot 64	231	57980	0.8	11.7674	0.9	2.6273	1.2	0.2243	0.9	0.72	1304.7	10.5	1308.3	9.1	1314.2	16.7	1314.2	16.7	99.7
-Spot 24	69	46109	4.3	11.7428	0.7	2.3823	1.3	0.2030	1.1	0.84	1191.3	12.2	1237.3	9.5	1318.3	13.8	1318.3	13.8	96.3
-Spot 36	383	40249	3.8	11.6683	0.6	2.7306	1.4	0.2312	1.2	0.89	1340.7	14.6	1336.8	10.1	1330.6	11.7	1330.6	11.7	100.3
-Spot 29	111	6958	2.1	11.2979	2.0	2.5937	2.4	0.2126	1.3	0.54	1242.8	14.8	1298.9	17.8	1392.8	39.2	1392.8	39.2	95.7
-Spot 54	298	158827	2.8	11.2446	0.6	3.0216	1.3	0.2465	1.2	0.91	1420.6	15.5	1413.1	10.3	1401.8	10.8	1401.8	10.8	100.5
-Spot 50	115	105974	1.9	10.8548	0.6	3.2751	1.1	0.2579	1.0	0.83	1479.3	12.6	1475.2	8.9	1469.1	12.0	1469.1	12.0	100.3
-Spot 110	274	43239	1.8	10.7915	0.6	3.3529	1.3	0.2625	1.1	0.89	1502.8	15.4	1493.5	10.1	1480.2	11.3	1480.2	11.3	100.6
-Spot 12	298	30383	1.7	10.7910	0.5	3.0352	1.1	0.2376	1.0	0.90	1374.5	12.3	1416.5	8.5	1480.3	9.4	1480.3	9.4	97.0
-Spot 99	274	30525	2.7	10.7542	0.7	3.3676	1.2	0.2628	1.0	0.81	1504.0	13.4	1496.9	9.6	1486.8	13.5	1486.8	13.5	100.5
-Spot 26	162	117304	1.8	10.6862	0.6	3.3554	1.0	0.2602	0.8	0.78	1490.7	10.9	1494.1	8.1	1498.8	12.2	1498.8	12.2	99.8
-Spot 82	57	57401	1.2	10.6665	0.8	3.3595	1.4	0.2600	1.1	0.83	1489.9	14.9	1495.0	10.6	1502.3	14.2	1502.3	14.2	99.7
-Spot 71	54	32362	1.6	10.4896	0.9	3.4422	1.3	0.2620	0.9	0.68	1500.0	11.4	1514.1	9.9	1533.8	17.3	1533.8	17.3	99.1
-Spot 11	146	347409	13.3	10.4642	0.8	3.5651	1.3	0.2707	1.1	0.82	1544.3	14.9	1541.8	10.5	1538.4	14.3	1538.4	14.3	100.2
-Spot 7	149	37562	0.7	10.0583	1.3	3.8021	1.8	0.2775	1.2	0.70	1578.7	17.5	1593.2	14.4	1612.4	24.0	1612.4	24.0	99.1
-Spot 39	461	109864	1.8	10.0472	0.6	3.8674	1.2	0.2819	1.0	0.85	1601.1	14.7	1606.9	9.8	1614.5	11.8	1614.5	11.8	99.6
-Spot 92	200	50594	1.8	9.9158	0.6	4.1263	1.0	0.2969	0.8	0.81	1675.8	11.7	1659.5	8.0	1639.0	10.5	1639.0	10.5	101.0
-Spot 68	131	45533	1.1	9.8692	0.8	3.9855	1.3	0.2854	1.0	0.80	1618.5	14.5	1631.3	10.3	1647.7	13.9	1647.7	13.9	99.2
-Spot 16	73	20704	1.3	9.8329	0.9	4.0217	1.2	0.2869	0.8	0.68	1626.2	12.0	1638.6	9.9	1654.5	16.5	1654.5	16.5	99.2
-Spot 84	70	39863	0.8	9.7904	0.8	4.0259	1.2	0.2860	1.0	0.79	1621.4	13.9	1639.4	10.0	1662.6	14.0	1662.6	14.0	98.9
-Spot 5	161	143703	2.4	9.7855	0.6	4.0174	1.1	0.2852	0.9	0.83	1617.7	12.6	1637.7	8.6	1663.5	10.9	1663.5	10.9	98.8
-Spot 31	128	42291	1.0	9.7774	0.8	4.1080	1.3	0.2914	1.0	0.80	1648.7	14.6	1655.9	10.3	1665.0	14.1	1665.0	14.1	99.6
-Spot 15	69	34004	2.2	9.7540	0.8	4.0095	1.2	0.2838	0.9	0.75	1610.3	12.8	1636.1	9.7	1669.5	14.7	1669.5	14.7	98.4
-Spot 47	227	406418	1.5	9.7096	0.7	4.2008	1.1	0.2960	0.8	0.78	1671.2	12.2	1674.2	8.7	1677.9	12.3	1677.9	12.3	99.8
-Spot 58	120	35899	1.4	9.6832	0.6	4.1109	1.2	0.2888	1.1	0.86	1635.7	15.2	1656.5	10.0	1682.9	11.5	1682.9	11.5	98.7
-Spot 59	202	49178	2.2	9.5020	0.7	4.5523	1.1	0.3139	0.8	0.76	1759.6	12.5	1740.6	8.9	1717.7	12.9	1717.7	12.9	101.1

-Spot 23	216	60114	2.5	9.3169	0.6	4.7163	1.2	0.3188	1.0	0.86	1784.0	15.8	1770.1	9.9	1753.8	10.9	1753.8	10.9	100.8
-Spot 10	208	49903	4.2	9.2008	0.6	4.7167	1.2	0.3149	1.0	0.87	1764.7	15.5	1770.2	9.7	1776.7	10.6	1776.7	10.6	99.7
-Spot 105	368	58375	2.2	9.1927	0.5	4.8560	1.6	0.3239	1.5	0.94	1808.7	23.3	1794.7	13.2	1778.3	9.5	1778.3	9.5	100.8
-Spot 77	44	22848	0.6	9.0144	0.8	4.6866	1.2	0.3065	0.9	0.75	1723.6	13.9	1764.8	10.2	1814.0	14.5	1814.0	14.5	97.7
-Spot 67	38	7697	1.5	8.8953	0.8	5.0594	1.3	0.3266	1.1	0.79	1821.6	16.7	1829.3	11.4	1838.1	15.0	1838.1	15.0	99.6
-Spot 102	92	169973	3.5	8.7733	0.7	5.3432	1.1	0.3401	0.8	0.76	1887.3	13.7	1875.8	9.4	1863.0	12.9	1863.0	12.9	100.6
-Spot 17	489	173772	1.5	8.5041	0.6	5.1689	1.1	0.3189	0.9	0.82	1784.6	14.0	1847.5	9.3	1919.1	11.0	1919.1	11.0	96.6
-Spot 91	9	2539	0.4	7.2678	2.6	6.8985	4.0	0.3638	3.1	0.77	2000.1	52.8	2098.5	35.5	2196.4	44.7	2196.4	44.7	95.3
-Spot 42	274	987	1.8	6.7244	6.7	7.3229	7.1	0.3573	2.3	0.33	1969.3	39.7	2151.6	63.7	2330.4	115.4	2330.4	115.4	91.5
-Spot 9	77	36533	0.8	5.4071	0.7	13.2604	1.1	0.5202	0.8	0.75	2700.2	18.1	2698.4	10.3	2696.9	11.9	2696.9	11.9	100.1
-Spot 69	139	97187	2.4	5.3923	0.8	12.8210	1.2	0.5016	0.9	0.75	2620.8	19.1	2666.6	11.1	2701.5	12.9	2701.5	12.9	98.3
-Spot 13	154	97582	1.8	5.3833	0.6	13.6656	1.0	0.5338	0.7	0.74	2757.4	15.8	2726.8	9.0	2704.2	10.7	2704.2	10.7	101.1
-Spot 52	167	46351	1.3	5.3630	0.6	11.4476	1.2	0.4455	1.0	0.86	2375.0	19.7	2560.3	10.8	2710.5	9.8	2710.5	9.8	92.8
-Spot 108	211	1361095	3.8	5.2815	0.6	14.2572	1.2	0.5464	1.0	0.83	2810.0	21.7	2767.0	10.9	2735.7	10.6	2735.7	10.6	101.6
-Spot 96	60	35846	0.7	5.2653	0.7	13.8737	1.0	0.5300	0.7	0.71	2741.6	16.1	2741.1	9.6	2740.8	11.6	2740.8	11.6	100.0
-Spot 53	104	31407	2.8	5.1593	0.7	14.4716	1.1	0.5417	0.9	0.78	2790.7	19.9	2781.1	10.7	2774.2	11.7	2774.2	11.7	100.3
-Spot 88	166	31250	1.5	5.0816	0.6	14.4626	1.2	0.5333	1.0	0.85	2755.2	23.0	2780.5	11.5	2799.0	10.5	2799.0	10.5	99.1
-Spot 98	77	13339	0.9	5.0140	0.6	15.0876	1.1	0.5489	1.0	0.84	2820.6	21.7	2820.8	10.7	2820.9	9.8	2820.9	9.8	100.0
-Spot 3	99	91129	0.9	3.7660	0.5	23.3689	1.1	0.6386	1.0	0.87	3183.4	23.9	3242.4	10.6	3279.1	8.3	3279.1	8.3	98.2

Concordia Plots

Normal Concordia Plots

Plot 1. STP-1

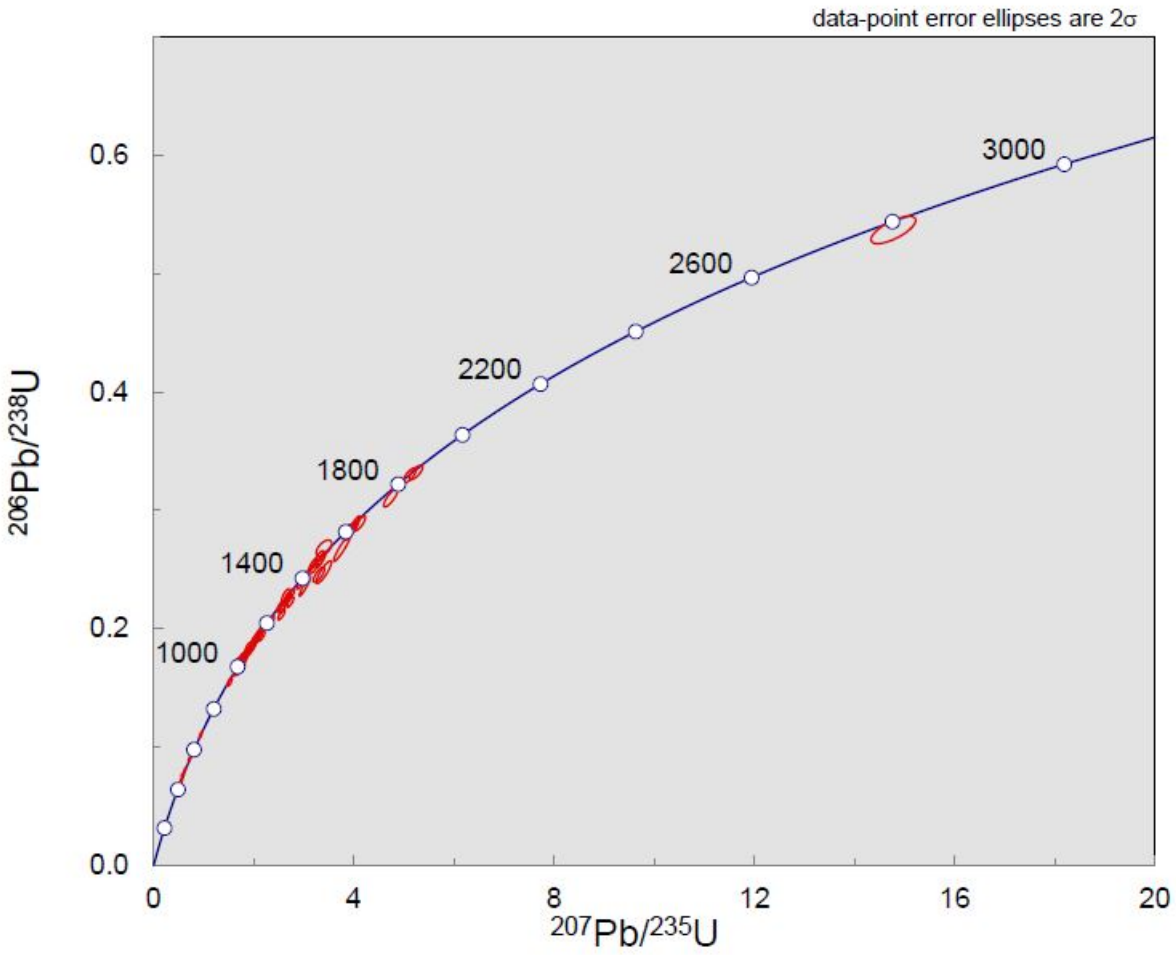

Plot 2. STT-1

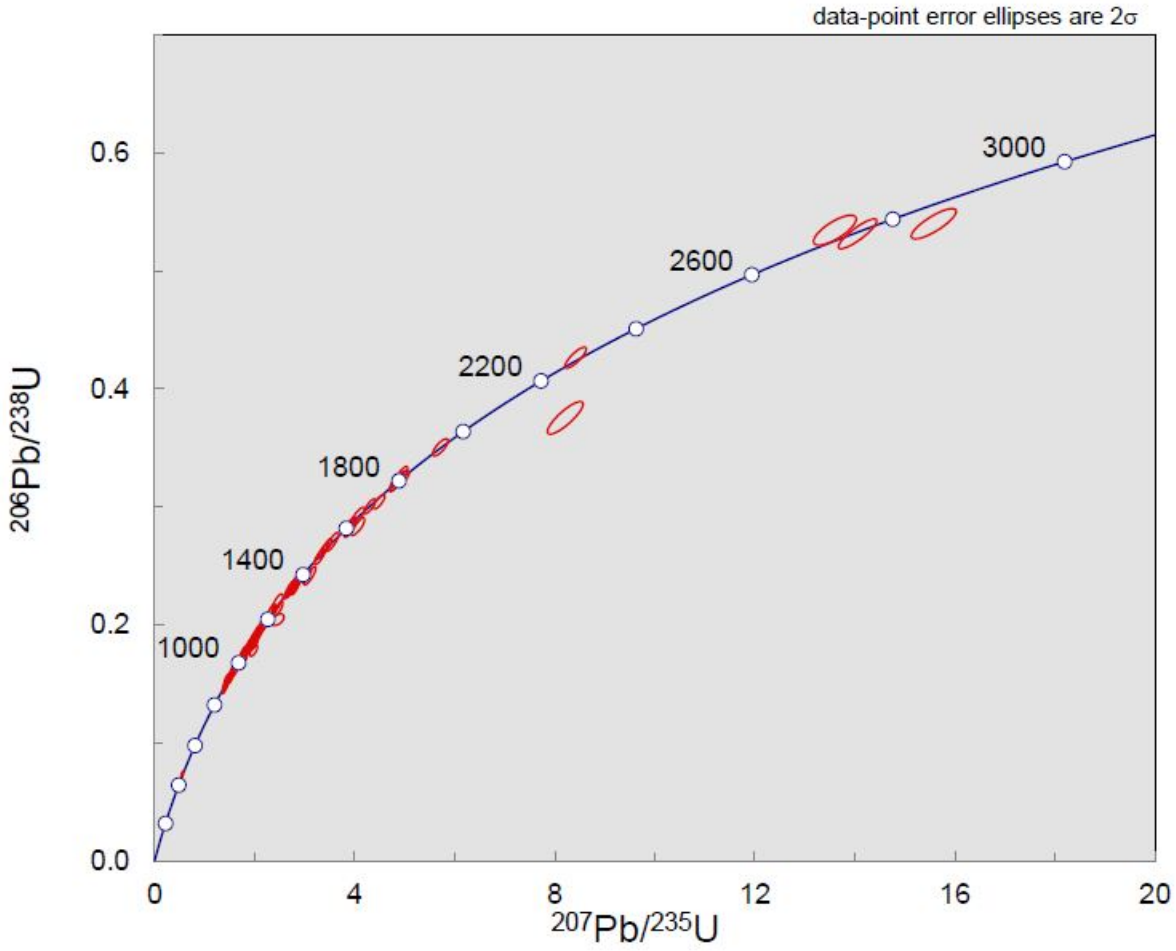
data-point error ellipses are 2σ
0.6
0.4
0.2
0.0
206Pb/238U
3000
2600
2200
1800
1400
1000
0
4
8
12
16
20
207Pb/235U

Plot 3. JFB-1

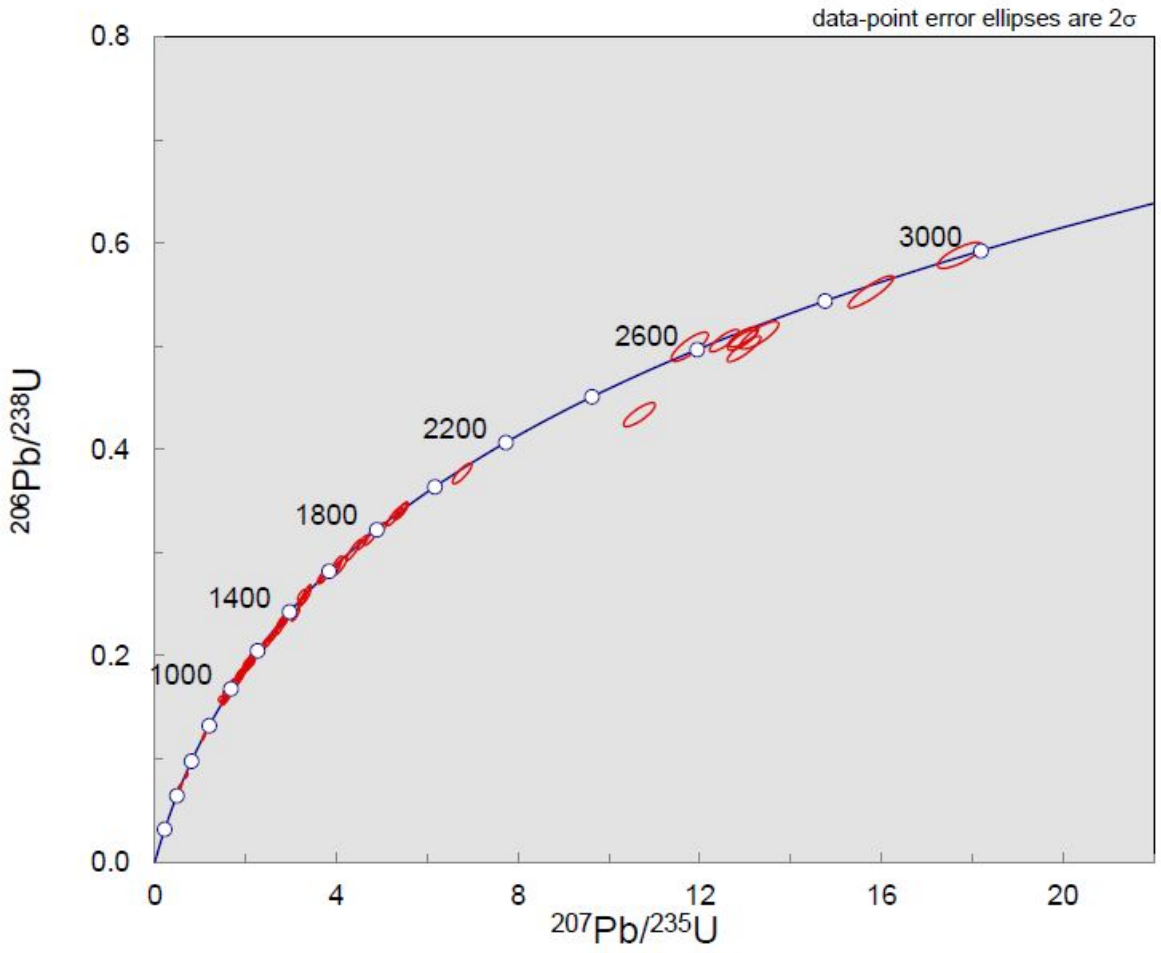
data-point error ellipses are 2σ
0.8
0.6
0.4
0.2
0.0
0
4
8
12
16
20
$^{206}Pb/^{238}U$
$^{207}Pb/^{235}U$
1000
1400
1800
2200
2600
3000

Plot 4. JFM-1

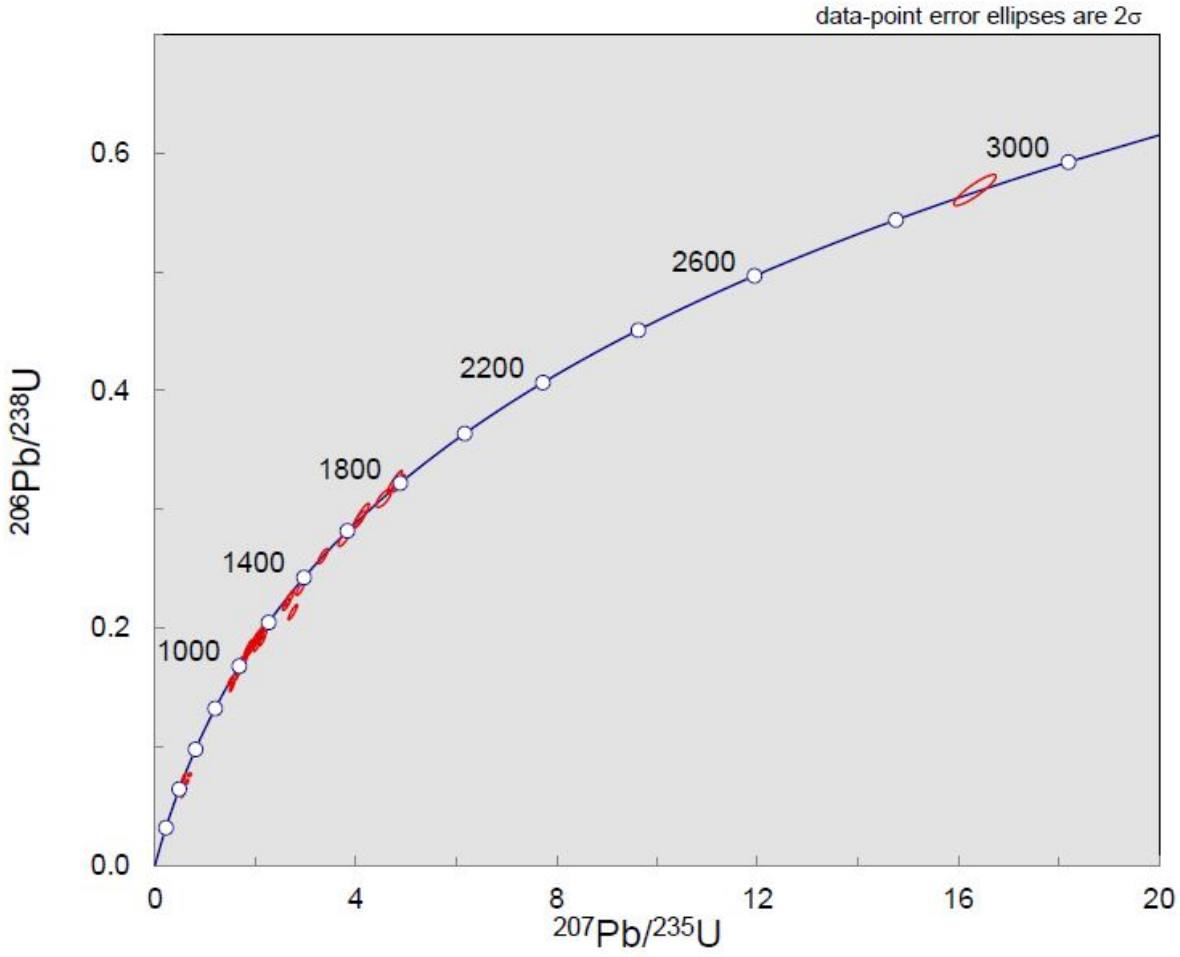
data-point error ellipses are 2σ
0.6
0.4
0.2
0.0
206Pb/238U
3000
2600
2200
1800
1400
1000
0
4
8
12
16
20
207Pb/235U

Plot 5. JFM-1 (Additional Analysis)

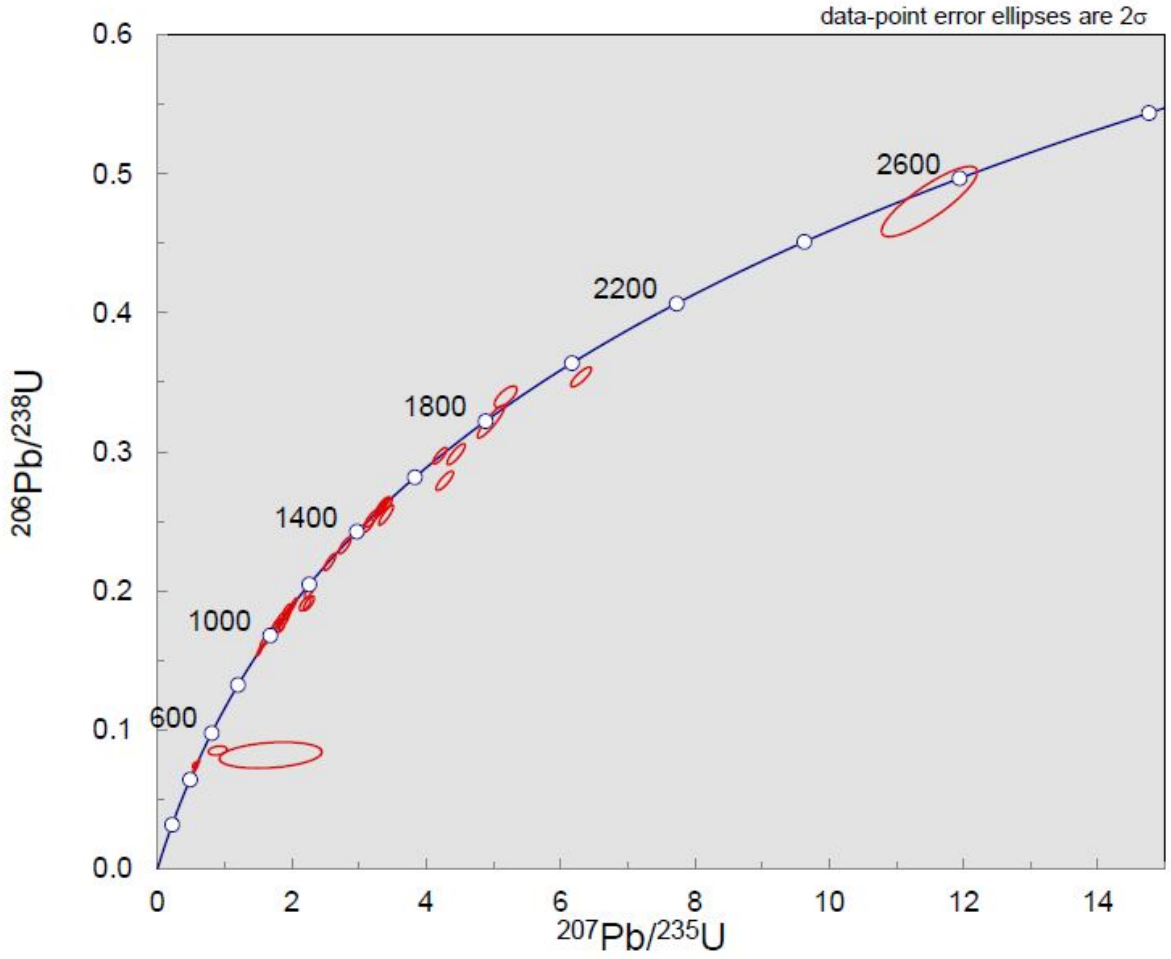

Plot 6. JFT-1

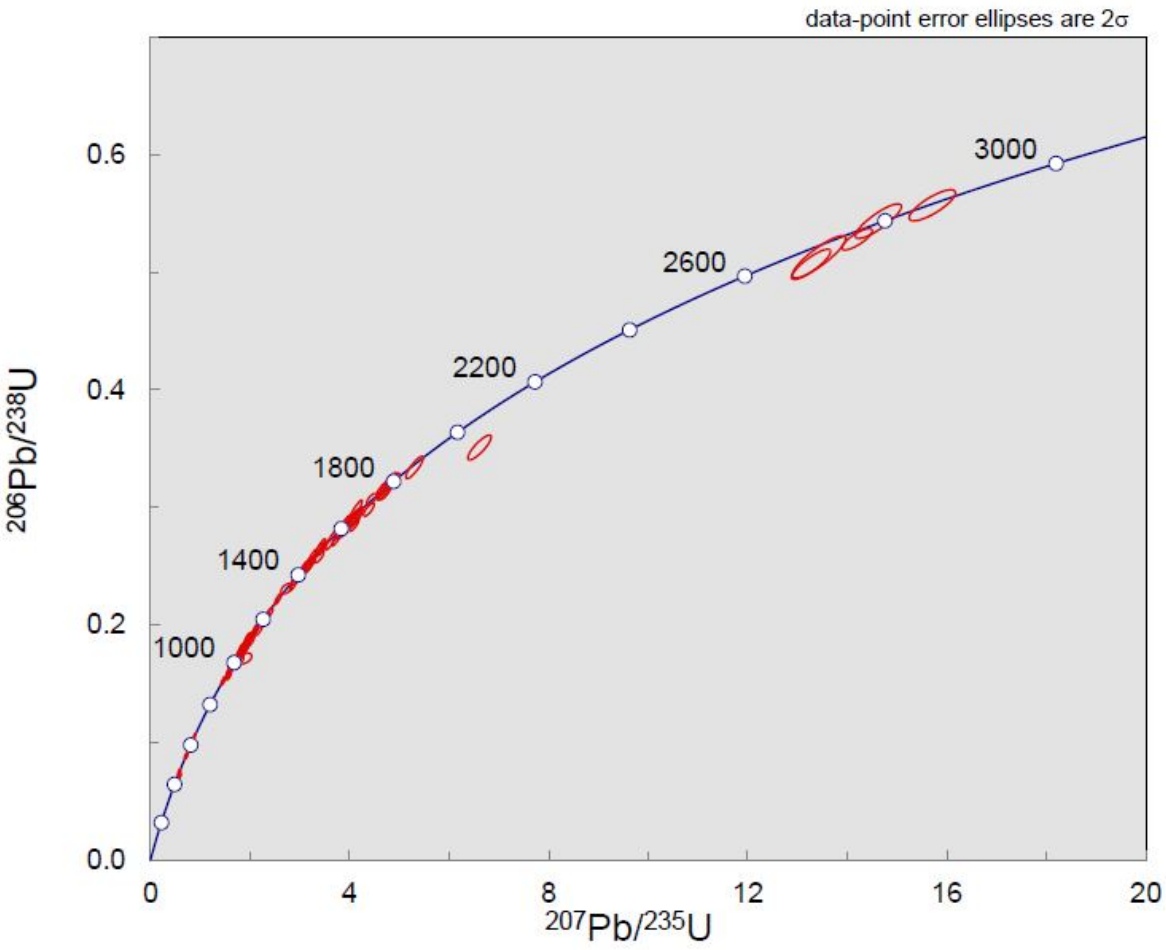
data-point error ellipses are 2σ
0.6
0.4
0.2
0.0
206Pb/238U
3000
2600
2200
1800
1400
1000
0
4
8
12
16
20
207Pb/235U

Plot 7. JV-1

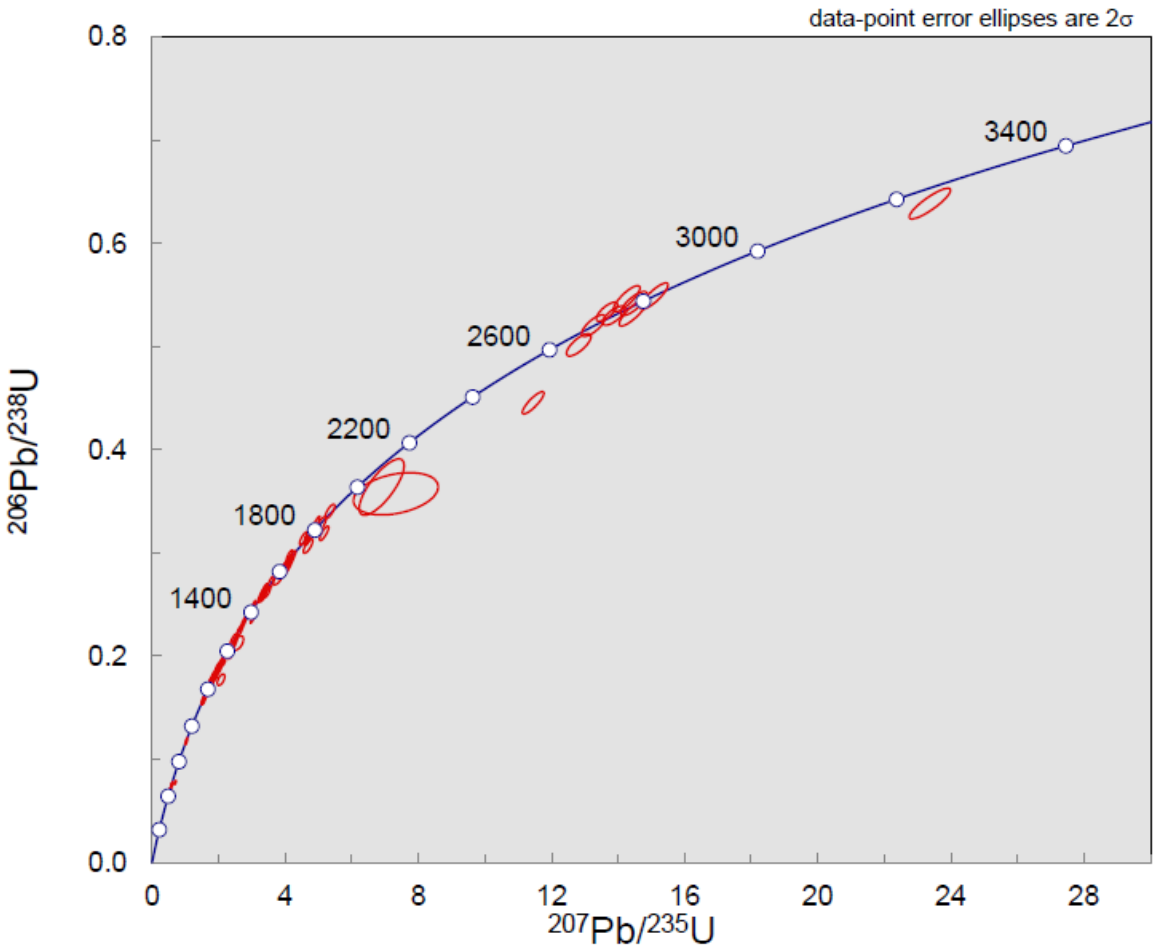
data-point error ellipses are 2σ
0.8
0.6
0.4
0.2
0.0
206Pb/238U
0
4
8
12
16
20
24
28
207Pb/235U
1400
1800
2200
2600
3000
3400

VITA

Personal Background	Shaun Prines Pittsburgh, Pennsylvania Born October 12, 1995, Pittsburgh, Pennsylvania Son of Leslie Prines and Grandson of Bonnie Gesinski
Education	Bachelor of Science in Geology, 2018 University of Pittsburgh, Pittsburgh, Pennsylvania Master of Science in Geology, 2020 Texas Christian University, Fort Worth, Texas
Experience	Geology Intern, Summer 2019 Pennsylvania Geological State Survey, Pittsburgh, PA Teaching Assistant, 2018-2020 Texas Christian University, Fort Worth, Texas
Professional Memberships	American Association of Petroleum Geologists Geological Society of America Fort Worth Geological Society

ABSTRACT

U-PB DETRITAL ZIRCONS OF THE SYN-OROGENIC CARBONIFEROUS DEEP-WATER CLASTIC DEPOSITS IN THE OUACHITA MOUNTAINS, ARKANSAS, UNITED STATES

Shaun T. Prines M.S, 2020

Department of Geological Sciences

Texas Christian University

Thesis Advisor: Dr. Xiangyang Xie

Committee Members: Dr. Helge Alsleben and Dr. Walter L. Manger

The southern margin of the North American continent transformed from a passive margin to an active margin during the Ouachita orogeny. Consequently, this tectonic activity resulted in depositing the thick and near-continuous syn-orogenic Carboniferous deep-water clastic deposits of the Ouachita Mountains in Oklahoma and Arkansas. The limited exposures of these syn-orogenic Carboniferous deep-water deposits in the Ouachita Mountains provided the prefect opportunity to further constrain the effects of the Ouachita orogeny on the sediment sourcing and dispersal patterns of the Southern Midcontinent during the Carboniferous.

In this study, a total of six outcrop samples (n=616) from the Mississippian Stanley Group and Lower-Middle Pennsylvanian Jackfork and Johns Valley Groups were collected and processed for U-Pb detrital zircon geochronologic analysis. Results show that the age distributions of the Carboniferous deep-water clastic deposits in the Ouachita Mountains are characterized by major peaks of the Paleozoic (~350-500 Ma), Grenville (~900-1350 Ma), and Midcontinental Granite-Rhyolite (~1350-1500 Ma), with minor peaks of Yavapai-Mazatzal (~1600-1800 Ma) and Superior (> ~2500 Ma) provinces. The detrital signatures of the six samples are relatively identical and were primarily derived from the recycled detritus of the

distal Appalachian orogenic belt and associated forelands with intermixed contributions from the Ouachita orogenic belt, the northern Midcontinent region, and western Laurentia. Additionally, the results of this study allow for furthered constraints to be placed on sediment dispersal pathways to the Southern Midcontinent in the Carboniferous.